UC Berkeley
UC Berkeley Electronic Theses and Dissertations

Title
Understanding Water and Solute Fluxes in Diverse Catchments

Permalink
https://escholarship.org/uc/item/2h47269n

Author
Godsey, Sarah

Publication Date
2009

Peer reviewed|Thesis/dissertation

eScholarship.org Powered by the California Digital Library
University of California

Understanding Water and Solute Fluxes in Diverse Catchments

by

Sarah Elizabeth Godsey

A dissertation submitted in partial satisfaction of the

requirements for the degree of

Doctor of Philosophy

in

Earth and Planetary Science

in the

Graduate Division

of the

University of California, Berkeley

Committee in charge:

Professor James W. Kirchner, Chair
Professor Michael Manga
Professor John Harte

Fall 2009

Understanding Water and Solute Fluxes in Diverse Catchments

Copyright 2009

by

Sarah Elizabeth Godsey

Abstract

Understanding Water and Solute Fluxes in Diverse Catchments

by

Sarah Elizabeth Godsey

Doctor of Philosophy in Earth and Planetary Science

University of California, Berkeley

Professor James W. Kirchner, Chair

Catchments integrate incoming hydrological and geochemical fluxes via the mixing and reaction processes occurring within their boundaries. The catchment science community still seeks realistic and internally consistent models which explain integrated catchment behavior. It is known that the amount of streamflow responds quickly to rainfall, that stream water is predominantly "old" water which has been stored for long periods within the catchment, and that streamflow chemistry varies with flow regime. To quantify these observed patterns of catchment behavior, I examined precipitation-runoff relationships, the distribution of travel times of water parcels falling on the catchment, and reactive tracer concentration-discharge relationships.

By examining water and solute fluxes across a wide range of catchments, I identified characteristics which catchment models should include in order to accurately represent these systems. Specifically, I showed that long-tailed travel time distributions are common in at least 20 European and North American catchments, and I tested the methods that are commonly used to estimate such distributions. I demonstrated that concentration-discharge relationships consistently exhibit power-law scaling at timescales of rainstorms and on an interannual basis in 59 hydrochemically diverse catchments. Finally, I showed that in snow-dominated catchments in California's Sierra Nevada mountains, summer low flows often respond more-than-proportionally to changes in snowpack volume.

I also showed that, although simple exponential mixing models are commonly used to represent catchment behavior, they cannot reproduce observed long-tail travel time distributions or power-law concentration-discharge relationships. Instead I showed that catchment travel time distributions are well-characterized by gamma distributions, and that a new reaction and transport model matches concentration-discharge relationships across our study catchments. Finally, I examined the effects of changing the phase of precipitation in a historical snowpack-low flow model. As more precipitation fell as rain instead of snow, the historical model was less accurate. I considered a mechanistic model to explore potential catchment responses to climate warming in Sierra Nevada catchments, and found that changes in the processes of groundwater recharge and evapotranspiration that were not considered in the historical model affected low flow responses to perturbed catchment inputs.

Introduction

Catchments are useful natural systems for studying hydrologic and hydrochemical processes. By definition, catchments integrate the fluxes of solutes and water that enter their boundaries. The mixing, reaction, storage, and mobilization processes operating within the catchment boundary all influence the water and solute fluxes leaving the catchment. Here I present and interpret data from a wide variety of catchments. I do this in order to quantify typical catchment travel time distributions, concentration-discharge relationships, and precipitation-flow relationships. Constraining the typical range of these three features can help catchment scientists to evaluate different models of catchment behavior, and understand how catchments might respond to perturbations, such as land-use change or climate change.

In chapters 1 and 2, I investigate catchment travel time distributions. First, I estimate travel time distributions for 20 catchments throughout North America and Europe, and find that they exhibit a fairly consistent shape with very long tails. The long tails implies that these catchments have a wide range of flowpath lengths and velocities. If a soluble contaminant were added to a catchment with a long-tailed travel time distribution, concentrations of that contaminant would be quickly detected in the stream and would persist for a very long time. Then in chapter 2, I evaluate the methods that are commonly used to estimate travel time distributions. I identify the situations in which different sampling and analysis methods can lead to problematic estimates.

In chapter 3, I shift from travel time distributions to an examination of the relationship between catchment inflows and outflows of water in a series of case studies from the Sierra Nevada. Specifically, I present the historical relationship between snowpacks and low flows in each catchment, and then I consider how summer low flow are likely to change as climate change shifts winter snowfall to rain. I analyze long-term data records from eight catchments, and model catchment-scale as well as subcatchment-scale processes. Subcatchment-scale changes in the timing and variability of groundwater recharge, and the timing of evapotranspiration are particularly important in understanding the catchment-scale response to a shift from snow-dominated to rain-dominated precipitation fluxes.

In chapter 4, I tackle the combined problem of mixing and reaction in 59 hydrochemically diverse catchments throughout the United States. I find that concentrations of major weathering products, such as Ca, Mg, Na, and Si, vary with changes in discharge, but only by a small amount. That is, most catchments exhibit nearly chemostatic behavior, on both the timescale of individual storms and on an inter-annual basis. I examine several simple hydrological and geochemical models, including a new model detailed in the appendix of this chapter. I find that only this new model can reproduce observed patterns of variation in reactive tracer concentrations with discharge, and still maintain internally consistent, plausible parameter values.

In addition to these contributions, there is still more work that could improve our understanding of catchment behavior building upon the results presented here. For example, one could evaluate the new mixing and reaction model introduced in chapter 4 by collecting intensive soil pore water data at sites where different mixing, transport and reaction processes occur. The

travel time distribution modeling work in chapter 1 could be extended to more diverse sites. The sampling protocols at each of these sites could be developed based on the results shown in chapter 2. As discussed in chapter 2, travel time distribution estimation methods which explicitly fit to noise in the frequency domain would be immediately useful to the catchment science community. It would also be helpful to develop a physical basis for travel time distribution shape. The effect of assuming a time-invariant travel time distribution should be quantified, especially in cases where small errors in the flow-time correction are introduced. Finally, as mentioned in chapter 3, collecting information to evaluate changes in recharge and evapotranspiration as precipitation phase changes is a difficult, but useful, step in evaluating the utility of catchment-scale precipitation-runoff models in the face of climate change.

Acknowledgements

My advisor Jim Kirchner has been extraordinarily generous with his time during my entire graduate career. Jim is enthusiastic about science, and his joy in scientific discovery is contagious. He has taught me how to carefully analyze data to test hypotheses. He has also helped me to improve my technical writing and presentation skills. Michael Manga and John Harte, my other dissertation committee members, provided insightful feedback on an earlier draft of this dissertation. Dave Clow, Tom Clair, Ivan Fernandez, Steve Kahl, Sarah Nelson, Steve Norton, Margaret Neal, Colin Neal, Christina Tague, Wenche Aas, Heleen de Wit, Brit Lisa Skjelkvale, Iain Malcolm, Doerthe Tetzlaff and Chris Soulsby contributed their time and data to the analyses included in this dissertation, and are co-authors on some of the manuscripts based on this work.

The geomorphology and HydroLunch groups at Berkeley helped me grow as a scientist. Bill Dietrich welcomed me into the geomorphology group during my first weeks at Berkeley, and has generously offered scientific and professional advice over the years. Many thanks also go to the geomorph group members: Leslie Hsu, Elowyn Yager, Johnny Sanders, Joel Rowland, Rebecca Leonardson, Taylor Perron, Ken Ferrier, Marisa Palucis, Mike Lamb, Christian Braudrick, Kathleen Swanson, Peter Nelson, Dino Bellugi, Tim Creyts, Roland Kaitna, Toby Minear, and Justine Owen. I also especially recognize two alumni of the geomorph group who died in the past year: Douglas Allen and Marie Bera. Beth Boyer provided early insights and encouragement, and was instrumental in creating a campus-wide community of people interested in water at Berkeley. The HydroLunch group, including Steve Sebestyen, Gretchen Miller, Madeline Solomon, Ben Runkle, Justin Lawrence, Ted Grantham, Newsha Ajami, Anne Short, Seth Shonkoff, Matt Cover, Jon Sanderman, Kevin Lunde, and Maria Goodrich, helped me to understand water resource issues from a variety of perspectives.

Eve-Lyn Hinckley, Maria Brumm, Lowell Miyagi, Mike Kiparsky, Ludmilla Aristilde, Trey Apel, and Julia LaRouche have all been supportive colleagues from near and far during the past years. I also thank the EPS and BWC staff, especially Margie Winn and Claire Legas, for their dedication, good humor, and patience. I am also especially grateful to the fellow members of my cohort – Vicky Lee, Christina Lee, Su-chin Chang and Nicole Schlegel – who have supported one another through ups and downs of graduate school.

Some field work that is not included in this dissertation was completed at sites in the Sierra Nevada and Coast Ranges in California. I thank researchers and staff at the Caspar Creek Experimental Forest, CAL FIRE, the Kings River Experimental Watershed, the US Forest Service, and the UC Reserve System's Sagehen Creek Field Station. In particular, Carolyn Hunsaker, Jason Adair, Tom Whittaker, Liz Keppeler, Sue Hilton, Brian Barrett, Fay Yee, Faerthen Felix, and Jeff Brown were very supportive. In addition, Evan Kha, David Swenson, Mike Cotton, Terry Smith, Madeline Solomon, Roger Davis, and Steve Dunn all helped with field work. Mike Cotton and Bill Walsh also provided computing assistance at critical times.

My "Fishing House" housemates, Don Koelpin, Eric Dubinsky and Theresa Grieco, always helped make day-to-day life in Berkeley richer. Carl Salk, Brian Meffle, David Sherwin, Mary Sherwin, David Swenson, Mike Cotton, Dave Jackson, Molly Stenhouse, Jamie Morrow,

Terry Smith, Beth Alsberg, Rahel Smith, M.C. Duboscq, Erin Sheepo, Kira Abrams, and Rick Kaplan shared good food, good stories, and lots of fun over the years.

Finally, I would like to thank my parents and sisters whose love and support helped me to complete my dissertation.

Chapter One

Generality of Fractal 1/f Scaling in Catchment Tracer Time Series and its Implications for Catchment Travel Time Distributions

Submitted to Hydrological Processes

Abstract

Catchment travel time distributions reflect how precipitation from different storms is stored and mixed as it is transported to the stream. Catchment travel time distributions can be described by the mean travel time and the shape of the distribution around the mean. Whereas mean travel times have been quantified in a range of catchment studies, only rarely has the shape of the distribution been estimated. The shape of the distribution affects both the short-term and long-term catchment response to a pulse input of a soluble contaminant. Travel time distributions are usually estimated from conservative tracer concentrations in precipitation and streamflow, which are analyzed using time-domain convolution or spectral methods. Of these two approaches, spectral methods are better suited to determining the shape of the distribution. Previous spectral analyses of both rainfall and streamflow tracer time series from several catchments in Wales showed that rainfall chemistry spectra resemble white noise, whereas the stream tracer spectra in these same catchments exhibit fractal 1/f scaling over three orders of magnitude. Here we test the generality of the observed fractal scaling of streamflow chemistry, using spectral analysis of long-term tracer time series from 22 catchments in North America and Europe. We demonstrate that 1/f fractal scaling of stream chemistry is a common feature of these catchments. These observations imply that catchments often exhibit an approximate power-law distribution of travel times, and thus retain a long memory of past inputs. The observed fractal scaling places strong constraints on possible models of catchment behavior, because it is inconsistent with the exponential travel time distributions that are predicted by simple mixing models.

Introduction

Catchment storage and mixing of solutes can be characterized by the catchment travel time distribution, which is defined by both the mean travel time and the shape of the distribution around the mean. Catchment responses to contamination or land use change, as well as biogeochemical responses linked to hydrological processes (Rodhe *et al.*, 1996; Wolock *et al.*, 1997; Tetzlaff *et al.*, 2007; Landon *et al.*, 2000; Burns *et al.*, 2005; Turner *et al.*, 2006), depend in part on the travel time distribution. The mean travel time describes the aggregate average flushing rate of the catchment, whereas the shape of the distribution is determined by the heterogeneity of the flowpath lengths and velocities. Quantifying this heterogeneity is crucial to understanding how streams respond to rainfall and how long water-borne contaminants might persist in the catchment (*e.g.*, Kirchner *et al.*, 2000).

Catchment travel times are typically modeled with the exponential distribution, a special case of the gamma family of distributions, expressed in a simplified form as

$$h(\tau) = \frac{1}{\tau_o} e^{-\tau/\tau_o} \tag{1}$$

where τ is the time for an individual parcel of tracer to reach the stream after falling as precipitation, and τ_o is the mean travel time. The exponential travel time distribution assumes that the catchment behaves as a single linear well-mixed reservoir (McGuire *et al.*, 2005). The exponential distribution scales with the mean travel time τ_o, and has a particular shape within the broader family of gamma distributions. That broader family of gamma distributions,

$$h(\tau) = \frac{\tau^{\alpha-1}}{\beta^{\alpha}\,\Gamma(\alpha)} e^{-\tau/\beta} = \frac{\tau^{\alpha-1}}{(\tau_o/\alpha)^{\alpha}\,\Gamma(\alpha)} e^{-\alpha\tau/\tau_o} \quad (2)$$

can take on a wide range of shapes as its shape factor α varies, including distributions that are strongly peaked at short time and have long tails (for small values of its shape factor α), as well as distributions that rise to a peak and then decline, resembling a typical storm hydrograph (for larger values of α), as shown in figure 1. The gamma distribution subsumes the exponential distribution as a special case when its shape factor α equals 1. Besides the shape factor α, the only other parameter in the gamma distribution is the mean travel time τ_o, or alternatively the scale factor $\beta = \tau_o/\alpha$. The incomplete gamma function $\Gamma(\alpha)$ serves as a normalization constant, making the area under the distribution equal to 1. The β-form of the gamma distribution is commonly found in the statistical literature, but the equivalent τ_o-form is also given in equation (2) to make its dependence on mean travel time explicit and to allow direct comparison with the exponential distribution in equation (1). The shape factor in the gamma distribution controls how much weight is found in the tails of the distribution, versus near the center, reflecting the heterogeneity in the catchment flowpath lengths and velocities. The smaller the value of α, the greater the variability in travel times compared to the mean; in fact, the coefficient of variation of the gamma distribution (the ratio of the standard deviation to the mean) equals the square root of $1/\alpha$. Following an analysis showing that some catchments are characterized by gamma travel-time distributions with shape factors near α=0.5 (Kirchner *et al.*, 2000), several physical interpretations of this behavior have been proposed, including advection and dispersion of spatially-distributed inputs (Kirchner *et al.*, 2001), variable subsurface advection (Lindgren *et al.*, 2004), and multiple well-mixed linear or coupled nonlinear reservoirs in series and in parallel (Shaw *et al.*, 2006).

Although other catchment travel time distributions are used, by far the most commonly employed is the exponential travel time distribution. It was used in 66% of the catchment travel time distribution models reviewed by McGuire and McDonnell (2006) whereas gamma distributions (except for the special case of the exponential distribution) were used in only ~2% of those studies. Other theoretical models that yield power-law travel time distributions sometimes exhibit means and other moments that are infinite (e.g., Scher *et al.* 2002, Cvetkovic & Haggerty 2002). These imply that there is an infinite accumulation of tracers in catchments which is not supported by field evidence, and therefore we do not consider these models further in this work. Other distributions, including the sine-wave, exponential-piston flow, dispersion, piston flow, and binomial models, have also been used in catchment travel time distribution studies. Here we consider only the gamma model, including the special case of the exponential model, because the exponential model is used more commonly than all other models combined, and the wide range of possible shapes of the gamma distribution encompasses shapes similar to many other possible catchment travel time distributions.

Kirchner *et al.* (2000, 2001) showed that in a series of Welsh catchments, the gamma travel time distribution with $\alpha \approx 0.5$ better reproduced the power spectral scaling of the catchments' tracer time series than the exponential distribution did. Here, we test whether this behavior is particular to the Welsh catchments, or whether these gamma distributions represent travel time distributions in other catchments as well. The distinction between different distribution shapes is particularly important when we consider how a catchment would flush out

a pulse of a soluble contaminant (Figure 2). The smaller the value of α, the greater the intensity of contamination in the stream in the short term, and the greater the persistence of the contaminant in the stream in the long term (Figure 2). Thus, both the short-term and long-term implications of contamination episodes will be underestimated if exponential distributions are mistakenly assumed to govern catchments that instead obey gamma distributions with $\alpha<1$.

Here we analyze tracer time series from 22 diverse catchments to determine whether the exponential model accurately represents their travel-time behavior. Characteristics of our study catchments are summarized in Table 1. The study sites are generally small headwater catchments, with drainage areas ranging from 0.3 km^2 to 295 km^2 (median 1.6 km^2) and average catchment slopes ranging from ~2 to 16 degrees. Gage elevation ranges from sea level to 580 m. Soil types include gleysols, histosols, and podzols, and the bedrock lithologies of the catchments include metamorphic and granitic rocks, as well as sandstones and shales. Vegetative cover varies across the catchments: most are forested to some extent, and several have been felled or burned at some point in the past 50-100 years. The catchments are typically sampled weekly and the record length varies from 4 to 29 years. This study focuses on catchments in maritime settings, with chloride deposition fluxes that are large compared to observed or estimated rates of biogeochemical cycling in soils and vegetation, so that chloride can be plausibly used as a tracer of hydrologic mixing and storage. Likewise the study catchments are temperate and generally humid (mean annual precipitation is typically ~1450 mm/yr, with one site as low as 350mm/yr, and most between 685 and 3900 mm/yr), limiting the potential effect of evapoconcentration on the stream chloride time series. We discuss the use of chloride, each site's mass balance, and the relevance of conservative tracers for this analysis below.

Methods

We analyzed chloride tracer time series in precipitation and streamflow for each site using spectral methods. We used spectral methods rather than the more commonly used time-domain convolution methods (McGuire and McDonnell 2006) because it can be difficult to distinguish between exponential and non-exponential gamma models in the time domain (Figure 3), but they appear distinct when analyzed with spectral techniques (Figure 4).

For all catchments in this study, we used the longest time series of chloride concentrations in precipitation and streamflow that were available (see Table 1 for the record length at each site). Chloride was used because it is more widely available than other potential conservative tracers such as deuterium or ^{18}O. A conservative tracer is one which reacts or fractionates slowly enough that it reflects the mixing processes of the system of interest (Turner and Barnes, 1998). If this is the case, the chloride tracer moves with the water, and mixing of waters of different ages will lead to damping of chloride fluctuations in the output (streamflow) relative to the input (precipitation) across a range of time scales. Concern about whether chloride is a sufficiently conservative tracer (Bastviken *et al.*, 2006) encouraged us to limit our analysis to sites where chloride input fluxes are high enough that reactions in the soil should be small in comparison. To check whether this was sufficient, we also estimated the chloride mass balance on an annually-averaged basis for each site (Table 2). We calculated the annual average chloride mass fluxes as the product of annual water fluxes in precipitation or streamflow and annual average concentration in precipitation and streamflow, respectively. Average annual mean

concentrations are calculated as numerical rather than volume-weighted mean concentrations. Chloride mass fluxes in precipitation and stream water are within 10% of each other at seven sites, and within 50% of one another at all but two sites (Cadillac and Hadlock streams; see Results and Discussion section for more information about these sites). At those sites where average annual mass fluxes in and out of the catchment differed by as much as 50%, stream chloride mass outflows typically exceeded inflows, suggesting that chloride inputs such as dry deposition may be important. At two sites (Mharcaidh and Svarttjern), chloride inflows exceeded outflows, which may be due to retention of inputs in these locations. Alternately, the mass balance may reflect an error due to underestimation of discharge, overestimation of chloride inputs, or sampling bias affecting the averaged results. Unfortunately, mass balance can be difficult to achieve in many field studies which employ natural or artificial tracers, and the accuracy of mass flux estimates can be influenced by non-stationarity of inputs, non-representative samples (e.g., due to the type or size of precipitation sampler) and short records (where the tail of the distribution is never measured).

For each site, the precipitation or streamflow time series was truncated so that both would cover the same span of time. The inverse of this time span is the so-called fundamental frequency. Spectral power was measured at all integer multiples of this fundamental frequency, up to the Nyquist frequency. Because some of the time series were unevenly sampled and all had occasional missing data, the Nyquist frequency was estimated from the median interval between samples. We calculated the spectral power for the rainfall and stream time series at each of these frequencies using the date-compensated discrete Fourier transform (DCDFT) method proposed by Ferraz-Mello (1981) and further elaborated by Foster (1996), because it avoids a potentially serious artifact that can arise in the better-known Lomb-Scargle Fourier Transform (Foster, 1995). We band-averaged the resulting power spectra with a triangular smoothing window with a width of ~0.1 log units in frequency (as shown in the top plot in Figure 4).

We filtered the resulting spectra to correct for the effects of aliasing, in which spectral power above the Nyquist frequency appears instead as spurious spectral power below the Nyquist frequency. Aliasing can lead to artificially shallow spectral slopes, particularly with power-law spectra such as those analyzed here (Kirchner, 2005). To account for possible aliasing effects, we passed these results through an aliasing filter with an assumed corner frequency of one hour, and a limiting frequency of twice the minimum (fundamental) frequency (Kirchner, 2005). We then calculated the ratio of the spectral power of the stream tracer time series to that of the precipitation tracer, to obtain the so-called transfer function (*e.g.*, lower plot in Figure 4). The transfer function is useful because the convolution theorem says that if the stream concentrations are determined by the convolution of the precipitation concentrations and a travel-time distribution, then the power spectrum of that travel-time distribution equals the transfer function (see Kirchner *et al.* 2001 for details). The power spectrum of the gamma distribution is, from equation (2),

$$\left|H(f)\right|^2 = \left(1 + \left(2\pi f \tau_o / \alpha\right)^2\right)^{-\alpha} \tag{3}$$

(Bain, 1983). From equation (3) one can see that at frequencies that are high compared to α/τ_o, the spectrum of the transfer function should follow a power law with a slope of approximately -

2α. Thus a first estimate of α can be obtained directly from the power-law slope of the transfer function, or equivalently, from the difference between the power-law slopes of the tracer spectra in streamflow and precipitation. To estimate the best-fit gamma travel-time distribution for each of the sites, we fitted equation (3) to each site's empirical transfer function. We adjusted the parameters of the hypothetical travel time distributions to minimize the sum of squared differences between the hypothetical and the empirical transfer function power spectra in logarithmic space.

Results and Discussion

Gamma distribution shape factors could be estimated for 20 of our 22 sites (all except Cadillac and Hadlock Brooks). At all 20 sites, the shape factor α was significantly less than 1, implying that the exponential distribution does not accurately represent the mixing behavior of any of these catchments (Figure 5 and Table 3). The best-fit transfer function slopes ranged from -0.69 to -1.56, implying shape factors ranging from 0.35 to 0.78. None of the transfer functions were as steep as a slope of -2, which would correspond to an exponential travel time distribution. This implies that the exponential travel time distribution, and its assumption of a well-mixed linear reservoir, does not describe catchment behavior. Instead, most catchments appear to exhibit more heterogeneous behavior with a wider range of flowpaths and travel times (shape factors less than 1), leading to more weight in the tails of the travel time distribution. Thus, in most catchments, a pulse input of a soluble contaminant would produce a sharper short-term peak in stream concentrations, and more persistent long-term contamination, than would be predicted from an exponential travel time distribution.

Although all slopes are shallower than -2, implying greater heterogeneity than predicted by an exponential model, the spectral slopes vary from site to site. Sites with a shallower slope, such as Upper Hafren and Dalelva, have more weight in the tails of the modeled travel time distribution. These sites would be expected to have some precipitation which very quickly reaches the stream as well as some very long slow flowpaths.

On the other hand, several sites have spectral slopes that are relatively steep, implying shape factors closer to 1. Four of the five sites with the steepest transfer function spectral power slopes -- and thus with travel time distributions that are closest to exponential -- have lakes in them. We would expect that lakes would act like true mixing tanks. True mixing tanks should exhibit an exponential travel time distribution (a shape factor of 1), and we see that most catchments with lakes have shape factors > 0.6. The Langtjern Inlet and Outlet sites are at the inlet and outlet of the Langtjern Lake, respectively. Thus they should offer a clear comparison of the effects of lake mixing on the travel time distribution shape factor, but several factors may obscure this relationship. First, low chloride concentrations affected by detection limits create a "floor" in the spectrum which may obscure possible steepening of the Langtjern Outlet spectrum relative to the Langtjern Inlet spectrum. Second, the Langtjern Inlet samples only a small portion of the total inlet catchment area, so that it does not just exclude the lake mixing itself. Broadly, the catchments in which there are no lakes have significantly smaller shape factors than those in which there are lakes. This method successfully reflects the impact of lakes on the mixing processes occurring within the catchment boundaries.

Other site characteristics (except for the presence or absence of lakes) do not appear to be correlated with variations in the shapes of the travel-time distributions across our study sites. In other studies, mean travel time has been found to be related to site hillslope gradient, mean hillslope length, and soil permeability classifications (McGlynn *et al.*, 2003; McGuire *et al.*, 2005; Tetzlaff et al, 2009; Hrachowitz *et al.*, 2009). Across our 22 sites, gamma distribution shape factors and mean transit times are not significantly correlated with any of the site characteristics listed in Table 1. One would expect catchment geometry and soil and geological characteristics to influence the heterogeneity of subsurface flowpaths and thus the shape of the travel-time distribution, but such an effect may not be strong enough to be seen in our data. In particular, many of the site characteristics in Table 1 are similar within each region, such that the effective number of substantially different sites is smaller than the total of 22 sites in our analysis.

Our analysis has considered only the family of gamma distributions, in comparison to the special case of the exponential distribution, which is widely assumed to describe catchment behavior (but which, as shown above, is inconsistent with the spectral scaling observed in the chloride tracer time series analyzed here). Other commonly used travel-time models are also inconsistent with the spectral behavior of our 22 sites. The exponential-piston flow model, for example, has the same transfer function as the exponential distribution, and thus does not match the spectral behavior of our sites any better. Dispersion models exhibit even steeper spectral scaling than the exponential distribution (Kirchner *et al.*, 2000), and so are even less compatible with the spectral behavior we have observed. We have also considered whether the estimated shape factor and scaling relationships leading to these inferences are predictably corrupted by the distance from mass balance. No significant relationship is seen between the best-fit shape factor (Table 3) and the ratio of chloride inflows to outflows (Table 2), suggesting that closer mass balance would not systematically alter the estimate of the distribution shape.

Although the spectral analysis method works well, some conditions can lead to problematic calculations of spectral signature. At Loch Ard B10 and B11, Oygaardsbekken and Pine Marten, for example, many of the sampling intervals are at weekly, biweekly or monthly intervals, that is, integer multiples of the median sampling frequency. Sampling at such intervals can lead to a partial violation of the Nyquist theorem, resulting in falsely inflated power at the high-frequency end of the spectrum. Such sampling patterns are common, and should be considered during the interpretation of the results of spectral analysis. In these cases, we split the records into shorter subsets (often with one predominant sampling interval) and re-ran the analyses. Because we observed the same spectral pattern in the shorter records, we have more confidence in the accuracy of the inferred travel time distributions. At the two sites in Maine, Cadillac and Hadlock Brooks, the method is unable to produce reasonable estimates of the travel time distribution. At these sites, output spectral power is always higher than the input spectral power, implying that (1) output variability is unusually large, (2) output variability has been amplified, or (3) at least one additional chloride input remains unsampled. Mass influxes differed from mass outfluxes by more than 50% at these sites (Table 2). Previous atmospheric deposition research at these sites found that Cl in throughfall (an estimate of wet + dry deposition) was 2.2-6.2 times greater than wet-only deposition, and winter deposition of Cl was much greater than that measured during the growing season, because of the marine origin of many winter storms (Nelson, 2007). Accounting for these additional sources and processes leading to the apparent

amplification of the output signal is necessary in order to accurately estimate the travel time distribution.

Conclusion

The shape of the catchment travel time distribution reflects the integrated catchment response to water inputs, and in turn, many soluble contaminants. The shape of the travel time distribution is often assumed to be well-represented by an exponential travel time distribution model, but we found that this was inappropriate at all sites for which the travel time distribution could be estimated because it was inconsistent with observed spectral scaling. The non-exponential gamma model with a shape factor < 1, implying significant weight in the distribution tails, can be applied at all sites. This implies that there is greater heterogeneity in the travel times of individual water parcels through catchments than would be inferred from the exponential travel time distribution. Catchment with large lakes should behave as large well-mixed reservoirs with shape factors near one, and most of our study sites with shape factors greater than 0.6 had prominent lakes or ponds within the stream network. However, where lakes were absent, the shape factor was not correlated with any other site characteristics. Although further work is needed to clarify how site characteristics influence the shape of the travel time distribution, our work demonstrated that the heavy-tailed non-exponential gamma model could be used to characterize the shape of the travel time distribution at all sites.

Acknowledgements

We thank the many field crews and lab technicians who created the data analyzed here. Our analysis was supported by NSF grant EAR-0125550 to JWK, by an NSF Graduate Research Fellowship to SEG, and by the Berkeley Water Center. The analysis of Scottish site data was supported by the Leverhulme Trust (F/00152/U). The collection and analysis of the Maine site data was supported by the US EPA, US National Park Service, US Geological Survey, Maine Department of Environmental Protection, and the University of Maine. Data collection in Nova Scotia was funded by Environment Canada.

References

Bain L. 1983. Gamma distribution. Encyclopedia of Statistical Sciences. (Eds. Kotz S and Johnson NL). New York, Wiley. 3: 292-298.

Bastviken D, Sandén P, Svensson T, Ståhlberg C, Magounakis M, Öberg G. 2006. Chloride Retention and Release in a Boreal Forest Soil: Effects of Soil Water Residence Time and Nitrogen and Chloride Loads. *Environmental Science and Technology* **40**: 2977–2982. DOI: 10.1021/es0523237

Brandt C, Robinson M, Finch JW. 2004. Anatomy of a catchment: the relation of physical attributes of the Plynlimon catchments to variations in hydrology and water status, *Hydrology and Earth System Science* **8**: 345-354.

Burns D, Vitvar T, McDonnell J, Hassett J, Duncan J, Kendall, C. 2005. Effects of suburban development on runoff generation in the Croton River basin, New York, USA. *Journal of Hydrology* **311**: 266–281.

Cvetkovic V, Haggerty R. 2002. Transport with multiple-rate exchange in disordered media. *Physical Review E* **65**: 051308. DOI: 10.1103/PhysRevE.65.051308

De Wit HA, Hindar A, Hole L. 2008. Winter climate affects long-term trends in stream water nitrate in acid-sensitive catchments. *Hydrology and Earth System Science Discussions* **4**: 3055-3085.

Ferraz-Mello S. 1981. Estimation of periods from unequally spaced observations. *Astronomical Journal* **86**: 619-624.

Foster G. 1995. The CLEANEST Fourier spectrum. *Astronomical Journal* **109**: 1889-1902.

Foster G. 1996. Wavelets for period analysis of unevenly sampled time series. *Astronomical Journal* **112**:1709-1729.

Hindar A, Tørseth K, Henriksen A, Orsolini Y. 2004. The significance of the North Atlantic oscillation (NAO) for sea-salt episodes and acidification-related effects in Norwegian rivers. *Environmental Science and Technology* **38**: 26–33.

Hrachowitz M, Soulsby C, Tetzlaff D, Dawson JJC, Dunn SM, Malcolm IA. 2009. Using long-term data sets to understand transit times in contrasting headwater catchments. *Journal of Hydrology* **367**: 237-248.

Kahl JS, Nelson SJ, Fernandez I, Haines T, Norton S, Wiersma GB, Jacobson G, Amirbahman A, Johnson K, Schauffler M, Rustad L, Tonnessen K, Lent R, Bank M, Elvir J, Eckhoff J, Caron H, Ruck P, Parker J, Campbell J, Manski D, Breen R, Sheehan K, Grygo A. 2007. Watershed Nitrogen and Mercury Geochemical Fluxes Integrate Landscape Factors in Long-term Research

Watersheds at Acadia National Park, Maine, USA. *Environmental Monitoring and Assessment* **126**: 9-25. DOI: 10.1007/s10661-006-9328-0.

Kaste Ø**,** Rankinen K, Lepisto A. 2004. Modelling the impacts of climate and deposition changes on nitrogen fluxes in northern catchments of Norway and Finland. *Hydrology and Earth System Science* **8**: 778-792.

Kirchner JW, Feng XH, Neal C. 2000. Fractal stream chemistry and its implications for contaminant transport in catchments. *Nature* **403**: 524-527.

Kirchner JW, Feng XH, Neal C. 2001. Catchment-scale advection and dispersion as a mechanism for fractal scaling in stream tracer concentrations. Journal of Hydrology **254**: 82-101.

Kirchner JW 2005. Aliasing in 1/ f_ noise spectra: Origins, consequences, and remedies. *Physical Review E* **71**, 066110.

Landon MK, Delin GN, Komor SC, Regan CP. 2000. Relation of pathways and transit times of recharge water to nitrate concentrations using stable isotopes. *Groundwater* **38**(3), 381-395.

Lindgren GA, Destouni G, Miller AV. 2004. Solute transport through the integrated groundwater-stream system of a catchment. *Water Resources Research* **40**.

McGlynn B, McDonnell J, Stewart M, Seibert J. 2003. On the relationships between catchment scale and streamwater mean residence time. *Hydrological Processes* **17**: 175-181.

McGuire KJ, McDonnell JJ, Weiler M, Kendall C, McGlynn BL, Welker JM et al (2005). The role of topography on catchment-scale water residence time. *Water Resources Research* **41**.

McGuire KJ, McDonnell. 2006. A review and evaluation of catchment transit time modeling. *Journal of Hydrology* **330**: 543– 563.

Neal C, Kirchner JW. 2000. Sodium and chloride levels in rainfall, mist, streamwater and groundwater at the Plynlimon catchments, mid-Wales: inferences on hydrological and chemical controls. *Hydrology and Earth System Science* **8**: 295-310.

Nelson SJ. 2007. Winter contribution to annual throughfall inputs of mercury and tracer ions at Acadia National Park, Maine. Ph.D. Dissertation. University of Maine, Orono, Maine, USA.

Rodhe A, Nyberg L, Bishop K.1996. Transit times for water in a small till catchment from a step shift in the oxygen 18 content of the water input. *Water Resources Research* **32**: 3497-3511.

Schauffler, M., S.J. Nelson, J.S. Kahl, G.L. Jacobson, T.A. Haines, W.A. Patterson and K.B. Johnson, 2007. Paleoecological Assessment of Watershed History in PRIMENet Watersheds at Acadia National Park, USA. *Environmental Monitoring and Assessment* **126**: 39-53. DOI: 10.1007/s10661-006-9330-6.

Scher H, Margolin G, Metzler R, Klafter J, Berkowitz B. 2002. The dynamical foundation of fractal stream chemistry: The origin of extremely long retention times. *Geophysical Research Letters* **29**: 1061. DOI: 10.1029/2001GL014123.

SFT. 2007. The Norwegian monitoring programme for long-range transported air pollutants. Annual report - Effects 2006 Report TA 2274/2007. The Norwegian Pollution Control Authority (SFT), Oslo, Norway. (In Norwegian.)

Shaw *et al.*, 2008 S.B. Shaw, A.A. Harpold, J.C. Taylor and T.M. Walter, Investigating a high resolution, stream chloride time series from the Biscuit Brook catchment, Catskills, NY, *Journal of Hydrology* **348**: 245–256.

Soulsby C, Malcolm R, Helliwell R, Ferrier RC, Jenkins A. 2000. Isotope hydrology of the Allt a Mharcaidh catchment, Cairngorms, Scotland: implications for hydrological pathways and residence times. *Hydrological Processes* **14**: 747-762.

Tetzlaff D, Malcolm IA, Soulsby C. 2007. Influence of forestry, environmental change and climatic variability on the hydrology, hydrochemistry and residence times of upland catchments. *Journal of Hydrology* **346**, 93– 111.

Tetzlaff D, Seibert J, McGuire KJ, Laudon H, Burns DA, Dunn SM, Soulsby C. 2009. How does landscape structure influence catchment transit time across different geomorphic provinces? *Hydrological Processes* **23**: 945–953. DOI: 10.1002/hyp.7240

Turner J, Albrechtsen HJ, Bonell M, Duguet JP, Harris B, Meckenstock R et al (2006). Future trends in transport and fate of diffuse contaminants in catchments, with special emphasis on stable isotope applications. *Hydrological Processes* **20**: 205-213.

Turner JV and Barnes CJ. 1998. Modeling of Isotopic and Hydrogeochemical Responses in Catchment Hydrology. In Isotope Tracers in Catchment Hydrology (eds. C. Kendall and JJ McDonnell) Elsevier Science BV, Amsterdam, 723-760.

Wolock, D.M., Fan, J., Lawrence, G.B., 1997. Effects of basin size on low-flow stream chemistry and subsurface contact time in the Neversink River watershed, New York. *Hydrological Processes* **11**: 1273–1286.

Yanni, S *et al.* 2000 Fog and Acidification Impacts on Ion Budgets of Basins in Nova Scotia, Canada, *JAWRA* **36**: 619-631

Figure Captions

Figure 1. Comparison of gamma distributions of travel times for different shape factors (α=0.5, 1, 2, and 4) as a function of lag time, expressed as a multiple of mean transit time. The shape factor of 1 is a special case of the gamma distribution and is equivalent to the exponential distribution.

Figure 2. Recovery time series of the concentration of a hypothetical soluble contaminant introduced in a pulse of 10 arbitrary units at time zero. The exponential model (solid black) shows a slow initial recovery relative to the low shape factor gamma model (dashed gray), and a faster recovery compared to the gamma model with shape factors above 1 (solid and dotted gray). After ~3 times the mean transit time, the contaminant shows more long-term persistence for gamma models with shape factors below 1 than would be expected if the exponential model described the catchment behavior. Gamma models with shape factors larger than 1 recover more quickly than the exponential model would predict, with concentrations that are ~10x lower after four mean transit times have elapsed.

Figure 3. Time series of measured (black dots) and modeled (lines) tracer concentrations in Hafren stream, one of the study sites. The modeled concentrations result from the convolution in the time domain of observed rainfall concentrations and the best-fit exponential (solid black, Eq. 1) or gamma (solid gray, Eq. 2) travel time distribution. The parameters in those equations are varied such that the modeled and measured concentrations match as accurately as possible in a least squares sense. It can be difficult to distinguish among different models in the time domain, but these same models can be shown to be significantly different in the spectral domain (see Figure 4).

Figure 4. (a) Power spectra vs. frequency for the input rainfall concentrations and output stream concentrations, showing the effect of alias-corrections at Hafren stream, one of the study sites. The ratio of the stream spectral power to rain spectral power equals the transfer function. (b) Power spectra vs. frequency plot showing the best-fit exponential and gamma travel time distributions in the spectral domain and the transfer function at Hafren. At the data-rich high frequencies, the differences between the spectral implications of two travel-time distributions are clear, with the gamma distribution corresponding more closely to the transfer function (the ratio of output power to input power).

Figure 5. Distribution of best-fit shape factors (lower x-axis) and corresponding high-frequency transfer function slopes (upper x-axis) for 20 catchments in this study. None of the shape factors are as large as 1, the shape factor that would imply an exponential travel time distribution accurately describes the mixing and storage processes. Instead they cluster around a shape factor of 0.5 and range within a relatively narrow band from 0.35 to 0.78. More weight of the travel time distribution is found in the tails of the distribution, implying that flowpaths and timing is more heterogeneous than an exponential model would predict.

Figure 6. Estimates of the shape factor for each site and its associated uncertainty, sorted from lowest to highest estimates. Lakes (indicated with an L) are more likely to be found within the catchment boundaries of the sites with larger shape factors.

Table Captions

Table 1. Site information for the 22 catchments included in this study. References are as follows: a = Tetzlaff *et al.*, 2007; b = Kahl *et al.*, 2007; c = Brandt *et al.*, 2004; d = Soulsby *et al.*, 2000; e= De Wit *et al.*, 2008; f= Kaste *et al.*, 2004; g = SFT, 2007; h=Hindar *et al.*, 2004; i=Yanni *et al.*, 2000; j = Schauffler *et al.*, 2007 ; k=Neal and Kirchner, 2000. P=reported precipitation values and chemistry from an average of 40 gages located throughout the catchment. K=Upper Hafren mean annual flow is estimated. Asterisk indicates that precipitation or streamflow chemistry sampling is ongoing.

Table 2. Summary of the average annual precipitation amount [mm], streamflow [mm], and Cl concentrations [mg/L], and calculated annual average chloride mass fluxes in precipitation and streamflow [Mg/km^2/yr] for each study catchment. The average Cl concentrations are numerical means rather than volume-weighted means. The ratio of the precipitation to stream mass fluxes is also listed, with 100% indicating equal inflows and outflows. Superscripts are as indicated in the caption for Table 1.

Table 3. Summary of best-fit travel time distribution parameters based on fitting Equation (3) to the calculated transfer function power spectra. Typical mean transit times are less than one year, and typical shape factors are ~0.5. Footnotes are as follows: a= quantities could not reasonably be determined. b=similar results obtained for Karpdalen precipitation record. c=similar results obtained for Ualand precipitation record.

Figures.

Figure 1.

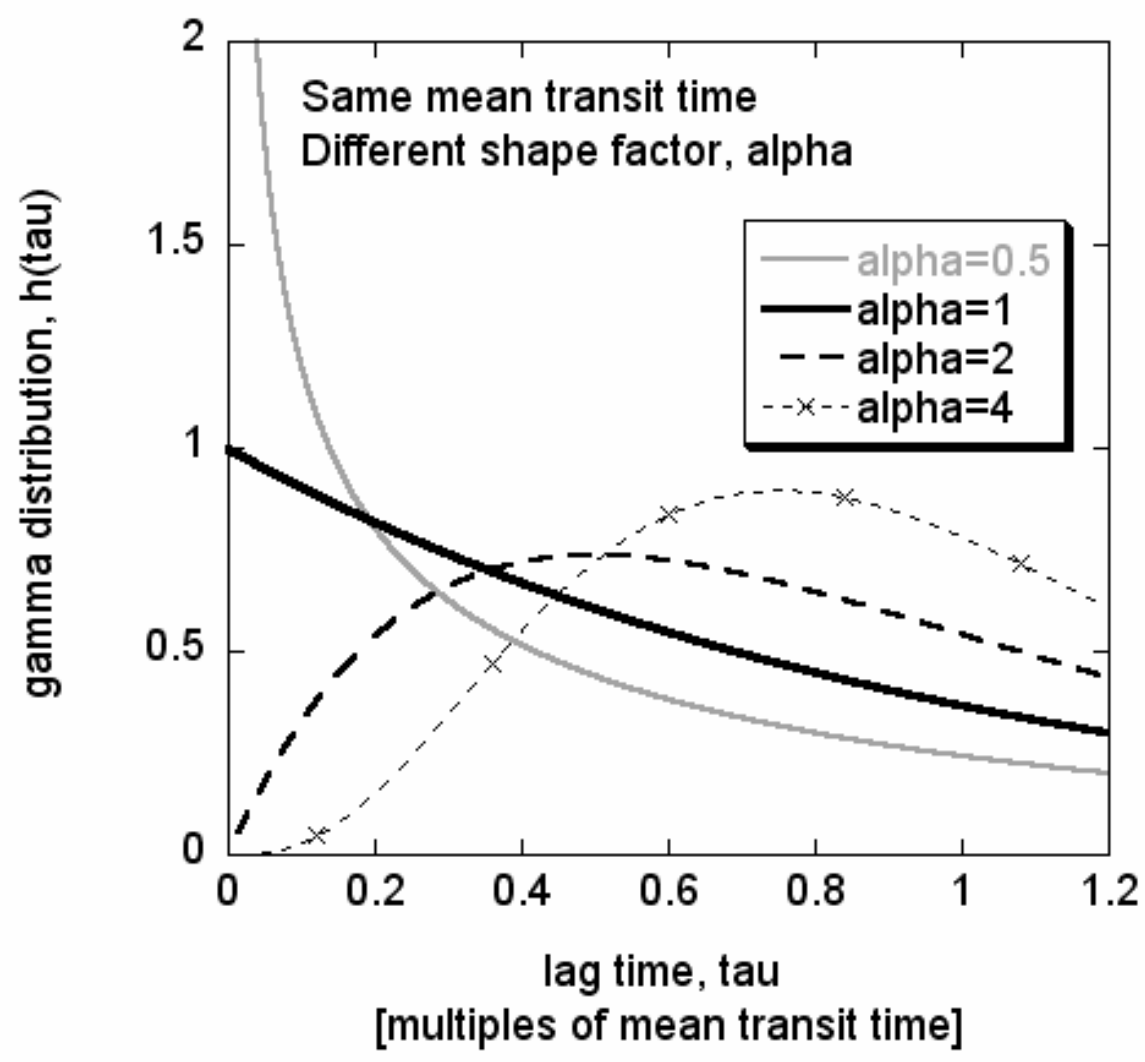

Figure 2.

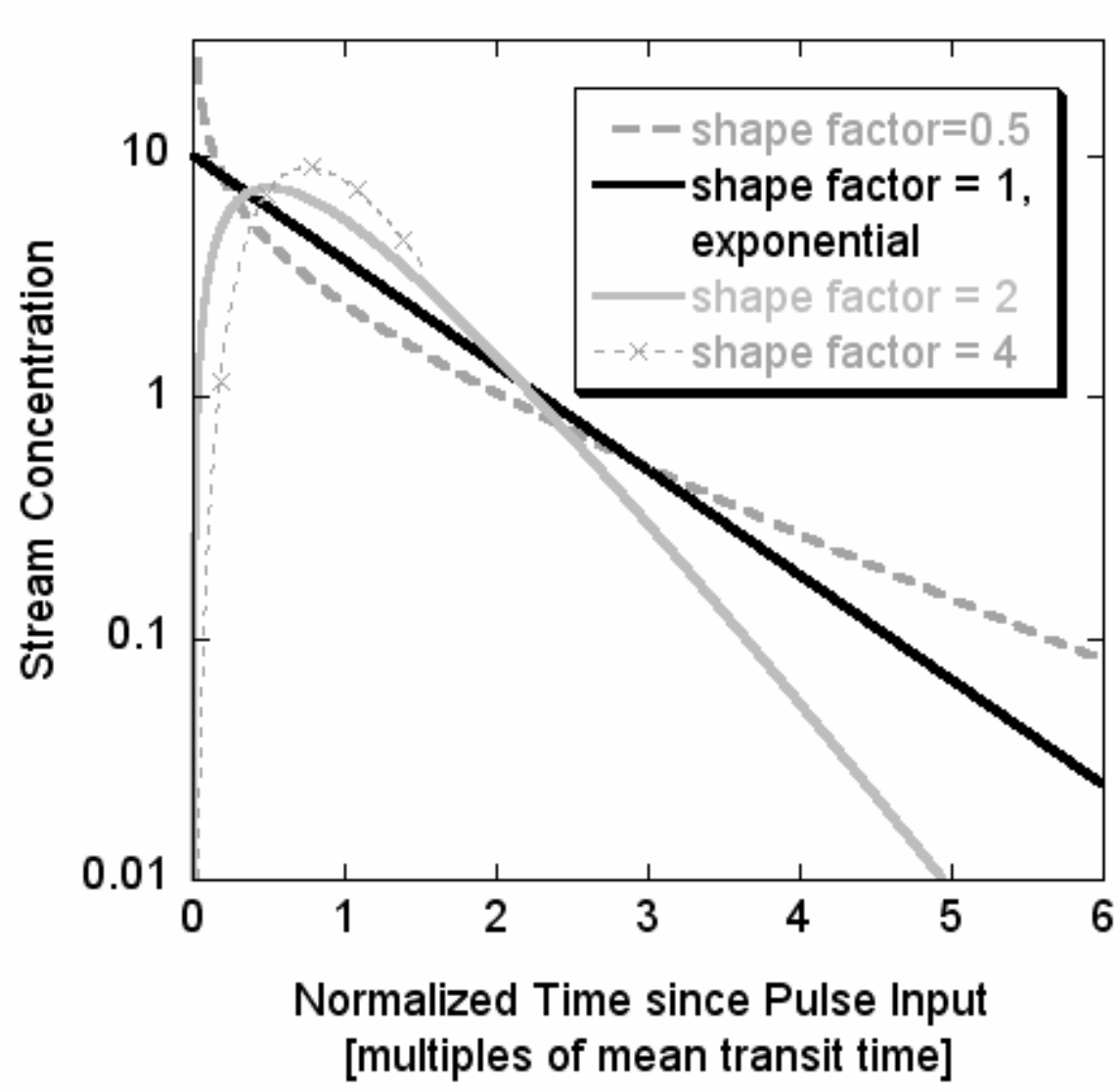
shape factor=0.5
shape factor = 1, exponential
shape factor = 2
shape factor = 4
Stream Concentration
10
1
0.1
0.01
0
1
2
3
4
5
6
Normalized Time since Pulse Input
[multiples of mean transit time]

Figure 3.

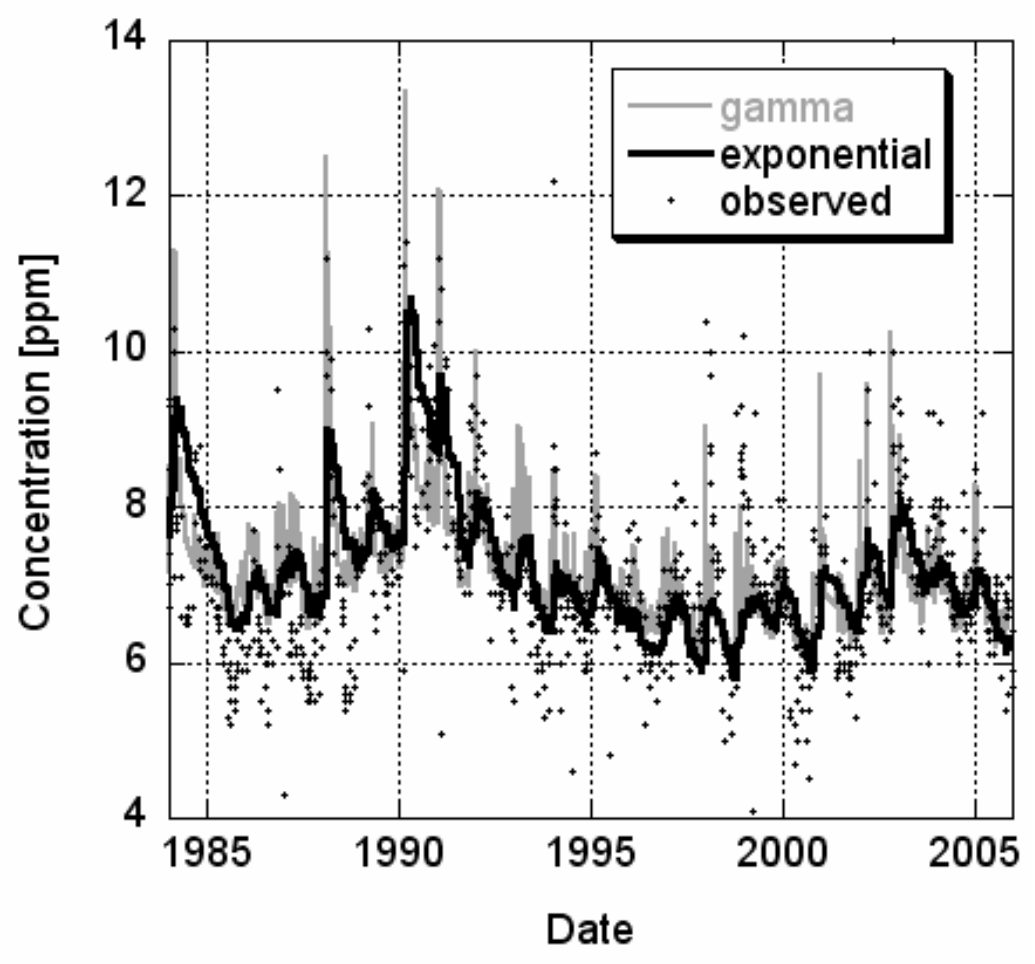
14
12
10
8
6
4
Concentration [ppm]
1985
1990
1995
2000
2005
Date
gamma
exponential
observed

Figure 4.

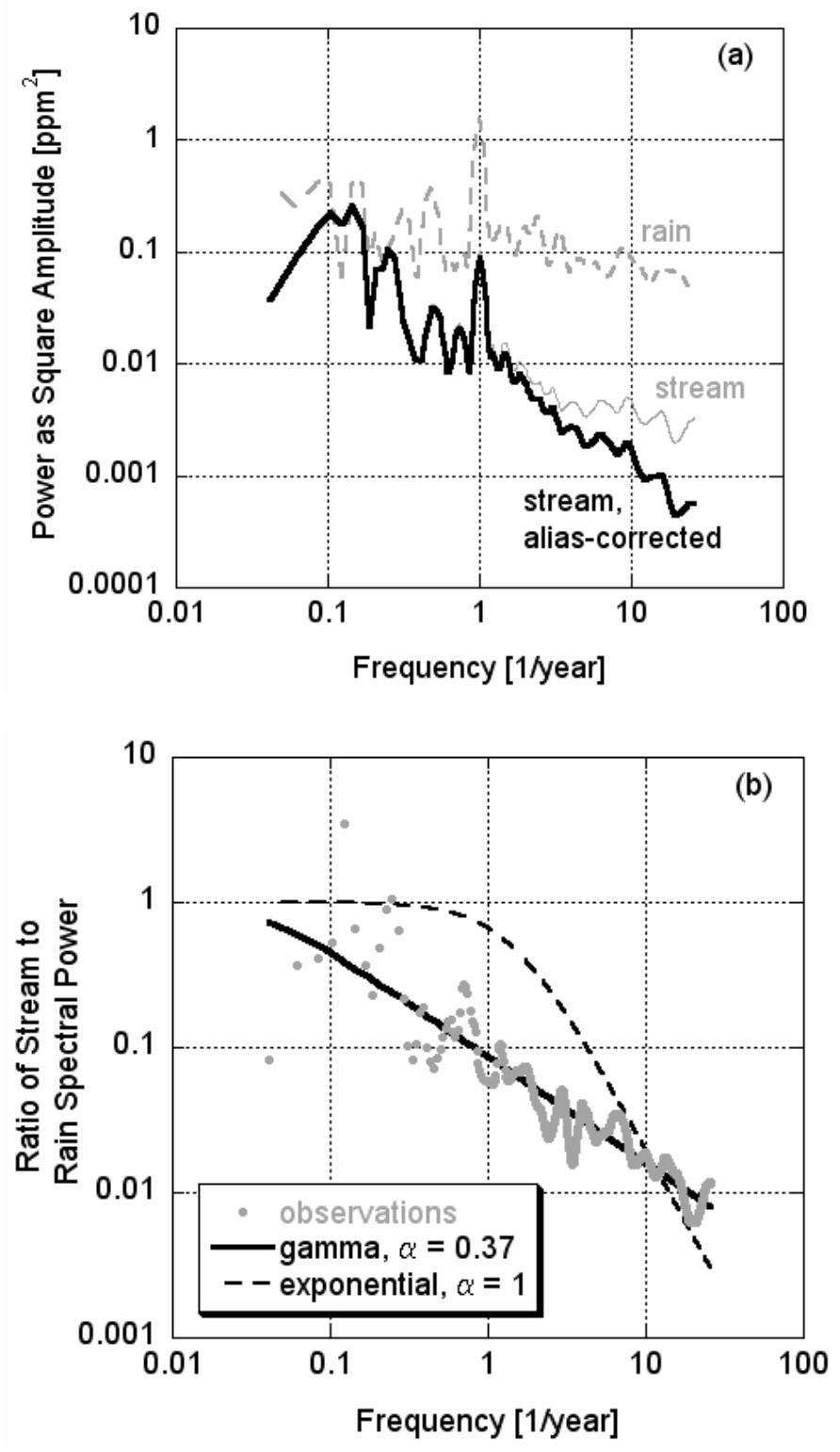
(a)
Power as Square Amplitude [ppm^2]
10
1
0.1
0.01
0.001
0.0001
0.01
0.1
1
10
100
Frequency [1/year]
rain
stream
stream,
alias-corrected
(b)
Ratio of Stream to
Rain Spectral Power
observations
gamma, α = 0.37
exponential, α = 1
Frequency [1/year]

Figure 5.

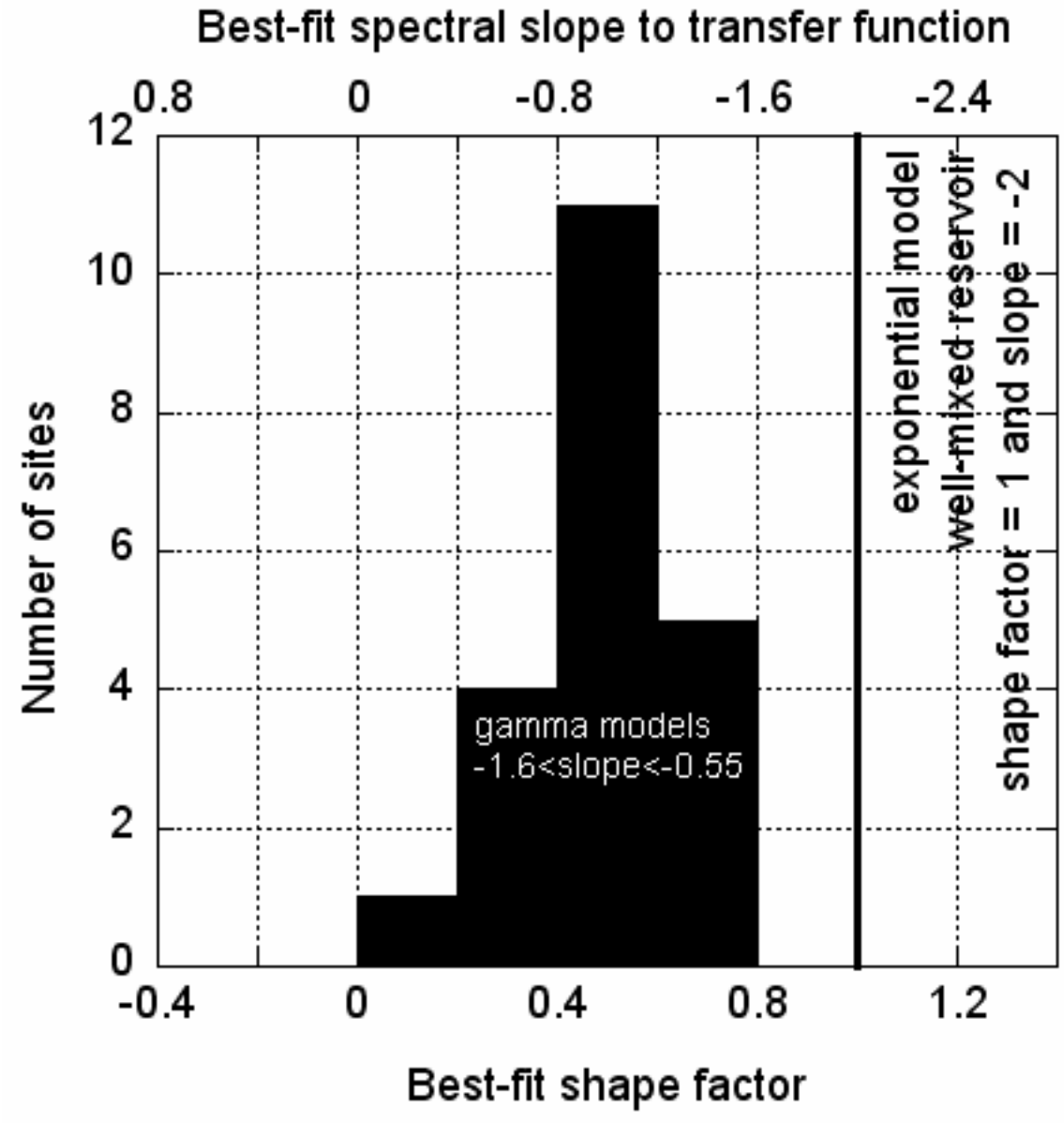
Best-fit spectral slope to transfer function
0.8
0
-0.8
-1.6
-2.4
12
10
8
6
4
2
0
Number of sites
gamma models
-1.6<slope<-0.55
exponential model
well-mixed reservoir
shape factor = 1 and slope = -2
-0.4
0
0.4
0.8
1.2
Best-fit shape factor

Figure 6.

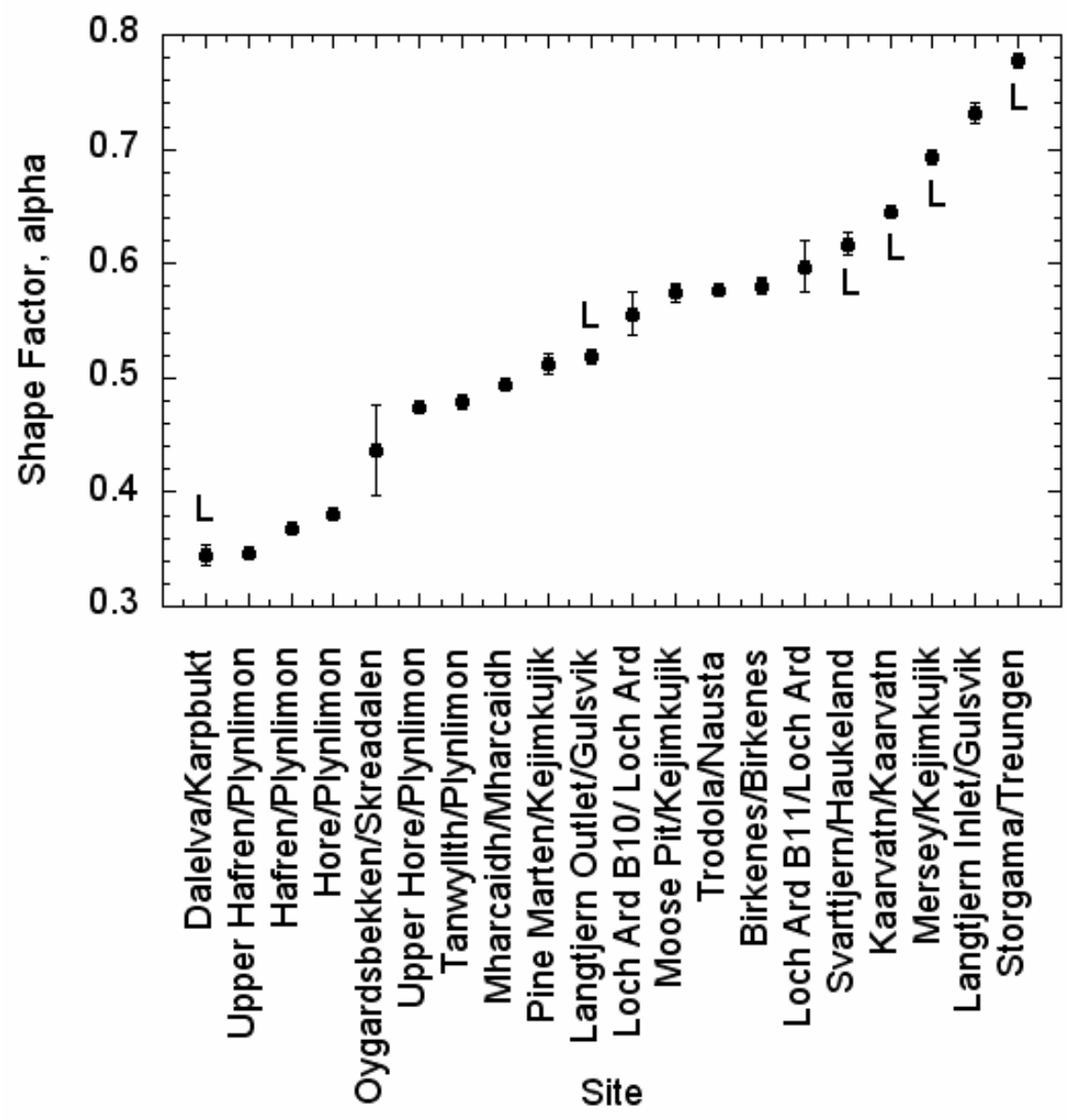
Shape Factor, alpha
0.8
0.7
0.6
0.5
0.4
0.3
Dalelva/Karpbukt
Upper Hafren/Plynlimon
Hafren/Plynlimon
Hore/Plynlimon
Oygardsbekken/Skreadalen
Upper Hore/Plynlimon
Tanwyllth/Plynlimon
Mharcaidh/Mharcaidh
Pine Marten/Kejimkujik
Langtjern Outlet/Gulsvik
Loch Ard B10/ Loch Ard
Moose Pit/Kejimkujik
Trodola/Nausta
Birkenes/Birkenes
Loch Ard B11/Loch Ard
Svarttjern/Haukeland
Kaarvatn/Kaarvatn
Mersey/Kejimkujik
Langtjern Inlet/Gulsvik
Storgama/Treungen
Site

Region	Stream and Precipitation Site Names	Catchment Outlet Locations [dd.ddd]		Precipitation Gage Location [dd.ddd]		Catchment Area	Mean Annual Precipitation	Mean Annual Flow	Catchment Outlet Elevation	Lake above catchment outlet?	Mean catchment slope	Soil Type/ Description
	citations in superscripts	Lat.	Long.	Lat.	Long.	[km^2]	[mm]	[mm]	[m]		[degrees]	
Central Scotland	Loch Ard B10/ Loch Ard^a	56.157	-4.465	56.085	-4.293	0.9	2000	1660	170	no	11	Hydrological responsive soils (Gleysols)
Central Scotland	Loch Ard B11/Loch Ard^a	56.157	-4.464	56.085	-4.293	1.4	2000	1670	170	no	9	Hydrological responsive soils (Gleysols, Peats)
Maine	Cadillac/NADP ME98^c,j	44.345	-68.216	44.377	-68.261	0.316	1332	968	122	no	16.26	Thin Spodosols over till, or Histosols
Maine	Hadlock/NADP ME98^b	44.332	-68.279	44.377	-68.261	0.472	1332	1110	137	no	11.54	Thin Spodosols over till, or Histosols
N Scotland	Mharcaidh/Mharcaidh^d	57.070	-3.510	57.056	-3.494	10	1200	850	330	no	15	Freely draining alpine soils (30%) and Humus Iron Podzols (35%) , hydrological responsive

												soils (Peats, 25%)
Norway	Birkenes/Birkenes^e	58.384	8.239	58.383	8.25	0.41	1400	1136	200	no	n/a	Podzols (90%), peats (7%)
Norway	Dalelva/Karpbukt (also Karpdalen)^f	69.685	30.386	69.667	30.367	3.2	350	497	0	yes	n/a	Leptosols (61%), podzols (20%), peats (4%)
Norway	Kaarvatn/Kaarvatn^e	62.780	8.891	62.783	8.883	25	1450	1843	200	yes	n/a	Bare rock and leptosols (76%), podzols (20%), peats, 2%
Norway	Langtjern Inlet/Gulsvik^e	60.371	9.732	60.367	9.65	1	685	595	510	no	n/a	Leptosols (74%), podzols (5%), peats (16%)
Norway	Langtjern/Gulsvik^e	60.372	9.727	60.367	9.65	4.8	685	595	510	yes	n/a	Leptosols (74%), podzols (5%), peats (16%)
Norway	Oygardsbekken/Skreadalen (also Ualand)^f	58.622	6.107	58.817	6.717	2.55	2140	1546	185	no	n/a	Leptosols (83%), podzols (4%), peats (6%)
Norway	Storgama/Treungen^e	59.052	8.654	59.017	8.517	0.6	960	956	580	yes	n/a	Bare rock and leptosols (59%), peats (22%), podzols (11%)
Norway	Svarttjern/Haukeland^g	60.831	5.568	60.817	5.583	0.57	3900	2848	302	yes	n/a	Podzols (68%), bare rock and leptosols (17%)
Norway	Trodola/Nausta^h	61.578	5.941	61.577	5.898	10	2388	2864	n/a	no	n/a	Leptosols and podzols

Nova Scotia	Mersey/Kejimkujik^i	44.437	-65.223	44.434	-65.206	295	1450	866	109	yes	2.481	shallow sandy loam, till
Nova Scotia	Moose Pit/Kejimkujik^i	44.462	-65.048	44.434	-65.206	17	1352	851	103	no	2.596	shallow sandy loam, till
Nova Scotia	Pine Marten/Kejimkujik^i	44.424	-65.213	44.434	-65.206	1.3	1352	850	114	no	3.326	shallow sandy loam, till
Wales	Hafren/Plynlimon^c,k	52.475	-3.705	52.47P	-3.71P	3.47	2378	2092	300	no	3.41	Peaty podzols and gleys
Wales	Hore/Plynlimon^c,k	52.471	-3.705	52.47P	-3.71P	3.35	2378	1884	300	no	4.04	Peaty podzols and gleys
Wales	Tanwyllth/Plynlimon^c,k	52.474	-3.706	52.47P	-3.71P	0.51	2378	4331	400	no	7.13	Sandy podzols and gleys
Wales	Upper Hafren/Plynlimon^c,k	52.487	-3.727	52.47P	-3.71P	1.17	2378	n/a	500	no	n/a	Sandy podzols and gleys
Wales	Upper Hore/Plynlimon^c,k	52.470	-3.722	52.47P	-3.71P	1.78	2378	1950	500	no	n/a	Sandy podzols and gleys

Stream and Precipitation Site Names	Geological Description	Vegetation	Land Cover Change	Stream Record		Ppt Record		Other notes	Drainage Density
citations in superscripts				Start date	End date for this analysis	Start date	End date for this analysis		[km/km^2]
Loch Ard B10/ Loch Ard^a	Quartz-rich metamorphics, glacial till	Forest plantation	Felling in parts in 1988/89, 2003/04/05	1988	2005	1988	2006	Validated based on field surveys and OS maps, generally at 10m resolution	2.82
Loch Ard B11/Loch Ard^a	Quartz-rich metamorphics, glacial till	Forest plantation	Felling in parts in 1997/98/99, 2003/04/05	1988	2005	1988	2006	Validated based on field surveys and OS maps, generally at 10m resolution; same rain gauge as for Loch Ard B10	2.87
Cadillac/NADP ME98^c,j	Cadillac Granite bedrock of Devonian age	60% Open/shrub/ scrub; 20% hardwood; 20% coniferous	"A large portion of this watershed burned severely in 1947 and probably more than once in the 1800s, and has supported heterogeneous successional forests for 200 years or longer." (Schauffler et al. 2007)	1999	2006	1981	2003*	MAP based on years for which there is stream data	2.0-4.1
Hadlock/NADP ME98^b	Cadillac Granite bedrock of Devonian age	23% Open/shrub/scrub; 7% hardwood; 70% coniferous	"The unburned watershed has been dominated by spruce (Picea rubens) and fir (Abies balsamea) for 500 years or more and has not recently burned or been substantially cleared." (Schauffler et al. 2007)	1999	2006	1981	2003*	MAP based on years for which there is stream data	2.4-5.3
Mharcaidh/Mharcaidh ^d	granite (with extensive drift)	Heather peatland (60%), montane rock (34%), rest conifers	Tree cover currently expanding due to reduced grazing by red deer (Cervus elaphus)	1985	2001	1985	2001	Validated based on field surveys and OS maps, generally at 10m resolution	2.14

Birkenes/Birkenes^e	glaciated, granite, biotite	Norway spruce	Felling of forest at 7% of catchment in 1985, otherwise no changes	1972	2006*	1977	2006*		n/a
Dalelva/Karpbukt (also Karpdalen)^f	glaciated, gneiss and other metamorphic rocks	Birch	Mature forest, no direct anthropogenic influences	1988	2006*	1998 or 1990	2006* or 1998		n/a
Kaarvatn/Kaarvatn^e	glaciated, gneiss and quartsite	Montane rock, heather, pine, birch	Mature forest, no direct anthropogenic influences	1978	2006*	1978	2006*		n/a
Langtjern Inlet/Gulsvik^e	glaciated, gneiss	Pine forest, spruce forest, peat	Mature forest, no direct anthropogenic influences	1973	2000*	1980	1997	Elevation estimated as equal to that at Langtjern	n/a
Langtjern/Gulsvik^e	glaciated, gneiss	Pine forest, spruce forest, peat	Mature forest, no direct anthropogenic influences	1973	2006*	1980	1997		n/a
Oygardsbekken/Skreadalen (also Ualand)^f	glaciated, gneiss, mignatites	Montane rock, heather, pine, birch	Mature forest, no direct anthropogenic influences	1992	2006*	1980 or 1991	2005* or 2000		n/a
Storgama/Treungen^e	glaciated, granite, biotite	Montane rock, heather, pine, birch	Mature forest, no direct anthropogenic influences	1974	2006*	1977	2006*		n/a
Svarttjern/Haukeland^g	glaciated, gneiss	Pine forest	Mature forest, no direct anthropogenic influences	1994	2006*	1981	2006*		n/a
Trodola/Nausta^h	glaciated, gneiss and other metamorphic rocks	Forest	Mature forest, no direct anthropogenic influences	1984	2004	1985	2006		n/a
Mersey/Kejimkujik^i	greywacke, sandstone	Spruce, fir, pine, maple, birch, beech, oak	maturing forest	1980	2007	1983	2004*	wetland veg in <1%, drainage density map resolution=20m	1.08
Moose Pit/Kejimkujik^i	greywacke, sandstone	Spruce, fir, pine, maple, birch	maturing forest	1983	2007	1983	2004*	wetland veg in <1%, drainage density map resolution=20m	0.90

Pine Marten/Kejimkujik^i	greywacke, sandstone	Spruce, fir, pine, maple, birch	maturing forest	1990	2007	1983	2004*	drainage density map resolution=20m	1.11
Hafren/Plynlimon^c,k	Lower Paleozoic shales, mudstones, sandstones	Sitka spruce	Afforested and actively managed forest planted on moorland/pastures in the 1930s	1983	2007*	1983	2007*	Outlet elevation estimated from CEH map for Plynlimon sites	n/a
Hore/Plynlimon^c,k	Lower Paleozoic shales, mudstones, sandstones	Sitka spruce	Afforested and actively managed forest planted on moorland/pastures in the 1930s	1983	2007*	1983	2007*		n/a
Tanwyllth/Plynlimon^c ,k	Lower Paleozoic shales, mudstones, sandstones	Sitka spruce	Afforested and actively managed forest planted on moorland/pastures in the 1930s	1991	2007*	1983	2007*		n/a
Upper Hafren/Plynlimon^c,k	Lower Paleozoic shales, mudstones, sandstones	Sitka spruce	Afforested and actively managed forest planted on moorland/pastures in the 1930s	1990	2007*	1983	2007*		n/a
Upper Hore/Plynlimon^c,k	Lower Paleozoic shales, mudstones, sandstones	Sitka spruce	Afforested and actively managed forest planted on moorland/pastures in the 1930s	1984	2007*	1983	2007*		n/a

Table 1.

Region	Stream and Precipitation Site Names	Mean Annual Precipitation	Mean Annual Flow	Avg Annual Precipitation Concentration	Avg Annual Stream Concentration	Precipitation Mass Flux	Stream Mass Flux	Ratio of precipitation:stream fluxes
	citations in superscripts	[mm]	[mm]	[mg/L]	mg/L	[Mg/km^2/yr]	[Mg/km^2/yr]	[%]
Central Scotland	Loch Ard B10/ Loch Ard^a	2000	1660	3.29	6.20	6.6	10.3	64
Central Scotland	Loch Ard B11/Loch Ard^a	2000	1670	3.29	8.00	6.6	13.4	49
Maine	Cadillac/NADP ME98^c,j	1332	968	1.05	5.44	1.4	5.3	27
Maine	Hadlock/NADP ME98^b	1332	1110	1.05	5.65	1.4	6.3	22
N Scotland	Mharcaidh/Mharcaidh^d	1200	850	3.25	3.55	3.9	3.0	129
Norway	Birkenes/Birkenes^e	1400	1136	2.52	4.61	3.5	5.2	67
Norway	Dalelva/Karpbukt (also Karpdalen)^f	350	497	6.10	4.09	2.1	2.0	105
Norway	Kaarvatn/Kaarvatn^e	1450	1843	2.27	2.05	3.3	3.8	87
Norway	Langtjern Inlet/Gulsvik^e	685	595	0.50	0.69	0.3	0.4	84
Norway	Langtjern/Gulsvik^e	685	595	0.50	0.60	0.3	0.4	96
Norway	Oygardsbekken/Skreadalen (also Ualand)^f	2140	1546	3.06	6.98	6.5	10.8	61
Norway	Storgama/Treungen^e	960	956	0.82	1.13	0.8	1.1	73
Norway	Svarttjern/Haukeland^g	3900	2848	3.53	3.46	13.8	9.9	140
Norway	Trodola/Nausta^h	2388	2864	1.99	2.90	4.8	8.3	57
Nova Scotia	Mersey/Kejimkujik^i	1450	866	3.18	5.62	4.6	4.9	95
Nova Scotia	Moose Pit/Kejimkujik^i	1352	851	3.18	3.61	4.3	3.1	140
Nova Scotia	Pine Marten/Kejimkujik^i	1352	850	3.18	4.36	4.3	3.7	116
Wales	Hafren/Plynlimon^c,k	2378	2092	3.93	7.09	9.3	14.8	63
Wales	Hore/Plynlimon^c,k	2378	1884	3.93	7.59	9.3	14.3	65
Wales	Tanwyllth/Plynlimon^c,k	2378	2208	3.93	7.81	9.3	17.3	54
Wales	Upper Hafren/Plynlimon^c,k	2378	2000K	3.93	5.80	9.3	11.6	80
Wales	Upper Hore/Plynlimon^c,k	2378	1950	3.93	7.38	9.3	14.4	65

Table 2.

Site Name	alpha	alpha s.e.	mean transit time [yr]	mean transit time s.e.
Dalelva/Karpbukt[b]	0.35	0.01	2.91	0.42
Upper Hafren/Plynlimon	0.35	0.01	4.44	0.39
Hafren/Plynlimon	0.37	0.00	1.62	0.09
Hore/Plynlimon	0.38	0.00	0.70	0.03
Oygardsbekken/Skreadalen[c]	0.44	0.04	0.09	0.01
Upper Hore/Plynlimon	0.47	0.00	0.42	0.01
Tanwyllth/Plynlimon	0.48	0.01	0.23	0.01
Mharcaidh/Mharcaidh	0.49	0.00	1.22	0.05
Pine Marten/Kejimkujik	0.51	0.01	0.49	0.03
Langtjern Outlet/Gulsvik	0.52	0.01	0.73	0.03
Loch Ard B10/ Loch Ard	0.56	0.02	0.08	0.00
Moose Pit/Kejimkujik	0.57	0.01	0.61	0.03
Trodola/Nausta	0.58	0.01	0.28	0.01
Birkenes/Birkenes	0.58	0.01	0.16	0.00
Loch Ard B11/Loch Ard	0.60	0.02	0.05	0.00
Svarttjern/Haukeland	0.62	0.01	0.18	0.01
Kaarvatn/Kaarvatn	0.65	0.01	0.23	0.00
Mersey/Kejimkujik	0.69	0.01	0.35	0.01
Langtjern Inlet/Gulsvik	0.73	0.01	0.10	0.00
Storgama/Treungen	0.78	0.01	0.08	0.00
Cadillac/NADP ME98	-[a]	-	-	-
Hadlock/NADP ME98	-[a]	-	-	-

Table 3.

Chapter Two

Accuracy of catchment mean transit times and travel time distribution estimates

Abstract

Travel time distributions reflect how catchments store and mix precipitation from different storms. Travel time distributions can be described by the mean travel time (MTT) and the shape of the distribution around the mean. Here we evaluate the sensitivity of travel time distribution estimation methods to possible analysis and sampling errors by fitting potential distributions to deliberately corrupted synthetic tracer time series, including output time series generated using known travel time distributions. We corrupt the synthetic time series by cutting them into finite lengths (2-6 times the MTT), subsampling them at specified frequencies (10-1000 samples per MTT), and adding noise to them. We then compare the best-fit distribution parameters to the known distribution parameters that we used to generate the time series. We also compare the estimates for different estimation methods (time- and frequency-domain convolution methods), distribution models, and different shapes of the "actual" travel time distribution. Time-domain methods are usually more robust than frequency-domain methods, except with sparsely sampled time series (<20 samples/MTT). Errors in the input and output time series affect the parameter estimates differently depending on the estimation method that is used. Frequency-domain-derived estimates depend strongly on errors in the output time series; dense sampling of noisy time series exacerbates estimation errors in the frequency domain. The shape of the distribution itself also affects parameter estimate accuracy. Different estimation methods are more accurate for different distribution shapes. Thus, independent estimates of the distribution shape would improve MTT estimates. If the exponential model is incorrectly assumed *a priori* to characterize the catchment travel time distribution, the MTT can be underestimated by up to an order of magnitude.

Introduction

Integrated catchment behavior can be characterized by the catchment travel time distribution, including the mean travel time – the average time that rainfall takes to reach the stream – and the shape of the distribution around that mean. Catchment geography, topography, soil type, and subsurface conductivity all influence the travel time distribution (McGuire *et al.* 2005, McGlynn *et al.* 2003, Simic and Destouni 1999, Uchida *et al.* 2006, Cardenas 2008, Tetzlaff *et al.* 2007 & 2009, Hrachowitz *et al.* 2009). The travel time distribution is a useful descriptor of catchment biogeochemistry related to hydrological processes (Rodhe *et al.* 1996, Wolock *et al.* 1997, Tetzlaff *et al.* 2007) as well as catchment response to human impacts, such as contamination events or land-use change (Landon *et al.* 2000, Burns *et al.* 2005, Turner *et al.* 2006). Catchments with short travel times or narrow distributions will have a rapid and large ("flashy") response to contamination events, whereas catchments with long travel times or heavy-tailed distributions will have a more persistent response to those same contamination events. The shape of the distribution refers to the heterogeneity of flowpath lengths and velocities whereas the mean travel time refers to the average flushing rate of the catchment.

The accuracy of travel time distribution estimates may be affected by several sampling and analysis choices. Some potential estimation errors can be avoided or corrected for, whereas others do not yet have solutions. Despite more than 75 studies (McGuire and McDonnell 2006) and an increased recent interest in travel time distributions, no one has yet completed a

systematic study showing how methodological choices concerning sampling and analysis affect the accuracy of travel time distribution estimates. Knowing the accuracy of travel time distribution estimates is important so that we can determine whether different results reflect real differences in catchment behavior. Researchers make at least four key choices as they estimate travel time distributions, and must account for at least two more sources of uncertainty which they cannot easily control, but which affect the accuracy of their estimates. The four choices are: (1) travel time distribution model (*e.g.,* exponential, gamma, piston-flow, dispersion); (2) sampling frequency; (3) record length; and (4) analysis method, *e.g.,* time-domain convolution, sine-wave, water balance, or frequency-domain convolution (power spectra). The two additional sources of uncertainty are: (5) sampling error or noise; and (6) the travel time distribution itself (*e.g.,* a narrower distribution may be easier to accurately model or vice versa). We now discuss the most common choices for (1) – (4) and highlight previous work which examines the effects of all of these potential sources of uncertainty on the estimation of travel time distributions.

Typically researchers choose to use time-domain estimation methods and sparsely sampled records of variable length. The records reviewed by McGuire and McDonnell (2006) are 1–34 years long, with most of them ~3 years in length. If the reported mean travel time estimates are assumed to be accurate, the record length is typically 2 to 5 times the mean travel time. Approximately 26% of the reviewed catchments were sampled on at least a weekly basis, ~47% at least biweekly, and ~91% at least monthly. This implies that ~83% of catchments have ≥10 samples per mean travel time, ~60% of catchments have ≥20 samples per mean travel time, and ~16% have ≥100 samples per mean travel time. Several time-domain methods are regularly used in travel time analyses, including convolution, mixing, sine wave, exponential averaging and water balance models. Frequency-domain convolution (or power spectra) methods are also sometimes used to estimate travel time distributions (see McGuire and McDonnell (2006) for a review of these methods). Approximately 80% of the studies reviewed by McGuire and McDonnell (2006) used sine wave and convolution methods in the time domain. The sine wave method can be used in a narrower range of conditions than the convolution method, and Stewart and McDonnell (1991) showed that convolution methods performed better than sine wave methods. For those reasons, we focus on convolution methods in this paper. In addition to considering convolution in the time domain, we also look at frequency-domain convolution methods. Duffy and Gelhar (1985) suggested that frequency-domain methods could improve travel time distribution estimates, and Kirchner *et al.* (2000) used frequency-domain (or power spectra) methods to reveal useful scaling properties of catchment behavior in a series of Welsh catchments.

Measurement and analysis errors can also affect the accuracy of travel time distribution estimates. Several potential sources of error have been explicitly identified and addressed, including errors introduced by aliasing due to infrequent sampling (Kirchner 2005) or due to irregularly sampled/gapped time series (Ferraz-Mello 1981, Foster 1996). Others have considered the effects of input characterization errors due to spatially variable precipitation (Rodhe *et al.* 1996, Nicotina *et al.* 2008) or changes in the tracer input signal during recharge (*e.g.*, Cl retention or isotopic fractionation: Dunn and Bacon 2008, Page *et al.* 2007, Bastviken *et al.* 2006). In some cases, researchers have attempted to correct for input characterization errors using weighting functions (*e.g.*, Weiler *et al.* 2003) or identifying the scales at which spatial variability in the inputs might overwhelm the signal of mixing in the catchment (Nicotina *et al.*

2008). Whereas input characterization errors due to spatially-variable inputs can be estimated by spatially-distributed sampling, one can estimate the effect of temporal variability and measurement error by comparing replicate samples at a given location. For five catchments at Plynlimon, Wales, the variation in replicate samples never exceeds ~1-2% of the measured variability in the rainfall input time series. These small differences could reflect real temporal variability which exists in the sample or could be an artifact of instrument drift or analysis errors.

Researchers usually choose *a priori* among several travel time distribution models, including the exponential, piston-flow, exponential piston-flow, dispersion and gamma models, which we briefly summarize below (also see Maloszewski and Zuber 1982, Cook and Bohlke 2000, McGuire and McDonnell 2006). Exponential models are among the simplest of several travel time distribution models, and are a special case within the gamma family of distributions. The exponential travel time distribution assumes that the catchment behaves as a well-mixed linear reservoir (*e.g.,* McGuire *et al.* 2005) and is the most commonly used model, used in 66% of catchment studies reviewed by McGuire and McDonnell (2006). The piston-flow and exponential piston-flow models assume that the catchment allows plug flow or behaves as a delayed linear reservoir (Asano *et al.* 2002, McGlynn *et al.* 2003) and these models are used in 14% of the reviewed studies. The dispersion model assumes that the one-dimensional solution to the advection-dispersion equation describes catchment behavior (Maloszewski and Zuber 1982) and is used in 15% of the reviewed studies. Although it was used in only ~2% of the reviewed studies, the gamma distribution has been shown to characterize catchment travel time distributions in some catchments better than any of the other models (Kirchner *et al.* 2000). Following Kirchner *et al.*'s (2000) analysis, the gamma model has elicited at least three physical interpretations, including advection and dispersion of spatially-distributed inputs (Kirchner *et al.* 2001), coupled nonlinear and multiple well-mixed linear reservoir in series and in parallel (Shaw *et al.* 2008), and variable subsurface advection (Lindgren *et al.* 2004). The gamma model can take on a wide variety of shapes, encompassing shapes similar to many other distributions, and is equivalent to the exponential model under certain conditions (discussed below). For those reasons, we focus on the gamma model, including the special case of the exponential distribution, in the rest of this paper.

The shape of the travel time distribution can exacerbate or offset the effects of different sampling and analysis choices. That is, the amount of weight in the tails of the distribution may affect how accurately one can estimate the travel time distribution itself. However, the expected shape of catchment travel time distributions, and particularly the importance of possible long-tail or late-time behavior, is still debated. Some argue that long-tail behavior is common and important in distinguishing among possible distributions (Haggerty *et al.* 2004, Lange *et al.* 1996, Kirchner *et al.* 2000, Godsey *et al.* in review). Others argue that distinctions in late-time behavior are not useful (Botter *et al.* 2008, Deng and Jung 2009) and may not be important in characterizing catchment behavior. In this paper, we consider how a range of distribution shapes, including those with short and long tails, affect the accuracy of the travel time distribution estimates.

When evaluating the accuracy of travel time distribution estimates, we assume that the distribution shape does not change over time, and further assume that the distribution characterizes the range of times over which water molecules exit the catchment. That is, we

estimate time-invariant travel time distributions rather than residence time distributions (see discussion in Kreft and Zuber 1978, Maloszewski and Zuber 1982, Botter *et al.* 2008, and Fiori and Russo 2008, among others). We assume that tracers are measured in flux and only enter and exit the catchment once. Botter *et al.* (2008) distinguish between residence and travel time distributions based on the amount or flux of preexisting water in a control volume (*i.e.*, 'old' water). For cases in which the rate of change of old water flux is small or the storage volume is small relative to the amount of inputs entering the system, the travel time and residence time distributions should be similar, assuming that the travel time distribution remains approximately time-invariant. We explicitly assume that the travel time distribution is time-invariant – unchanging despite changes in soil moisture, dominant flowpaths, or other dynamic controls on catchment hydrologic response – as is done in many travel time distribution studies. Although this assumption is often violated, the problems that it causes can be at least partially addressed by analyzing tracer fluxes instead of concentrations (Niemi 1977), employing time-variant travel time distributions (Turner *et al.* 1987), or most commonly, by using flow-corrected time rather than calendar time (Rodhe *et al.* 1996). Except during long periods without rain (Fiori and Russo 2008), using flow-corrected time can lead to reliable solute transport modeling even without explicitly allowing for a time-variant travel time distribution. In this paper, we assume the simplest scenario wherein flow-corrected time is equal to calendar time. Therefore errors due to the timing and volume of inputs are already accounted for (at least in non-drought conditions), and we can evaluate the sensitivity of parameter estimates to other sampling and analysis errors. We further assume that spatial variability in inputs and any difference between rainfall and recharge concentrations (McGuire and McDonnell 2006) are accurately reflected in the input time series, are incorporated into an introduced stochastic error, or are small enough to be ignored. Thus the results presented in this work should be used with caution in catchments which experience long droughts or exhibit large spatial variations in inputs which are not otherwise accounted for, and in studies in which calendar time is not accurately flow-corrected.

We illustrate the effects of sampling frequency, measurement error and record length with a data set of tracer concentrations from Plynlimon, Wales. Although we cannot know by how much these reported concentrations deviate from the actual concentrations in the stream or rainfall at any given time, we present this data set to demonstrate some of the effects considered throughout the rest of this study. The data plotted in Figure 1a-c show the effects of sampling at weekly, monthly, and bimonthly intervals. Because the precipitation samples are averaged over the sampling interval, one can clearly observe the decreased variability in the precipitation tracer record as sampling frequency decreases. We also demonstrate the effects of short- and medium record lengths (Figure 1d&e), and the addition of a small amount of white noise (equivalent to ~2% of the rainfall standard deviation; see Figure 1f). In each panel, we include the best-fit travel time distribution parameters estimated using frequency-domain methods for this real data set at the given sampling frequency and record length, with or without additional noise.

By working with synthetic catchments in the rest of this paper, we can quantify how accurately one can estimate the travel time distribution in comparison to the known distribution underlying the synthetic data. We can then evaluate the effects of each of the four choices outlined above (model choice, sampling frequency, record length, and analysis method) plus two additional factors (sampling error/noise and actual travel time distribution) on the estimates of

the mean travel time and the shape of the travel time distribution for a range of different synthetic catchments.

Methods

First, we generate synthetic time series with particular specified travel time distributions; then, we corrupt those synthetic time series, and estimate the travel time distribution of the corrupted time series using typical methods. We can then compare the estimated travel time distribution to the specified travel time distribution to see how similar they are. In this section, we elaborate on this process to outline the motivation and critical details of each step.

We generate a synthetic time series to represent the concentration of a potentially conservative tracer such as deuterium, ^{18}O, or chloride in the precipitation. The inputs are specified to be a random normal distribution of values similar to the white noise precipitation tracer time series observed in real-world catchments (*e.g.,* Kirchner *et al.* 2000). Although these inputs are not universally realistic, they represent the simplest possible scenario for testing the accuracy and reproducibility of travel time distribution methods. We also specify the length of the synthetic input time series, and express the length as a multiple of the mean travel time, T_r, to permit scaling of these results to any catchment. We then specify a gamma travel time distribution of the form:

$$h(\tau) = \frac{\tau^{(\alpha-1)}}{(T_r/\alpha)^{\alpha} * \Gamma(\alpha)} * \exp(-\tau\alpha/T_r) . \qquad \text{(Eq. 1)}$$

The gamma distribution is characterized by two parameters: the mean lag time, τ, and the shape factor, α. Changes in the mean travel time will shift the timing of the bulk catchment response. Changes in the shape factor will shift the weight of the distribution to or from the tails. When the shape factor α equals 1, Equation (1) simplifies to an exponential distribution. By convolving the synthetic rainfall time series with the travel time distribution, we generate the output time series, which is the concentration of the conservative tracer in the streamflow. Usually variability in the stream concentrations is damped relative to the variability in rainfall concentrations due to the mixing of waters from different storms within the catchment (Buttle 1994, Kirchner 2003). For the purposes of this paper, we refer to these synthetic time series and their associated travel time distribution parameters as the "actual" values.

In the real world, we do not have access to these "actual," perfect, continuous rainfall and streamflow concentration values, but we instead sample the rain and stream waters at discrete intervals and inevitably introduce a (hopefully) small amount of measurement error into our samples. We test the effect of discrete sampling and measurement error by corrupting the "actual" rainfall and stream time series. To corrupt the time series, we first sample the "actual" rainfall and stream time series at evenly-spaced intervals so that we have 10, 20, 50 or 100 samples per "actual" mean travel time. We also sample every point in the time series to simulate the 'no subsampling' case. Because rainfall gauges typically hold a mixture of water from all storms since the previous sampling, we take the mean of all of the "actual" values in the sampling interval for the input time series. On the other hand, stream concentrations are typically determined from a grab sample taken at a particular time, and we similarly take just one (evenly-

spaced) value for each sampling interval for the output time series. We then introduce random normally-distributed errors scaled to 0, 1 and 2 % of the standard deviation of the sampled "actual" rainfall concentration time series. We consider the same range of errors for the rainfall and stream concentration time series individually and in combination to see whether errors in just one of these measurements could substantially affect the accuracy of the travel time distribution estimate. We repeat this process with records that are 2, 3, 5, and 6 times as long as the mean travel time. For each scenario, we repeat the analysis 1000 times with different "actual" rainfall concentration time series and random errors. For a real-world example of the potential effects of noise, record length and sampling frequency on travel time distribution estimates, see Figure 1.

We then use non-linear least-squares fitting algorithms (*e.g.,* lsqcurvefit in MATLAB) to determine the best-fit parameters of the travel time distribution (Equation 1). In the time domain, we convolve the corrupted input time series with the estimated travel time distribution to generate the estimated output time series. We vary the parameters of the estimated travel time distribution (Equation 1) so that the estimated output time series matches the corrupted output time series as closely as possible. In the frequency domain, we calculate the power spectrum of the corrupted inputs and the corrupted outputs. We then calculate the ratio of these spectra, which termed the transfer function. The convolution theorem implies that the transfer function should equal the power spectrum of the travel time distribution (i.e., the convolution kernel). The power spectrum of the gamma distribution is, from Equation (1),

$$\left|H(f)\right|^2 = \left(1 + \left(2\pi f T_R / \alpha\right)^2\right)^{-\alpha} \qquad \text{(Eq.2)}$$

(Bain 1983). We then vary the parameters of the travel time distribution such that the power spectrum of the estimated transfer function (Equation 2) matches the power spectrum of the corrupted transfer function as closely as possible. We then compare the estimated travel time distribution parameters (obtained by either method) to the "actual" travel time distribution parameters to evaluate the sensitivity of the methods to different forms of corruption. A schematic explanation of the methods we used in this study is shown in Figure 2.

Finally, we examine the accuracy of the mean travel time estimate when the shape factor is incorrectly specified instead of fitted as part of the estimation procedure. The travel time distribution is often assumed *a priori* to be represented by an exponential distribution, which is equivalent to assuming a gamma distribution with a shape factor of 1. We test the effect of the different combinations of measurement error and sampling intervals when an incorrect shape factor of 1 is assumed when the "actual" shape factor is less than 1.

Results and Discussion

Mean travel time estimates are sensitive to the estimation method and sampling frequency as well as how noisy the sample is. Broadly speaking, the time-domain method (Figure 3a-f) is more robust to all of the factors influencing the accuracy of the travel time distribution parameter estimates than is the frequency-domain method (Figure 3g-l). The frequency-domain method can be useful for sparsely sampled time series (*e.g.*, Figure 3c vs. Figure 3i). Estimates using either method are not very sensitive to record lengths (Figure 3b&c,

e&f, h&i, k&l), although very slight improvements occur with increased record length for sparsely sampled time series with "actual" α=0.5 (*e.g.,* 3b&h). For corrupted time series with errors equal to 2% of the rainfall s.d., however, this is not the case, and shorter records produce more accurate parameter estimates using the frequency-domain method (Figure 3i, lower left). Record lengths are normalized to the mean travel time so they can be generalized to any catchment. For sparsely sampled time series estimated with the frequency-domain method, record lengths longer than approximately five times the mean travel time improve the parameter estimate accuracy as long as the introduced error is less than approximately 1.5% of the rainfall standard deviation (Figure 3h). This implies that it would be useful to know the amount of noise and the "actual" mean travel time before sampling begins. Although neither is typically known ahead of time, an estimate of their order of magnitude may be possible based on pilot tests or studies in similar catchments. The hypothesized values used in the planning stages should be verified later to assess the accuracy of the estimates.

Shape factor estimates are generally more accurate than mean travel time estimates made under the same conditions (Figure 3 vs. 4). Using the time-domain method (Figure 4a-f), we show that the shape factor is accurately estimated regardless of the record length, the amount of noise which corrupts the signal, or the sampling frequency. Sampling frequency affects the accuracy of the frequency-domain method estimates for shape factors, especially for noisy samples (Figure 4g,i,j,l). Although the shape factor estimates are generally better than the corresponding mean travel time estimates, they can still be up to 40% over- or underestimated (Figure 4g,i,k,j,l). Frequency-domain estimates of the shape factor at the higher "actual" shape factor of α=1 are very sensitive to error corrupting the signal, leading to underestimates of >20% in some cases (Figure 4j-l). Shape factor estimates are actually less accurate than the mean travel time estimates for sparsely sampled time series evaluated using the frequency-domain method (far left side of Figures 3g&11g and far bottom of Figures 3i&11i). Despite the accurate mean travel time estimates in these cases, the shape factor estimates are off by ~20%. Record length and signal-to-noise ratio do not strongly influence the shape factor estimates in these cases. Because the mean travel time estimates generally appear more sensitive to changes in the factors affecting each analysis, we often report and discuss mean travel time estimates instead of shape factor estimates throughout this paper.

Errors as large as 2% of the rainfall variability have little effect on the time-domain method estimates (Figure 3a,b,d,e). On the other hand, when using frequency-domain methods, errors added to the signal are more problematic (Figure 3g,h,j,k), particularly for densely sampled time series (Figure 3i,j,l) or large (*e.g.,* α=1) shape factors (Figure 3j,k,l). Because additive white noise errors, such as the kind we use to corrupt the time series, strongly affect the stream power spectra at high frequencies, it is possible to modify the frequency-domain method to fit the transfer function (Equation 2) only at frequencies below which the signal-to-noise ratio is at least one. If one could accurately estimate the measurement error, and thus the frequency below which the signal-to-noise ratio would be at least one, then this modified frequency-domain method would work quite well regardless of record length, added noise or sampling frequency. Parameter estimates would be consistently within ~5% of "actual" values in this (unlikely) situation. However, because this situation is so unrealistic, we do not show these results. Nonetheless we are currently pursuing a method in which measurement noise can be explicitly fitted.

Noise in the stream and rain tracer time series affect the accuracy of the travel time distribution estimates to a different degree for the different methods used. Noise in the rainfall tracer time series is slightly more important than in the stream tracer time series for the time-domain method: note that the subparallel lines in Figure 5a&b have slopes closer to zero than +/-1. For the frequency-domain method, errors in rainfall concentration measurements result in no variation in the accuracy of the best-fit travel time distribution parameters for α=1 (Figure 5d). However, errors in the stream concentration measurements have a measurable effect on the fit of the time series (*e.g.,* subparallel vertical lines in Figure 5d). For α=0.5 using the frequency-domain method, errors in both rainfall and streamflow tracer concentrations influence the accuracy of the parameter estimates (Figure 5c).

Based on these results, we recommend using the time-domain method, except in cases of sparsely sampled time series which are either nearly noise-free or very short. Specifically, if fewer than 10-20 samples per MTT are available, and the time series is shorter than four times the MTT or the error is known to be $\leq$~0.5% of the rainfall variability, the frequency-domain method gives a more accurate travel time distribution estimate. The frequency-domain method appears to be very sensitive to noise contaminating the signal, so it is important to either fit to the noise or avoid using the method with noisy time series. We need to evaluate the error in available time series to choose the best technique to estimate the travel time distribution. These recommendations may not apply to cases in which the time invariance assumption fails, especially if there are errors in the correlation of the input and output time series, as discussed in the Future Directions section below.

The "actual" shape factor also influences the accuracy of parameter estimates. For example, when using the time-domain method, mean travel time estimates are less accurate if the "actual" shape factor equals 0.5 (left column, Figure 3a-c) than if it equals 1 (right column, Figure 3d-f). The opposite is true for the frequency-domain method (Figure 3g-i vs. 3j-l). We compare the influence of estimation method, sampling frequency and added noise on the accuracy of parameter estimates across a wider range of "actual" shape factors (Figure 6). Using time-domain methods, one can use a relatively small number of samples (*e.g.,* 10 samples per "actual" mean travel time) to accurately estimate travel time distribution parameters if the "actual" shape factor is $\geq$0.7 (Figure 6b,d). These estimates are as accurate as those based on 10 times as many samples per mean travel time. For an "actual" shape factor of 0.5, ~80-100 samples per mean travel time are needed to accurately estimate the mean travel time, and the required sampling frequency for an accurate estimate increases as the "actual" shape factor decreases (Figure 6b). For catchments in which the shape factor is lower, more of the travel time distribution is in the tail, suggesting that there is a wider range of flowpaths and flow velocities to the stream compared to those sites in which the shape factor is higher. For "actual" shape factors below 0.5, more samples are typically required to accurately reproduce the travel time distribution using either method (Figure 6b,d,f,h). However, for "actual" shape factors greater than 0.5, a denser sampling frequency can be problematic when using the frequency-domain method on a noisy signal (Figure 6f,h, upper right corners). In most cases, the time-domain method leads to parameter estimates that are accurate to within 5-10% (Figure 6a-d), and the time-domain method is usually more reliable than the frequency-domain method (Figure 6a-d vs. 6e-h). However, for sparsely sampled time series (<20 samples per mean travel time) from catchments with an "actual" shape factor between ~0.4 and ~0.6, the frequency-domain method

is more reliable than the time-domain method (Figure 6b vs. 6f). Fewer than 20 samples per mean travel time were collected in 38% of studies reviewed by McGuire and McDonnell (2006). For the catchments in these studies, it would be useful to independently know the "actual" shape factor for a given catchment in order to choose the most accurate travel time distribution estimation method.

Predicting the shape factor of the travel time distribution based on physical characteristics of the catchment could improve the efficiency and accuracy of travel time distribution parameter estimates (Figure 6). Specifically, *a priori* knowledge of the shape factor could influence the choice of analysis method and sampling frequency. When the "actual" shape factor is less than ~0.4, the mean travel time is difficult to estimate regardless of the method used in the analysis (Figure 6a,b,e,f). Because the time-domain method overestimates mean travel time whereas the frequency-domain method underestimates mean travel time when the shape factor is less than ~0.4, one could use both methods to verify the consistency of the mean travel time estimate (Figure 6a,b,e,f). Despite many studies characterizing travel time distributions, we do not yet know of independent methods to estimate the shape factor using catchment characteristics. Qualitatively, we know that shape factors closer to 1 should act more like mixing tanks and those much less than 1 should have a wider distribution of flowpaths and timing, as discussed in the Introduction. However, those qualitative observations have not been translated to quantitative ones; further work to quantify an independent means of estimating the distribution shape factor would be useful.

Finally, when the shape factor is incorrectly specified *a priori* to be higher than the "actual" shape factor, the mean travel time is consistently underestimated for both time-domain and frequency-domain methods (Figure 7). Underestimation of the mean travel time may be a common occurrence. Approximately 66% of the catchments reviewed by McGuire and McDonnell (2006) were modeled with an exponential model, which implicitly assumes a shape factor of 1. We have shown elsewhere (Godsey *et al.* in review) that 20 catchments in North America and Europe have shape factors in the range of 0.35-0.78. When the exponential model is incorrectly assumed to characterize the catchment travel time distribution for this range of shape factors, mean travel times are underestimated by up to an order of magnitude (Figure 7). Estimates improve as the "actual" shape factor approaches 1, the *a priori* assumed value. This large error in the characterization of the travel time distribution can be avoided by fitting both the mean travel time and the shape factor simultaneously.

Conclusions and Future Directions

The methods currently used to estimate the travel time distribution parameters – the mean travel time and the distribution shape factor – are subject to several kinds of errors which can make the parameter estimates unreliable. We showed here that the sampling frequency and analysis method can have a large impact on the accuracy of the parameter estimates. Time-domain methods are generally more resilient to noisy signals except when fewer than ~20 samples are collected per mean travel time. In this case, collecting samples more frequently leads to much better estimates of the shape factor and minimizing errors helps to constrain the mean travel time estimates. Given a way to independently determine the shape factor, experimental designs and error estimates could be improved. We point out that if a non-exponential gamma

distribution with a relatively small shape factor actually describes the catchment response, assuming an exponential travel time distribution can lead to extreme underestimation of the mean travel time. Frequency-domain methods are more sensitive to noisy data than are time-domain methods, but are faster and a more accurate choice for relatively noise-free sparsely sampled time series.

Additional work could make this analysis more applicable to real-world scenarios. For example, we intend to explore the assumption of time-invariant travel time distributions in more detail. This assumption is critical in nearly all studies, and we expect that the parameter estimates may be sensitive to flow-time correction methods. In particular, we plan to test the effect of corrupting the time series with slight decorrelations in the timing of the input and output time series. We will explore the effects of small errors in flow-time corrections, including the effect of shrinking or stretching time too much, or inadvertently misaligning the corrected time series. We are also working on a method that improves the travel time distribution estimates by simultaneously fitting to the noise and signal in the frequency domain. Initial results suggest that correctly accounting for the signal-to-noise ratio strongly improves frequency-domain parameter estimates.

Acknowledgements

The National Science Foundation grant EAR 0125550, the Miller Institute for Basic Research and the Berkeley Water Center funded this research. Thanks to B. Walsh for technical assistance and to E.W. Boyer and C. Neal for helpful discussions

References

Asano Y, Uchida T, Ohte N. 2002. Residence times and flow paths of water in steep unchannelled catchments, Tanakami, Japan. Journal of Hydrology 261: 173-192.

Bain L. 1983. Gamma distribution. Encyclopedia of Statistical Sciences. (Eds. Kotz S and Johnson NL). New York, Wiley. 3: 292-298.

Bastviken D, Sandén P, Svensson T, Ståhlberg C, Magounakis M, Öberg G. 2006. Chloride Retention and Release in a Boreal Forest Soil: Effects of Soil Water Residence Time and Nitrogen and Chloride Loads. Environmental Science and Technology 40: 2977–2982. DOI: 10.1021/es0523237.

Botter G, Peratoner F, Putti M, Zuliani A, Zonta R, Rinaldo A, Marani M. 2008. Observation and modeling of catchment-scale solute transport in the hydrologic response: A tracer study. Water Resources Research 44: DOI:10.1029/2007WR006611

Burns D, Vitvar T, McDonnell J, Hassett J, Duncan J, Kendall C. 2005. Effects of suburban development on runoff generation in the Croton River basin, New York, USA. Journal of Hydrology 311: 266-281.

Buttle JM. 1994. Isotope hydrograph separations and rapid delivery of pre-event water from drainage basins. Progress in Physical Geography 18: 16-41.

Cardenas MB. 2008. Surface water-groundwater interface geomorphology leads to scaling of residence times. Geophysical Research Letters 35: DOI:10.1029/2008GL033753

Cook PG, Bohlke JK. 2000. Determining timescales for groundwater flow and solute transport. In Environmental Tracers in Subsurface Hydrology (Eds. Cook and Herczeg), Kluwer, Boston: pp. 1-30.

Deng Z, Jung H. 2009. Variable residence time–based model for solute transport in streams. Water Resources Research 45: W03415, DOI:10.1029/2008WR007000.

Duffy CJ, Gelhar LW. 1985. Frequency domain approach to water quality modeling in groundwater: theory. Water Resources Research 21: 1175–1184.

Dunn SM, Bacon JR. 2008. Assessing the value of Cl^- and $\delta^{18}O$ data in modeling the hydrological behaviour of a small upland catchment in northeast Scotland. Hydrology Research. 39: 337-358, DOI: 10.2166/nh.2008.134.

Ferraz-Mello S. 1981. Estimation of periods from unequally spaced observations. Astronomical Journal 86: 619-624.

Fiori A, Russo D. 2008. Travel time distribution in a hillslope: Insight from numerical simulations. Water Resources Research 44: W12426, DOI:10.1029/2008WR007135.

Foster G. 1996. Wavelets for period analysis of unevenly sampled time series. Astronomical Journal 112:1709-1729.

Haggerty R, Harvey CF, von Schwerin CF, Meigs LC. 2004. What controls the apparent timescale of solute mass transfer in aquifers and soils? A comparison of experimental results. Water Resources Research 40: W01510, DOI:10.1029/2002WR001716.

Hrachowitz M, Soulsby C, Tetzlaff D, Dawson JJC, Dunn SM, Malcolm IA. 2009. Using long-term data sets to understand transit times in contrasting headwater catchments. Journal of Hydrology 367: 237-248.

Kabeya N, Katsuyama M, Kawasaki M, Ohte N, Sugimoto A. in press. Estimation of mean residence times of subsurface waters using seasonal variation in deuterium excess in a small headwater catchment in Japan. Hydrological Processes. DOI: 10.1002/hyp.6231.

Kirchner JW. 2003. A double paradox in catchment hydrology and geochemistry. Hydrological Processes 17: 871-874.

Kirchner JW 2005. Aliasing in 1/ f_ noise spectra: Origins, consequences, and remedies. Physical Review E 71, 066110.

Kirchner JW, Feng XH, Neal C. 2000. Fractal stream chemistry and its implications for contaminant transport in catchments. Nature 403: 524-527.

Kirchner JK, Feng X, Neal C. 2001. Catchment-scale advection and dispersion as a mechanism for fractal scaling in stream tracer concentrations. Journal of Hydrology 254:82-101.

Kreft A, Zuber A. 1978. On the physical meaning if the dispersion equation and its solutions for different initial and boundary conditions. Chemical Engineering Science 33: 1471–1480.

Landon MK, Delin GN, Komor SC, Regan CP. 2000. Relation of pathways and transit times of recharge water to nitrate concentrations using stable isotopes. Ground Water 38: 381-395.

Lange H, Lischeid G, Hoch R, Hauhs M. 1996. Water flow paths and residence times in a small headwater catchment at Gardsjon, Sweden, during steady state storm flow conditions. Water Resources Research 32: 1689-1698

Lindgren GA, Destouni G, Miller AV. 2004. Solute transport through the integrated groundwater-stream system of a catchment. Water Resources Research 40: DOI:10.1029/2003WR002765.

Maloszewski P, Zuber A. 1982. Determining the Turnover Time of Groundwater Systems with the Aid of Environmental Tracers .1. Models and Their Applicability. Journal of Hydrology 57: 207-231.

McGuire KJ, McDonnell JJ, Weiler M, Kendall C, McGlynn BL, Welker JM, Seibert J. 2005. The role of topography on catchment-scale water residence time. Water Resources Research 41, W05002, DOI:10.1029/2004WR003657.

McGuire KJ and McDonnell JJ. 2006. A review and evaluation of catchment transit time modeling. Journal of Hydrology 330:543-563.

McGlynn B, McDonnell J, Stewart M, Seibert J. 2003. On the relationships between catchment scale and streamwater mean residence time. Hydrological Processes 17: 175-181.

Nicotina L, Celegon EA, Rinaldo A, Marani M. 2008. On the impact of rainfall patterns on the hydrologic response. Water Resources Research 44: W12401, DOI:10.1029/2007WR006654.

Niemi AJ. 1977. Residence time distribution of variable flow processes. International Journal of Applied Radiation and Isotopes 28: 855–860.

Page T, Beven KJ, Freer J, Neal C. 2007. Modelling the chloride signal at Plynlimon, Wales, using a modified dynamic TOPMODEL incorporating conservative chemical mixing (with uncertainty). Hydrological Processes 21: 292–307.

Rodhe A, Nyberg L, Bishop K. 1996. Transit times for water in a small till catchment from a step shift in the oxygen 18 content of the water input. Water Resources Research 32: 3497-3511.

Shaw SB, Harpold AA, Taylor JC, Walter MT. 2008. Investigating a high resolution, stream chloride time series from the Biscuit Brook catchment, Catskills, NY. Journal of Hydrology 348: 245– 256, DOI:10.1016/j.jhydrol.2007.10.009.

Simic E, Destouni G. 1999. Water and solute residence times in a catchment: stochastic–mechanistic model interpretation of ^{18}O transport. Water Resources Research 35: 2109–2119.

Stewart MK, McDonnell JJ. 1991. Modeling base flow soil water residence times from deuterium concentrations. Water Resources Research 27: 2681–2693.

Tetzlaff D, Malcolm IA, Soulsby C. 2007. Influence of forestry, environmental change and climatic variability on the hydrology, hydrochemistry and residence times of upland catchments. Journal of Hydrology 346: 93– 111.

Tetzlaff D, Seibert J, McGuire KJ, Laudon H, Burns DA, Dunn SM, Soulsby C. 2009. How does landscape structure influence catchment transit time across different geomorphic provinces? Hydrological Processes 23: 945–953. DOI: 10.1002/hyp.7240.

Turner J, Albrechtsen HJ, Bonell M, Duguet JP, Harris B, Meckenstock R, McGuire K, Moussa R, Peters N, Richnow HH, Sherwood-Lollar B, Uhlenbrook S, van Lanen H. 2006. Future

trends in transport and fate of diffuse contaminants in catchments, with special emphasis on stable isotope applications. Hydrological Processes 20: 205-213.

Turner JV, Macpherson DK, Stokes RA. 1987. The mechanisms of catchment flow processes using natural variations in deuterium and oxygen-18. Journal of Hydrology 94: 143–162.

Uchida T, McDonnell JJ, Asano Y. 2006. Functional intercomparison of hillslopes and small catchments by examining water source, flowpath and mean residence time. Journal of Hydrology 327: 627– 642, DOI:10.1016/j.jhydrol.2006.02.037

Weiler M, McGlynn BL, McGuire KJ, McDonnell JJ. 2003. How does rainfall become runoff? A combined tracer and runoff transfer function approach. Water Resources Research 39: 1315. DOI:10.1029/2003WR00233.

Wolock DM, Fan J, Lawrence GB. 1997. Effects of basin size on low-flow stream chemistry and subsurface contact time in the Neversink River Watershed, New York. Hydrological Processes 11: 1273-1286.

Figure Captions

Figure 1. Example time series of input (rainfall, in gray) and output (stream, in black) tracer data from Hafren stream in Plynlimon, Wales. The subpanels illustrate the effects of changing sampling frequency and record length as well as adding noise to a signal, and best-fit mean travel time estimates are calculated for the time series shown in each panel. (a) The weekly time series over a record length of 24 years. (b) Subsampled monthly time series. Precipitation tracer concentrations are averaged over the sampling period whereas stream output time series are not averaged in order to simulate "grab" samples. (c) Same as (b) except subsampled on a bimonthly basis. (d) Short record length of five years (approximately 1.5*MTT calculated in (a).) (e) Medium record length of 10 years (approximately 3*MTT calculated in (a).) (f) Original weekly time series of 24 years with added white noise equal to 2% of the standard deviation of the rainfall tracer time series. Note that parameter estimates are affected by record length and sampling frequency whereas adding noise has an undetectable effect. However the "actual" values are not available to make a robust comparison (see Methods text for more details).

Figure 2. A conceptual model of the approach utilized in this study. Random normally-distributed time series centered on a constant zero mean are convolved with a selected travel time distribution to generate output time series. Both of these "actual" time series are corrupted by sampling at discrete intervals or by adding in random noise or by both sampling and adding noise. New best-fit travel time distribution parameters are then estimated using non-linear least squares fitting procedures with the "corrupted" time series. The best-fit travel time distribution parameters are then compared to the "actual" travel time distribution parameters.

Figure 3. Ratio of the estimated to "actual" mean travel time as a function of sampling frequency, error added to the signal, and record length for "actual" shape factors of 0.5 (left column: a-c, g-i) and 1 (right column: d-f,j-l). Results for the time-domain (top three rows, a-f) and frequency-domain (bottom three rows, g-l) methods are shown. Color in the plots indicates the mean ratio of estimated to "actual" MTT for 1000 independent analyses with yellow representing estimates near the "actual" parameter. Cooler colors represent underestimates of the "actual" parameter values and warmer colors represent overestimates. A ratio of 1 indicates perfect reproduction of the "actual" parameter value. Note that most time-domain estimates of the mean travel time are quite accurate except when there are fewer than ~20 samples per mean travel time. Frequency-domain estimates are generally worse, and, perhaps surprisingly, the presence of noise in the signal is exacerbated by higher sampling frequencies, especially for large values of the shape factor, α.

Figure 4. Same as Figure 3 for estimates of the shape factor, α, instead of estimates of mean travel time. Estimates of the shape factor are generally more accurate than estimates of mean travel time.

Figure 5. Ratio of the estimated to "actual" mean travel time as a function of error added to the input and output time series for "actual" shape factors of 0.5 (left column, a&c) and 1 (right column, b&d) as calculated using time-domain (top row, a&b) and frequency-domain (bottom row, c&d) methods. The accuracy of the reproduced mean travel time is generally more sensitive to errors in the rainfall time series than to errors in the streamflow time series for the

time-domain method (a&b) whereas estimates using the frequency-domain method are more sensitive to errors in both time series or primarily in the streamflow time series (c&d). Uncertainty in the mean travel time estimates grows as more error is introduced into the time series, and the effect is most pronounced when using the frequency-domain method with α=1. Estimates using the time-domain method are relatively robust to errors in either time series.

Figure 6. Ratio of the estimated to "actual" travel time distribution parameters for a range of "actual" shape factors as a function of added error (left column, a,c,e,g) and sampling frequency (right column, b,d,f,h) as calculated using time-domain (top two rows, a-d) and frequency-domain (bottom two row, e-h) methods. Ratio of the estimated mean travel time (MTT_{hat}, 1st and 3rd rows) and estimated shape factor ($alpha_{hat}$, 2nd and 4th rows) to "actual" parameters are both shown. The "actual" shape factor that describes the catchment travel time distribution influences the accuracy of the estimates of the travel time distribution parameters (a,b,e-h). Mean travel time estimates using frequency-domain methods are often overestimated for larger "actual" shape factors (e&f). Mean travel time estimates are far less accurate for smaller "actual" shape factors using either method (a&b,e&f). Furthermore, smaller shape factors are more difficult to accurately estimate using either the time-domain (c&d) or frequency-domain (g&h) methods. At low "actual" shape factors, the time-domain method is biased toward overestimates of the mean travel time whereas the frequency-domain method tends to underestimate the mean travel time. For this reason, with smaller shape factors, it is worthwhile to verify the parameter estimates using both methods.

Figure 7. The ratio of the estimated to "actual" mean travel time when the shape factor is specified incorrectly for time-domain (a&b, top row) and frequency-domain methods(c&d, bottom row). The "actual" shape factor is specified on the x-axis. For fitting purposes, however, the shape factor is assumed *a priori* to be equal to 1; that is, we assume an exponential distribution best describes the catchment travel time distribution. For "actual" shape factors less than 0.5, the estimated mean travel time is underestimated by as much as an order of magnitude. Estimates are slightly better using the time-domain method (a&b) and are insensitive to error and sampling frequency when alpha is incorrectly specified. Frequent sampling with an incorrectly assumed shape factor leads to even less accurate mean travel time estimates using the frequency-domain method (c&d).

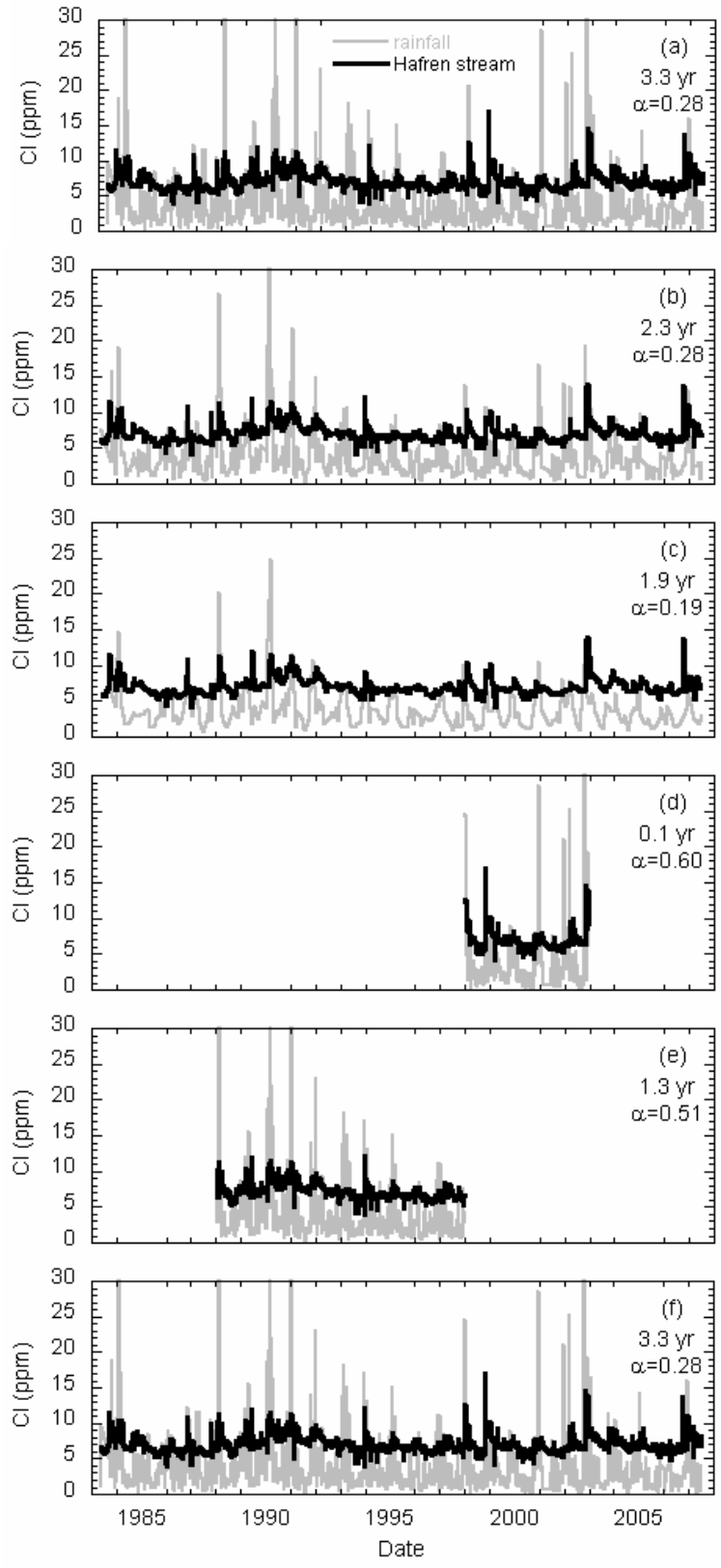
rainfall
Hafren stream
(a)
3.3 yr
α=0.28
(b)
2.3 yr
α=0.28
(c)
1.9 yr
α=0.19
(d)
0.1 yr
α=0.60
(e)
1.3 yr
α=0.51
(f)
3.3 yr
α=0.28
Cl (ppm)
Date
1985
1990
1995
2000
2005

Figure 1 a-f.

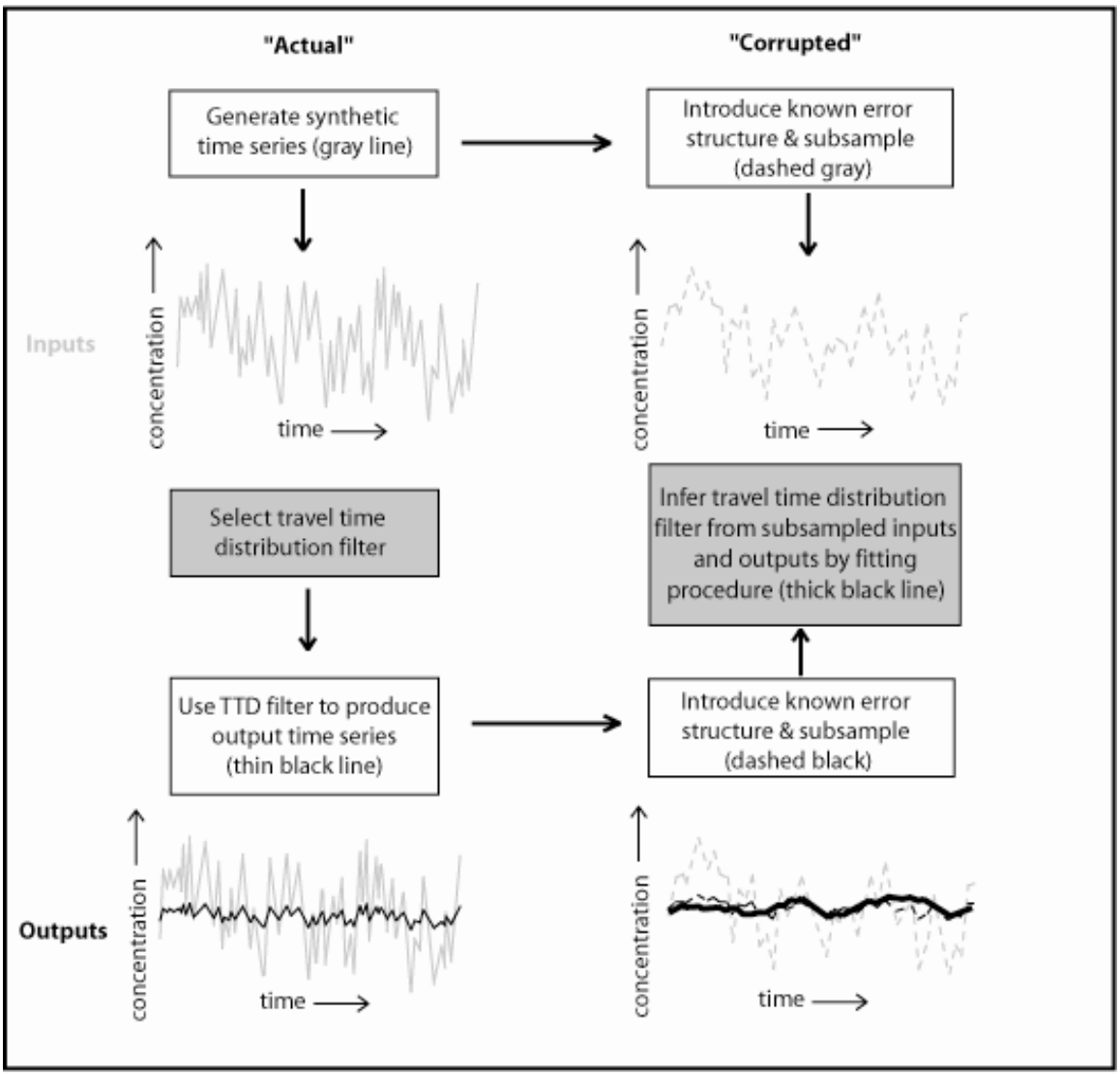
"Actual"
"Corrupted"
Generate synthetic time series (gray line)
Introduce known error structure & subsample (dashed gray)
Inputs
concentration
time
concentration
time
Select travel time distribution filter
Infer travel time distribution filter from subsampled inputs and outputs by fitting procedure (thick black line)
Use TTD filter to produce output time series (thin black line)
Introduce known error structure & subsample (dashed black)
Outputs
concentration
time
concentration
time

Figure 2.

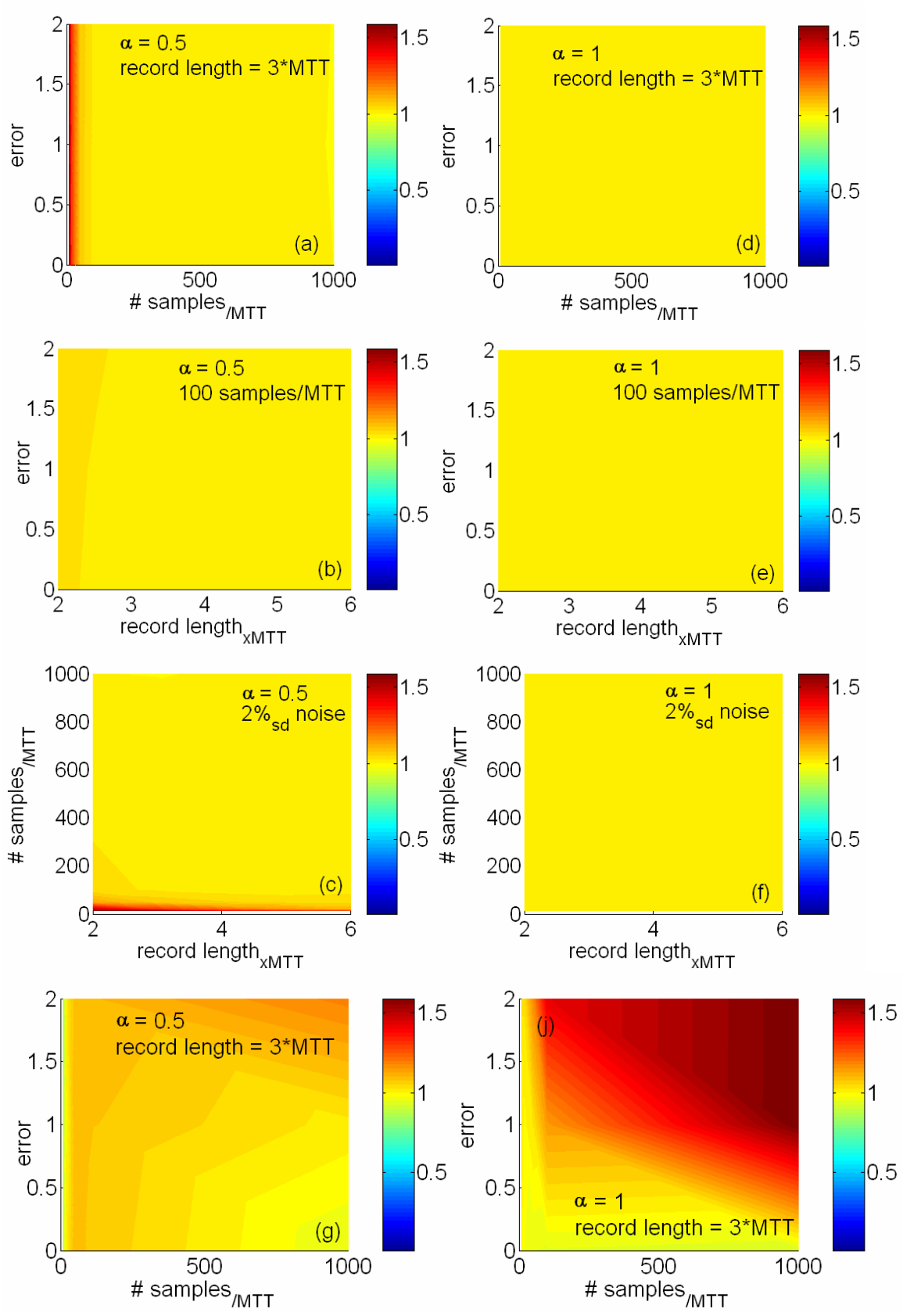
α = 0.5
record length = 3*MTT
(a)
α = 1
record length = 3*MTT
(d)
α = 0.5
100 samples/MTT
(b)
α = 1
100 samples/MTT
(e)
α = 0.5
2%sd noise
(c)
α = 1
2%sd noise
(f)
α = 0.5
record length = 3*MTT
(g)
(j)
α = 1
record length = 3*MTT
error
samples/MTT
record lengthxMTT

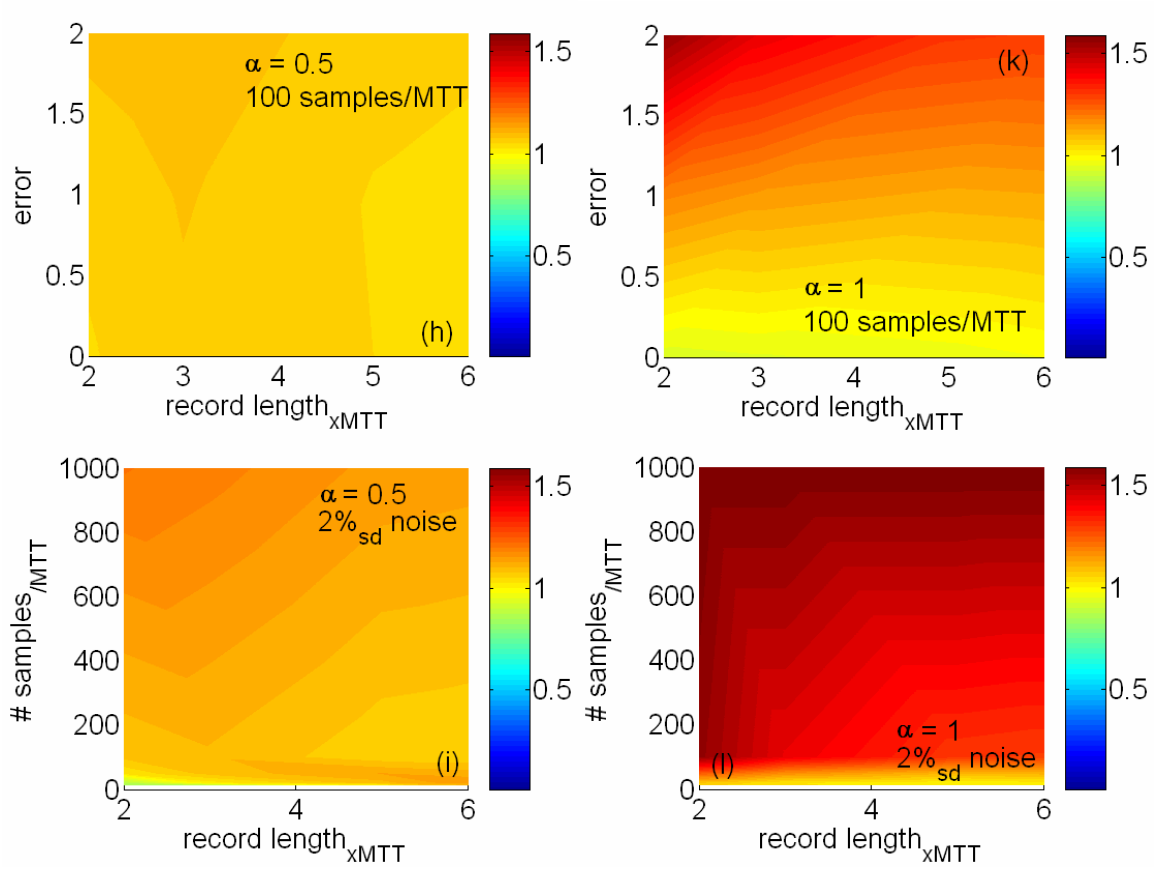
α = 0.5
100 samples/MTT
(h)
error
record length xMTT
(k)
α = 1
100 samples/MTT
α = 0.5
2% sd noise
(i)
samples /MTT
(l)
α = 1
2% sd noise

Figure 3 a-l.

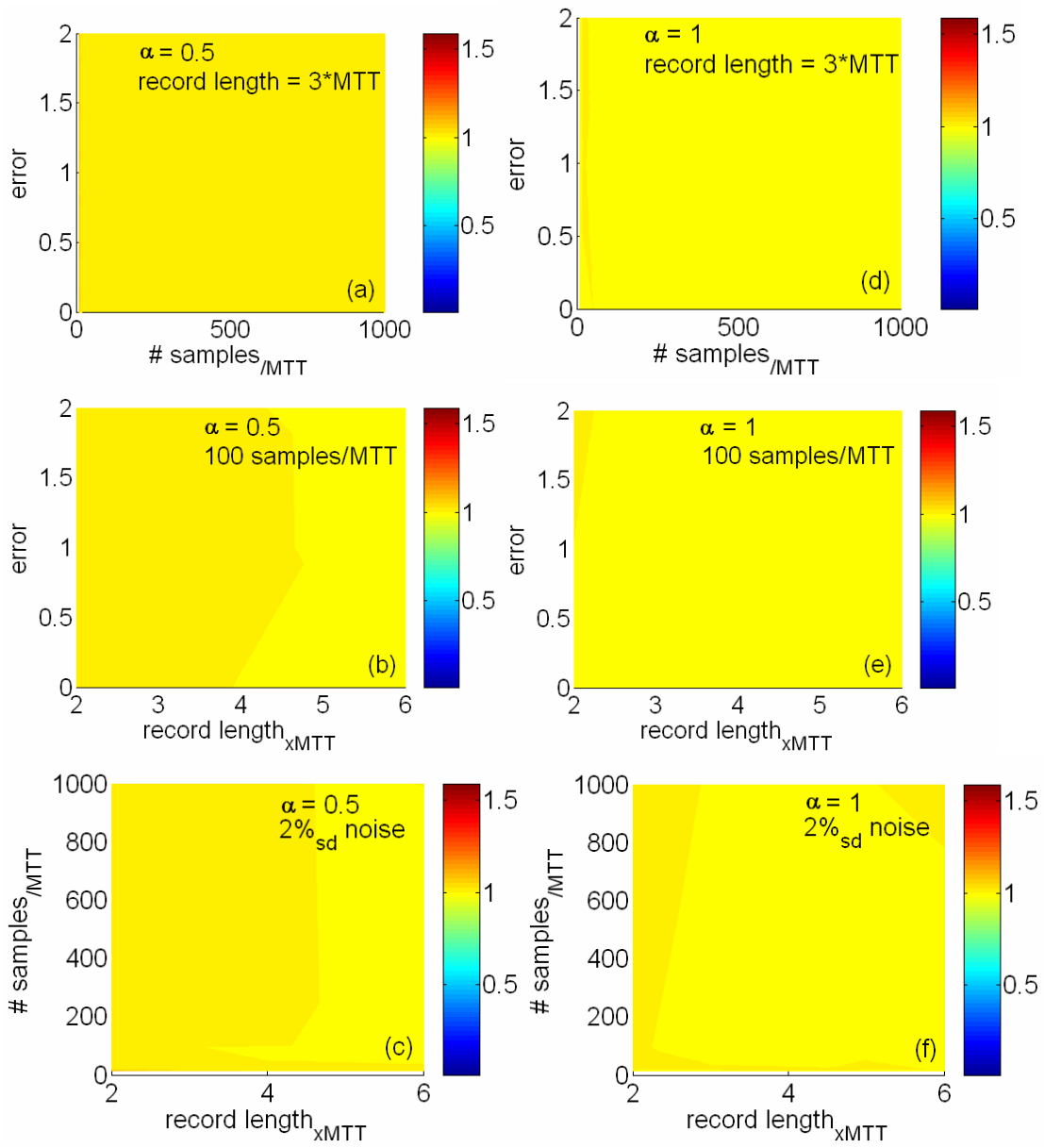
α = 0.5
record length = 3*MTT
(a)
error
samples/MTT
α = 1
record length = 3*MTT
(d)
α = 0.5
100 samples/MTT
(b)
record length xMTT
α = 1
100 samples/MTT
(e)
α = 0.5
2%sd noise
(c)
samples/MTT
α = 1
2%sd noise
(f)

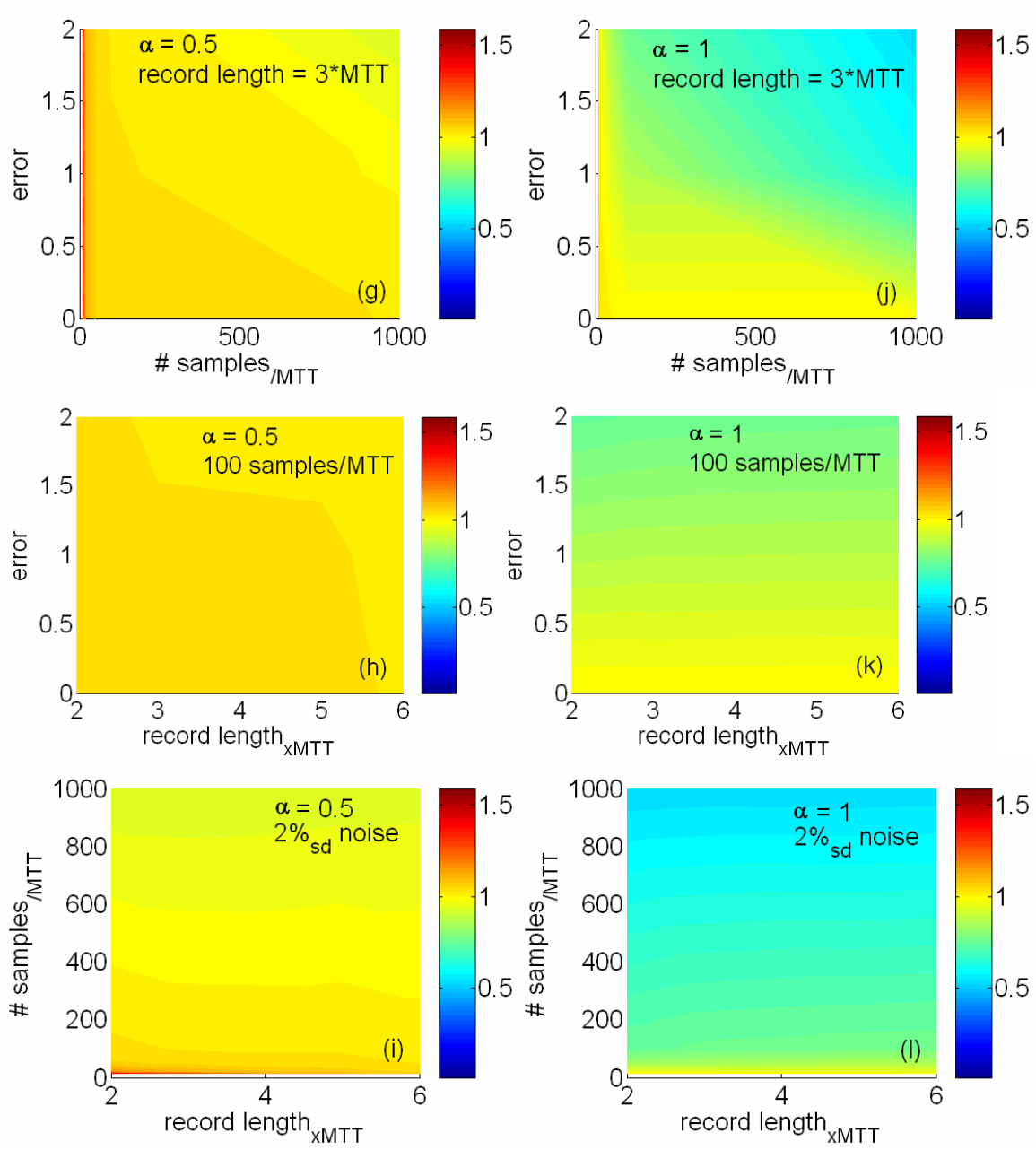
α = 0.5
record length = 3*MTT
(g)
α = 1
record length = 3*MTT
(j)
α = 0.5
100 samples/MTT
(h)
α = 1
100 samples/MTT
(k)
α = 0.5
2%sd noise
(i)
α = 1
2%sd noise
(l)
error
samplesxMTT
record lengthxMTT

Figure 4a-l.

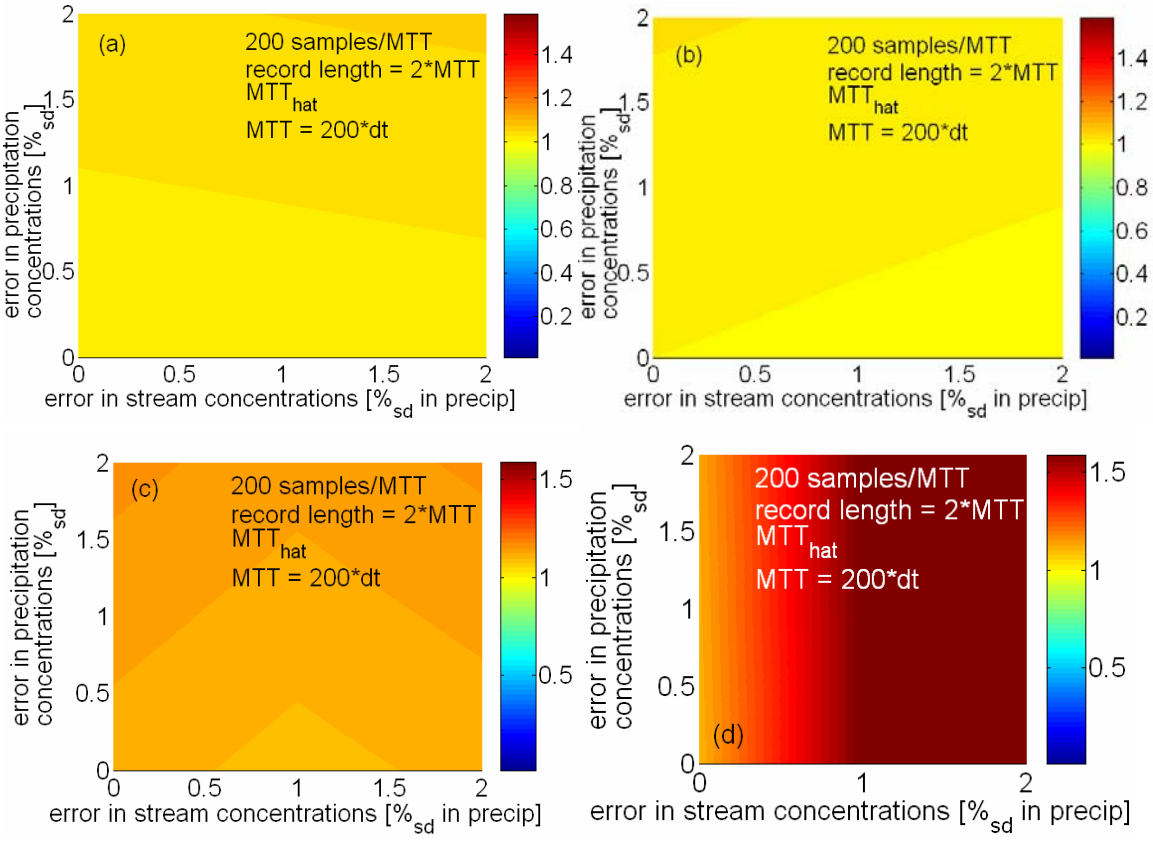
(a)
200 samples/MTT
record length = 2*MTT
MTT_hat
MTT = 200*dt
error in precipitation concentrations [%sd]
error in stream concentrations [%sd in precip]
(b)
200 samples/MTT
record length = 2*MTT
MTT_hat
MTT = 200*dt
error in precipitation concentrations [%sd]
error in stream concentrations [%sd in precip]
(c)
200 samples/MTT
record length = 2*MTT
MTT_hat
MTT = 200*dt
error in precipitation concentrations [%sd]
error in stream concentrations [%sd in precip]
200 samples/MTT
record length = 2*MTT
MTT_hat
MTT = 200*dt
(d)
error in precipitation concentrations [%sd]
error in stream concentrations [%sd in precip]

Figure 5a-d.

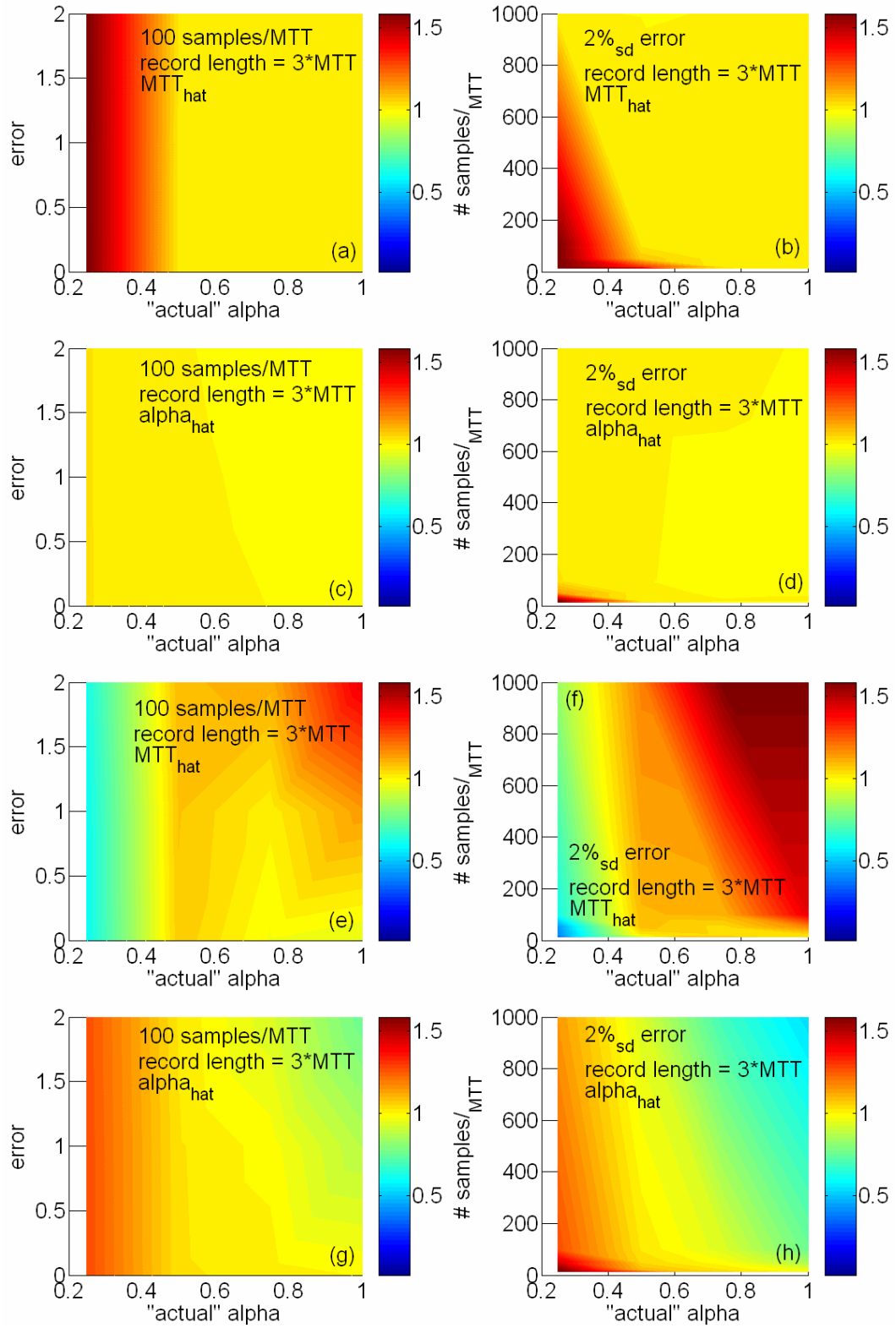
100 samples/MTT
record length = 3*MTT
MTT_hat
(a)
2%_sd error
record length = 3*MTT
MTT_hat
(b)
100 samples/MTT
record length = 3*MTT
alpha_hat
(c)
2%_sd error
record length = 3*MTT
alpha_hat
(d)
100 samples/MTT
record length = 3*MTT
MTT_hat
(e)
(f)
2%_sd error
record length = 3*MTT
MTT_hat
100 samples/MTT
record length = 3*MTT
alpha_hat
(g)
2%_sd error
record length = 3*MTT
alpha_hat
(h)
error
samples/MTT
"actual" alpha

Fig 6a-h.

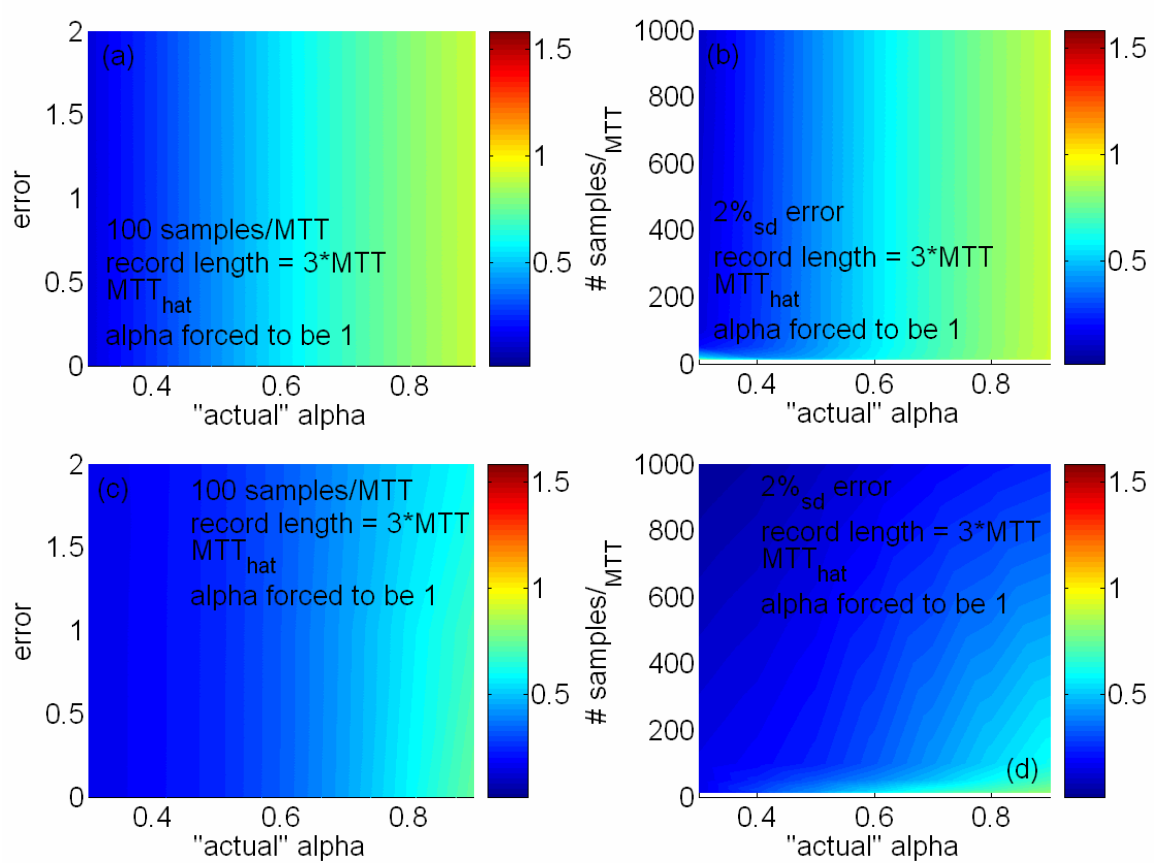
(a)
100 samples/MTT
record length = 3*MTT
MTT hat
alpha forced to be 1
error
"actual" alpha
(b)
2% sd error
record length = 3*MTT
MTT hat
alpha forced to be 1
samples/MTT
"actual" alpha
(c)
100 samples/MTT
record length = 3*MTT
MTT hat
alpha forced to be 1
error
"actual" alpha
(d)
2% sd error
record length = 3*MTT
MTT hat
alpha forced to be 1
samples/MTT
"actual" alpha

Figure 7a-d.

Chapter Three

Effects of changes in winter snowpacks on summer low flows: case studies in the Sierra Nevada, California, USA

1. Abstract

Seasonal low flows are important for sustaining ecosystems and for supplying human needs during the dry season. In California's Sierra Nevada mountains, low flows are sustained largely by groundwater that is recharged during snowmelt. As the climate warms over the next century, the volume of the annual Sierra Nevada snowpack is expected to decrease by ~40-90%. In eight snow-dominated catchments in the Sierra Nevada, we analyzed 10-33 years of snow water equivalent (SWE) and unimpaired streamflow records. Linear extrapolations of historical SWE-streamflow relationships suggest that annual minimum flows in some catchments could decrease to zero if peak SWE is reduced to roughly half of its historical average. For every 10% decrease in peak SWE, annual minimum flows decrease 9-22% and occur 3-7 days earlier in the year. In two of the study catchments, Sagehen and Pitman Creeks, seasonal low flows are strongly correlated with not only the current year's snowpack but also the previous year's as well. We used the distributed hydrologic model RHESSys to simulate the response of two study catchments to various warming scenarios. Model results suggest that a 10% decrease in peak SWE will lead to a 1-8% decrease in low flows. The modeled streams do not dry up completely because of increased fall or winter recharge and shifts in the timing of peak evapotranspiration. We consider how the current balance between rain and snow, the importance of groundwater contributions to streamflow, and the extent of vegetative cover all influence catchment response to warming.

2. Introduction

Flows during dry periods between storms, often called baseflows or low flows, are important for sustaining aquatic ecosystems and meeting human needs. Low flows are particularly important in Mediterranean climates like California's, in which a ~6-month dry season coincides with peak water demand. For example, in California base flows are critical to sustaining agricultural production during the rainless summer growing season. Fish also depend on base flows remaining high enough to provide in-stream habitat refugia with cool, oxygenated water (*e.g.*, May & Lee 2004). Sufficient low flows are also required to prevent saltwater intrusion into freshwater intake pumps in the Sacramento River Delta (Hayhoe *et al.* 2004, Knowles & Cayan 2002). Seasonal low flows are sustained by the release of water stored as groundwater, as snowpacks, or as impoundments behind dams. In California's Sierra Nevada mountains, significant winter precipitation is typically stored aboveground in seasonal snowpacks that persist beyond the end of the winter precipitation season (Hayhoe *et al.* 2004). These snowpacks melt in late spring or early summer, depending on altitude, aspect, shading, and other factors (Lundquist *et al.* 2004). Snowmelt sustains flows through the spring and early summer, and infiltrates into the ground to recharge belowground storage. Some of this recharged groundwater then slowly feeds low flows later in the season (Panagoulia & Dimou 1996). Some of the water is stored as shallow soil moisture available for evapotranspiration. In semi-arid and Mediterranean regions like California, groundwater as deep as 2-6 m below the ground surface also directly supplies water for transpiration (*e.g.*, White 1932, Nichols 1994). Because seasonal low flows are important for human and ecosystem needs, and because they are dependent on recharged water and evapotranspiration losses, it is important to understand how low flows respond to changes in the temporal distribution of recharge and evapotranspiration.

Both evapotranspiration and the temporal distribution of recharge are expected to change as the climate warms. Evapotranspiration losses may change as plants experience more widespread water stress in a warmer climate (Bates *et al.* 2008, Table 3.2), or as leaf-level water use efficiency increases in an atmosphere with a higher CO_2 concentration (Bates *et al.* 2008). In snow-dominated regions, such as the mountainous western US, the temporal distribution of recharge will largely be a function of the timing and volume of snowmelt, as well as the phase of precipitation (*i.e.*, the fraction falling as snow versus rain) (Earman *et al.* 2004, Winograd *et al.* 1998). Recharge from rainstorms is expected to differ from snowmelt-derived recharge because: (a) the timing and intensity of the arrival of the liquid (infiltrating) phase differ (Kingsmill 2006, Lundquist *et al.* 2009), (b) the antecedent soil moisture – and thus the conductivity and infiltration capacity – differs (Perkins and Jones 2008, Brady and Weil 2008), and (c) the immediate losses of near-surface water to evapotranspiration differ (Christensen *et al.* 2008). Climate change is expected to affect the volume and timing of snowmelt across the western United States (*e.g.*, Bates *et al.* 2008, Hayhoe *et al.* 2004, Mote *et al.* 2005). Compared to historical averages from the mid- to late-20th century, Sierra Nevada snowpack volumes are expected to decrease 40-90% by 2100 (Knowles & Cayan 2002, Leung & Wigmosta 1999, Hanson *et al.* 2004, Hayhoe *et al.* 2004). The projected decrease in snowpack volume may be due to (1) more frequent melt events throughout winter (Mote *et al.* 2005), (2) warmer temperatures that shift the phase of precipitation from snow to rain (Cayan *et al.* 1993, Gleick & Chalecki 1999, Lettenmaier & Gan 1990, Dettinger & Cayan 2003, Lettenmaier & Sheer 1991, Lettenmaier *et al.* 1999, Leung *et al.* 2004), or (3) lower total precipitation (*e.g.*, Dettinger *et al.* 2004). Current downscaled global climate model predictions for the Sierra Nevada suggest that total precipitation may increase or decrease by 10% or less (*e.g.*, Leung & Wigmosta 1999, Dettinger *et al.* 2004), so we do not focus on changes in precipitation amount in this study. Instead, we focus on the anticipated changes in the phase of precipitation and their impacts on the temporal distribution of recharge. We also consider the effect of the anticipated earlier melt-out of the entire snowpack (Cayan *et al.* 2001a, Cayan *et al.* 2001b, Mote *et al.* 2005). We recognize that these effects are expected to vary with elevation (Gleick 1987), and elevation is considered explicitly in our modeling work.

Here we explore the primary controls on catchment low flow response to changes in climate by examining historical trends and model predictions under possible warming scenarios. We ask, how will warming change the phase and timing of precipitation? How will these changes affect the temporal distribution of recharge and subsequent seasonal low flows? How important is the effect of warming on evapotranspiration, and in turn, on seasonal low flows? Are changes in evapotranspiration or precipitation more important in controlling low flow amount and timing? Specifically, we explore the potential impact of significant reductions in snowpack volume, and the anticipated changes in the temporal distribution of recharge and evapotranspiration, on low flows in Sierra Nevada streams and rivers. We estimate the historical sensitivity of streams to recharge as indicated by changes in snowpack volume and snowmelt timing. We also use the RHESSys model to examine warming-induced changes in precipitation phase and evapotranspiration.

3. Historical snow-recharge-low flow relationships

Sierra Nevada hydrology is dominated by California's Mediterranean climate, in which precipitation falls predominantly in the winter, snowmelt generates a broad peak of streamflow in late spring or early summer, and flows decline to annual minima in the late summer and autumn (*e.g.*, Figure 1). We quantified the relationship between snowpack volume and stream flow at eight snowmelt-dominated Sierra Nevada catchments with unimpaired flows (*i.e.*, free of dams and diversions). It is worth noting that because many streams in the Sierra Nevada are gauged only below dams or other impairments, the number of catchments that were suitable for this analysis was limited by the availability of unimpaired stream gauges rather than snow pillows. For our analysis, we included all catchments with at least a 10-year overlap of daily streamflow and snowpack information. In catchments with multiple snow sensors, we used the sensor with the longest continuous record. At the eight sites that met our criteria for analysis in the Sierra Nevada (Table 1 and Figure 2), the elevation of the snow pillows varies between 2022 and 3547 meters, and the stream gauges are located at elevations between 607 and 2184 meters. Drainage areas range from 25 to 1373 km^2 (median = 118 km^2). Average annual runoff varies from 8 to 86 cm/year (median = 52 cm/year) over the available flow records.

3.1 Flow-snowpack relationships

For each of our study sites, we calculated the 15-day running median daily flow and snow water equivalent (SWE). We used 15-day running medians to minimize the effect of individual, potentially spurious, values in the raw time series. For each year at each site, we calculated the annual low flow as the minimum of the 15-day running median flow following the spring snowmelt. We also calculated the annual peak SWE as the maximum of the 15-day running median SWE for each water year (*i.e.*, the maximum SWE that occurred in the winter or spring preceding the low flow for a given calendar year). We then normalized all flows and snow water equivalents by dividing each year's value by the average for all the years at each site. For example, for a given site, each year's minimum flow was divided through by the average of all years' minimum flows. We then determined the best-fit relationship between the normalized maximum SWE and the normalized minimum flows for each location.

Using these best-fit regressions, we established that there are predictable relationships between normalized maximum SWE and minimum flow at all of the study catchments (Figure 3). Flows are relatively sensitive to changes in SWE at six of the eight study sites (Pitman, Trout and Ward Creeks, South Fork Kern, Upper Truckee and South Fork Mokelumne Rivers). Linear extrapolations of the relationship between maximum SWE and minimum flow imply that minimum flows at these six gauge locations could decrease to zero if peak winter SWE were reduced to roughly half of its historical average (Figure 3). The best-fit normalized SWE-minimum flow slopes are significantly steeper than one at these six sites, which means that they exhibit a more-than-proportional relationship between maximum SWE and minimum flow. For these catchments, a 10% decrease in SWE results in a ~12-25% decrease in minimum flow (Table 1 and Figure 3). Low flows in the other two streams and rivers (Sagehen Creek and the Upper Merced River) respond proportionally or less-than-proportionally to changes in maximum SWE. In these catchments, a 10% decrease in peak SWE corresponds to a ~8-11% decrease in low flows.

We propose the following potential explanations for the more-than-proportional and less-than-proportional relationships between peak SWE and low flows in the Sierra Nevada mountains. The more-than-proportional relationship between minimum flows and maximum SWE might be understood by looking at examples of wet and dry years: in dry years, with lower peak SWE, snow would melt slowly and completely in early spring. Therefore, evapotranspiration losses from subsurface storage in the early growing season would not be recharged by snowmelt in the late spring and early summer, because the snowpack would have already melted away. Low flows would be lower than would be expected due to the decrease in precipitation. The opposite is true of wet years: the peak in snowmelt occurs later and although groundwater recharge may be a smaller fraction of total precipitation, that total volume is higher. Furthermore, evapotranspiration losses can be recharged for a portion of the growing season from melting of aboveground water stored in the snowpack. Groundwater stores therefore remain higher because of the coincident timing of melt and evapotranspiration demand in wet years. Therefore, low flows are higher than expected due solely to the increased precipitation. A possible explanation for the less-than-proportional relationships between low flows and peak SWE can be similarly divided into wet and dry years, and relies on the assumption that evapotranspiration predominately relies on a groundwater source. In dry years, the groundwater table may drop below the typical rooting depth, forcing a reduction in evapotranspiration rates and thus limiting the decrease in low flows. Conversely, in wet years, the water table may rise into the more densely rooted zone, thus raising evapotranspiration rates and limiting the increase in low flows.

3.2 Melt-out and low-flow timing

Low-flow discharge and timing depend on both melt-out timing and the volume of peak SWE. In low-SWE years, low flows are smaller and occur earlier (Figure 4). To understand the role of melt timing, we recorded the first day on which the snow water equivalent was zero – the day of melt out – at each snow sensor location for each year of record. We also defined the low-flow period as the range of days with flows below the 25th percentile of all historical flows. We chose this range because at most sites it encompasses at least one day in most years while excluding most snowmelt and autumn storm days in drought years. In a Mediterranean climate with a long dry period, the recession limb of the hydrograph is relatively flat near the end of the dry season, so low flows may occur for several days or weeks, depending on site conditions and the onset of autumn or winter storms. With this in mind, we also noted the first, mean and last day on which the low- flow period occurred (in Julian days). There is a strong correlation between maximum snowpack and the day of melt out. Melt-out occurs 3-7 days earlier for each 10% decrease in peak snowpack SWE (Figure 5a). The mean day of the low-flow period also occurs earlier in years with less snow and later in years with a larger snowpack, and varies by as much as ~3 months across all locations (Figure 5b).

The scatter in the relationship between low-flow timing and maximum SWE is larger than the scatter in the relationship between melt-out timing and maximum SWE (Figure 5a and b). Melt-out is typically expected to be a function of elevation, aspect and temperature (Lundquist *et al.* 2004). Low flow timing is expected to depend on additional factors including geology (Jefferson *et al.* 2008), leading to more scatter in its dependence on peak SWE (Figure

5b). To understand the low-flow timing response, we considered both the length of the low-flow period and the timing of the low-flow period during the year. The start date of the low-flow period is significantly correlated with melt-out timing at all sites. In contrast to the consistent strong relationship between melt-out timing and the start date of the low-flow period, the length of the low-flow period is significantly correlated with melt-out timing at only half of the sites (Ward, Trout, SF Mokelumne, and Upper Truckee). After the low-flow period begins, the influence of the melt-out timing appears to fade in some catchments. Low-flow recession characteristics often reflect both geologic and vegetative controls on water movement (Hall 1968, Singh 1968, Tallaksen 1995 & references in each), although sometimes baseflow recessions are independent of evapotranspiration signals (Post and Jakeman, 1996) or assumed to reflect predominately geological controls (Tague and Grant, 2009). At all eight sites, a fall rainstorm that quickly raises streamflows often marks the end of the low-flow period. End dates of the low-flow period in any given year rarely coincide across sites, implying local-scale storms may play a large role in determining the length of the low-flow period.

3.3 Memory

At some locations, low flows exhibit a "memory effect" in which they depend not only on the current year's snowpack, but also on the previous year's snowpack. To illustrate this memory effect, we divided the snowpack and low flow data at Sagehen Creek into two groups (Figure 6a): years for which the previous year's snowpack was above average (closed symbols) and years for which it was below average (open symbols). Flows are more sensitive to a given year's snowpack when the previous year's snowpack is above average (as seen in the steeper slope of the best-fit line for the solid symbols in Figure 6a). Thus, a wet year following a wet year produces higher flows than a wet year following a dry year. Note that low flows in dry years are approximately the same, regardless of whether the previous year was wet or dry. Risbey and Entekhabi (1996) showed that streamflow is less responsive to precipitation after a drought year at the larger Sacramento Basin scale. They attributed this "drought memory" to atmospheric, geologic, and vegetative effects, but did not explore which tributaries to the Sacramento might be more likely to exhibit a memory effect. At each of our sites, we performed a multiple regression of low flows against peak SWE for up to three previous winters to determine the persistence and significance of the memory effect. The only two sites with statistically significant memory effects were Sagehen Creek (Figure 6a) and Pitman Creek (Figure 6b) where the memory effect persisted for the two previous winters. At Pitman Creek, the statistical significance of the memory effect depends on the above-average SWE years in 1983 and 1998. These are the only two years at Pitman Creek in which an above-average snowpack follows an above-average snowpack, and it is possible that the Pitman memory effect is an artifact of a limited record.

At Sagehen Creek, the persistent effect of past snowpacks on low flows likely reflects the catchment hydrogeology. Unlike the other sites in this study, Sagehen is underlain by a layer of volcanics, including pyroxene and basaltic andesite (Sylvester *et al.* 2007). The other study sites are generally underlain by granites, which usually have more limited groundwater storage capabilities (Kakue and Kishi 2003, Price 2009). At least 14 springs are found within the Sagehen catchment boundaries, and 15- to 28-year-old groundwater contributes nearly all the streamwater at low flows, and up to 70% of streamwater at high flows (Erman and Erman 1995, Rademacher *et al.* 2005). Shun and Duffy (1999) report that inter-annual signals indicating long-

term memory are strengthened at sites in the Great Salt Lake basin where groundwater dominates streamflow. Thus, sites with a strong memory effect may reflect an important groundwater contribution to streamflow. Conversely, sites without a strong memory effect may have a smaller groundwater signal in streamflow. Memory and groundwater contributions may also indicate an insensitivity to climate warming. Groundwater contributions to streamflow above a certain threshold mediate summer streamflow response to warming in the Oregon Cascades (Tague *et al.* 2008). More specifically, low flows in catchments with more efficient subsurface drainage (implying a potentially larger groundwater contribution) are relatively insensitive to changes in recharge that might be expected as a result of climate change (Tague and Grant 2009).

As discussed in the introduction, climate model projections for California suggest that warmer temperatures will result in smaller snowpacks that melt earlier in the year. The relationship between changes in snowpack volume and melt timing for the eight sites in the Sierra Nevada (shown in Figures 3 and 5) suggest that in many streams, one would expect to see a significant decrease in flows and a shift to earlier arrivals of low flows. Historically, higher peak SWE generally corresponds to wetter years and lower peak SWE to drier years because most precipitation falls as snow. As a larger fraction of precipitation falls as rain, it is difficult to know whether the historical relationships between peak SWE and low flows will accurately describe catchment behavior. Extending the approach used in Figure 3, we performed multiple regressions of low flows against three potentially explanatory factors: peak SWE, total rainfall during snow-covered periods, and total rainfall during snow-free periods. Rainfall, either during snow-covered or snow-free periods, is not significantly correlated with low flows at any of our study sites, except at Sagehen Creek. At Sagehen, a 10% increase in rain falling during snow-free periods coupled with a 10% decrease in peak SWE would lead to a ~12% decrease in low flows, whereas without the additional rainfall, low flows would be expected to decrease by ~8%. Low flows were not significantly correlated with rain falling during the snow season at any site, implying that the impact of shrinking snowpacks on low flows would not be offset by increased winter rainfall.

4. Future precipitation-recharge-low flow relationships

In the rest of this paper, we report model simulations exploring how warming may alter the phase of precipitation, the temporal distribution of recharge, and the evapotranspiration demands of vegetation, and estimate their effects on low flows. We used the RHESSys model to simulate low flow-snowpack relationships under a variety of warming scenarios (outlined below), for comparison with the historical low flow-snowpack relationships discussed above. RHESSys is a spatially distributed watershed hydrologic model (Tague and Band 2004). Modeled hydrologic processes include interception, snow accumulation and melt, infiltration, evaporation, transpiration, and vertical drainage between unsaturated and saturated stores, as well as lateral redistribution of shallow groundwater and drainage to deeper groundwater stores. Snowmelt is estimated by combining an energy budget approach for radiation-driven melt with a temperature-index based approach for latent-heat driven melt processes. For a detailed evaluation of the elevation effects of warming on vegetation water use as represented by the RHESSys model, see Christensen *et al.* (2008).

4. 1 Site, Model and Scenario Descriptions

We modeled two sites in the Sierra Nevada: Sagehen Creek, in the northern part of the range, and the Upper Merced River, which flows through Yosemite National Park in the central part of the range (Figure 2). The catchments are quite different: Sagehen is ~27 km^2, with a peak elevation of 2672 m, volcanic geology, and nearly complete vegetative cover, whereas the Upper Merced is ~469 km^2 with a peak elevation of 3997 m, granitic geology, and vegetation covering ~75% of the catchment area. We examined each component of the water budget to compare the two catchments' responses to climate change. A complete description of RHESSys implementation and calibration for Sagehen Creek and Upper Merced can be found in Tague and Grant (2009). We compared modeled results with the historical record for the Upper Merced and Sagehen. The Upper Merced had a Nash-Sutcliffe efficiency of 0.58 (and an R^2 of 0.80 for log-transformed flow) over the 43-year record whereas Sagehen Creek had a Nash-Sutcliffe efficiency of 0.22 (and an R^2 of 0.66 for log-transformed flow) over a 41-year record.

We modeled the response of each catchment to five different scenarios: (1) a no-forcing case with the historic temperature and precipitation regimes, (2) a 2°C warming case in which precipitation is partitioned between snow and rain based on temperature, and vegetation water use also depends on temperature (3) a 4°C warming case with both precipitation and vegetation respond to temperature as in the previous case, (4) a 2°C warming case in which only the phase of precipitation changes, but no vegetation changes due to warming are permitted, and finally, (5) a 4°C warming case with only precipitation phase change permitted as in the previous case. We chose these scenarios because they encompass the range of warming scenarios that are expected in the region over the coming century (*e.g.*, Hayhoe *et al.* 2004), but are far less complex than a downscaled global climate model for the region. We deliberately excluded possible changes in the amount of precipitation in order to focus on quantifying the effects of changing the temporal distribution of melt and rainfall. The same precipitation record is used for each scenario (*i.e.*, no change in total precipitation), but because RHESSys partitions precipitation between snow and rain based on the temperature at each location within the catchment, the proportions of snow vs. rain will differ among the scenarios. Transpiration is largely driven by the spatial distribution of leaf area index (LAI), which is estimated from the Normalized Difference Vegetation Index based on summer Thematic Mapper Remote Sensing imagery at each site (White *et al.* 1997). Although shifts in vegetation patterns may be important in shaping catchments' response to climate change (Alo and Wang, 2008), little information exists to constrain the pace and pattern of possible vegetation shifts at our sites, and we did not include them in our modeling scenarios.

Net groundwater recharge is calculated using a mass balance approach where:

$$\text{net recharge} = \text{melt} + \text{rain} - \text{evapotranspiration} - \text{streamflow} \quad (1)$$

Melt is assumed to be equal to the difference in daily SWE on days where the size of the snowpack is diminishing, which is likely a slight underestimate of total melt in these catchments because snow falling and melting within the same day is categorized as rain. Evapotranspiration also includes canopy interception losses in which precipitation falls to the canopy and evaporates without ever reaching the ground. Transpiration varies in cases (1)-(3) based on the availability of soil water and based on potential evapotranspiration, which is a function of temperature and other factors. In cases (4) and (5), potential transpiration remains the same as in the base case.

Actual transpiration may decrease if insufficient water remains available, or it may increase if water availability no longer limits actual transpiration. The 2ºC and 4 ºC warming scenarios yield qualitatively similar results, differing only in magnitude, so for clarity, we display only the base and 4ºC results below (*i.e.*, cases (1), (3), and (5) from above).

4.2 Modeled snowpack- flow relationships

We tested whether the historical precipitation-low flow relationships seen in Figure 3 are consistent with model simulations of future climates in which more precipitation falls as rain and the temporal distribution of groundwater recharge shifts to earlier in the year. According to our modeling results, the historical relationships provide insight into the future hydrology of Sierran streams, but may eventually break down. The relationships between peak SWE and low flows are similar in the warming scenario and in the base case (Figure 7), but in the warming scenario, the data points occupy a smaller region in the lower left corner of the low flow-peak SWE plot. There also may be some flattening of the relationship, particularly at Sagehen (Figure 7b), whereas the slopes for the base case and the 4°C scenario remain statistically indistinguishable at the Upper Merced (Figure 7a)

The historical records indicate that the mean day of the low flow period advances by ~3-7 days for each 10% decrease in maximum snow water equivalent (Figure 5b), which matches the average timing shift of ~20 days at the Upper Merced between the base case and the 4°C scenario, in which peak SWE decreases by an average of 35%. The historical trend also matches the ~25 day shift in low-flow timing observed at Sagehen in the 4°C scenario, in which average peak SWE decreases by 82% from the base case (Table 2). If the 3-7 day advance per 10% loss in SWE holds for most Sierra Nevada locations, like it does for the Upper Merced and Sagehen, and peak SWE decreases by ~70% over the next century (Leung & Wigmosta 1999), the middle of the low-flow period should advance by ~20-50 days. This range is similar to the ~5 to >35 day advance in the "center time" of flows (or mean flow-weighted time, by water year) predicted by Stewart *et al.* (2004) over the next century using NCAR's Parallel Climate Model under 'Business as Usual' conditions for the Sierra Nevada. This model corresponds to ~2-3°C temperature increase and a modest change in precipitation of ±10%.

4.3 Modeled Water Balance Response to Both Precipitation Phase and Vegetation Water Use

We systematically compared the effects of precipitation phase change and vegetation water use changes on key components of the catchment water balance to identify controls on catchment warming response (Figures 8-9 and 10-11). First we examined the "full" 4°C warming scenario (case 3) in which precipitation phase and vegetation both respond to warmer temperatures (Figures 8-9). We compared these results to the 4°C warming scenario where only precipitation phase changes (case 5, Figures 10-11). Results for both sites and both scenarios are summarized in Table 2. Unsurprisingly, more rain falls when it is warmer than in the base case (Figure 8a-b and 9a-b, Table 2) and peak snowpack water content drops. Melt out and peak flows occur earlier in the year, and minimum 15-day running median flows decrease, occur earlier in the year, and become less variable from year to year (*e.g.*, Figures 8 and 9c, Table 2). We also considered changes in components of the water balance in each of the seasons, which we defined

as four approximately equal (91-92 day) periods. For convenience, we refer to them by their approximate seasons (spring=Julian days 61 to 152, summer=Julian days 153 to 245, autumn/fall = Julian days 246 to 334, winter=Julian days 335 to 60).

4.3.1 Net Recharge Response

Warmer temperatures affect the temporal distribution of recharge. Annual net recharge does not change under a warmer climate, but the timing and variability of net recharge both shift within the year (Figures 8 and 9e, Table 2). Peak 15-day running median net recharge shifts earlier in the year by approximately two months at the Upper Merced and to late autumn at Sagehen in the warming scenario (Table 2). There is a large decrease in spring net recharge, shifting the regime from a positive change in net storage to a near-zero or negative change in net storage. The lack of spring recharge is partially compensated by increases in recharge in fall (and, to a lesser degree, in winter, Table 2).

As seen in the brief excursions from the long-term average in late autumn and winter (Figures 8e and 9e), net recharge depends strongly on particular storm events and whether precipitation falls as snow or rain. Net recharge has a long-term average near zero (i.e., no long-term change in storage). Seasonal net recharge standard deviations increase due to warming by up to ~50% in fall and winter. The hydrologic response to this earlier and more sporadic flux of water to belowground storage partially determines how low flows will change in response to warming. Gross fluxes into groundwater storage increase in the warming case when more precipitation falls as rain (Table 2). Because there is no net change in storage, we know that gross fluxes out of storage increase proportionally to the increased fluxes into storage, which implies that average subsurface residence times will decrease under warmer temperatures.

Our model results of increased gross fluxes to groundwater in the warming case contradict observations made elsewhere. Two studies of the catchment-scale effect of the phase of precipitation on groundwater recharge in the southwestern US have suggested that snowmelt disproportionately contributes to groundwater recharge compared to the fraction of precipitation that falls as snow (Earman *et al.* 2006, Winograd *et al.* 1998). In these studies, precipitation that fell as rain was less effective at recharging the groundwater system, which is the opposite of the result seen in our modeling work. The discrepancy between our model results and this previous work may be partially explained by the differences in the studied catchments and the timing of the rainfall. For example, Winograd *et al.* (1998) found that summer rain in Nevada, which often falls in intense storms when potential evapotranspiration is very high, contributes proportionally less to groundwater recharge than does snowmelt in winter and spring. Lower intensity winter rain in the Sierra Nevada might contribute more to recharge than the summer rain in Winograd *et al.*'s (1998) study due to differences in both storm characteristics and potential evapotranspiration losses. RHESSys also assumes that rain falls evenly throughout the day unless precipitation duration time series are included as model inputs. Because sub-daily weather information is not available at these sites over the entire period of record, we use the default duration scheme, which may lead to overestimates of recharge during rainfall in all scenarios. However, we do not expect that actual rainfall intensities would regularly be high enough to exceed the infiltration capacity at the study sites, and therefore we expect that RHESSys's assumption of evenly distributed rainfall introduces minimal error in the net recharge estimates.

Infiltration to the subsurface appears to increase as the climate warms, which may help to sustain low flows.

4.3.2 Evapotranspiration Response

Warming also shifts the timing of vegetative evapotranspiration demand, which can, in turn, alter low flows. Total evapotranspiration over the period of record changes little from the base case to the 4°C warming scenario (Table 2), but the magnitude and direction of change are not evenly distributed throughout the year (Figure 8d and 9d). At the Upper Merced, spring evapotranspiration is slightly higher in the warming scenario than in the base case whereas summer evapotranspiration is lower in the warming case. At Sagehen, spring evapotranspiration is higher with warming than in the base case, and summer and winter evapotranspiration are lower (Figures 8 and 9d). Peak 15-day running median evapotranspiration occurs ~2-4 weeks earlier in an average year. That is, evapotranspiration demands shift in timing relative to the base case by about the same amount as low flows do (~20-25 days). This pattern allows low flows to remain higher than they would be if the growing season were to lengthen and total evapotranspiration were to increase. Historically, the timing of peak flows is approximately in phase with peak evapotranspiration and radiative fluxes. As warming occurs, both evapotranspiration and flows shift earlier in the year, and are increasingly out of phase with peak light availability. For some plants, light limitations may affect water use and net primary productivity. The coincident shift in timing of evapotranspiration and low flows suggests that it is important to understand when light may limit plant water use and under which conditions the growing season might lengthen.

4.3.3 Site-to-site differences

Recharge and evapotranspiration changes due to warming lead to larger changes in low flows at Sagehen Creek than at the Upper Merced. The large drop in SWE at Sagehen and the sustained higher evapotranspiration demand during the low-flow period exceed any increased winter net recharge. Apparently, the increases in winter recharge are relatively transient and insufficient to sustain flow later in the dry season. This transience is reflected in the distinct recession characteristics of the basins (Tague and Grant 2009). Sagehen Creek tends to be more groundwater-dominated (Rademacher *et al.* 2005) than much of the Sierra Nevada. For example, during high flows, Sagehen streamflow is composed of ~70% groundwater (Rademacher *et al.* 2005) whereas at the Upper Merced, flows are composed of only 0-10% groundwater (and 0-20% “lateral subsurface flows”) (Conklin and Liu 2008). Jefferson *et al.* (2008) found that in streams with a large groundwater component, like Sagehen Creek, low flows decrease in response to decreasing precipitation by more than streams with a smaller groundwater component, like the Upper Merced River. Our work differs from Jefferson *et al.* (2008) because we compare changes in the phase of precipitation and do not alter the total amount of precipitation. Modeling results from these two sites suggest that precipitation phase change, which alters the temporal distribution of recharge, can decrease low flows more in groundwater-dominated streams. We now explore how sensitive low flows are to changes in both precipitation phase and vegetative water demand vs. only changing the phase of precipitation from snow to rain.

4.4 Modeled Water Balance Response to Warming-Induced Precipitation Phase Change Only

Warming-induced changes in the phase of precipitation can be distinguished from changes due to warming effects on vegetative evapotranspiration demand. We modeled the same warming scenarios without any warming-induced changes in the timing of vegetation growth and water demand (cases 4 and 5, as outlined above). Results from the base case and warming scenario 5 from both Sagehen and the Upper Merced are shown in Figures 10 and 11 and columns 2 and 5 of Table 2. Nearly all of the decrease in peak SWE at Sagehen is due solely to precipitation phase change, and precipitation phase change accounts for most of the decrease at the Upper Merced as well (Figures 8b vs. 10b, Figure 9b vs. 11b, Table 2). The rest of the decrease in peak SWE at the Upper Merced occurs when warming-induced changes in vegetative evapotranspiration demands are permitted. This implies that more melting occurs as potential evaporation (and, typically, actual evapotranspiration) increases, perhaps due to a local warming feedback due to increased transpiration. We believe that this effect is probably also active at Sagehen, but is difficult to observe because changes in precipitation phase already affect the snowpack size so dramatically. More than half of the shift in timing of melt out occurs only when vegetative evaporative demand responses to warming are modeled (Figure 8b vs. 10b and 9b vs. 11b, Table 2). Average winter recharge is sensitive to both changes in the phase of precipitation and vegetation response to warming and differs between the sites. Although the total amount of evapotranspiration varies little as climate warms, most of the shift in the timing of peak evapotranspiration occurs only when vegetation effects due to warming are included (Figures 8d vs. 10d, Figure 9d vs. 11d, Table 2). Changes in the minimum flow amount are due to changes in both the precipitation phase and vegetation response, but the entire shift in minimum flow timing is due solely to the change in the phase of precipitation (Table 2). Thus, precipitation phase alone strongly affects snowpack volume and the timing of low flows. Changes in the timing of peak evapotranspiration and melt-out timing are observed in the warming scenarios in which plants respond to higher temperatures with higher potential evapotranspiration rates. Low flows and net winter recharge depend on both precipitation phase changes and vegetation warming response.

The two sites do not respond identically to warmer temperatures. Shifts in the phase of precipitation from snow to rain, in the absence of changes in the total amount of precipitation or evapotranspiration, affect the timing and magnitude of flow much more at Sagehen than at the Upper Merced (Figures 10c and 11c). At the Upper Merced, the timing of peak flows is unaffected by changes in the precipitation phase alone whereas at Sagehen peak-flow timing shifts substantially earlier due solely to changes in the precipitation phase. Peak evapotranspiration timing exhibits almost the opposite response with almost no change at Sagehen and a two-week advance at the Upper Merced due solely to changes in precipitation phase. Site-to-site differences in the original base-case fraction of precipitation falling as rain, the vegetative cover and the hydrogeology moderate the effects of warming and lead to distinct low flow responses.

4.5 Additional Considerations

We do not explicitly account for vegetation growth phenology shifts (*e.g.*, Price and Waser 1998, Royce and Barbour 2001, Loheide *et al.* 2008), frost damage due to reduced snow cover (*e.g.*, Weih and Karlsson 2002, Cleavitt *et al.* 2008), or vegetative diebacks and changes in species composition that may occur with warmer temperatures (*e.g.*, Lenihan *et al.* 2008). Vegetation growth phenology in mountainous ecosystems is usually strongly tied to snowmelt (*e.g.*, Price and Waser 1998, Royce and Barbour 2001), suggesting that our model results may underestimate the shift in evapotranspiration depending upon the seasonal changes in LAI. On the other hand, our results may overestimate evapotranspiration if frost damage is prevalent due to a decrease in insulating snow cover. Bare ground is more exposed to cold winter temperatures, and roots, seedlings and saplings can be damaged by colder temperatures than they would experience if the ground were snow-covered (*e.g.*, Weih and Karlsson 2002, Cleavitt *et al.* 2008). Although we assume that vegetation diebacks and species composition shifts are minimal over the time and space scales of this study, possible vegetation changes and the ensuing hydrologic response in the Sierra Nevada is worth further research. For example, if soils became very dry for a longer period during the summer, potential evapotranspiration would exceed actual evapotranspiration, and water stress might kill plants. Widespread drought stress could lead to long-term shifts in the vegetative cover, toward species that could better take advantage of winter rains or drier conditions (Lenihan *et al.* 2008). Such changes could shift the timing or amount of transpiration demand and in turn the timing and magnitude of low flows. Dettinger *et al.* (2004) identified possible feedbacks among evaporation, soil moisture and vegetation dynamics in the Sierra Nevada and argued that these feedbacks may be important for accurately predicting hydrologic response to climate change. However, these interactions at the daily to decadal time scales are still too uncertain to model accurately in both the Sagehen and Upper Merced basins at the catchment scale.

Plant growth and mortality can also reveal information about how vegetation responds to changes in temperature and the temporal distribution of available water. Millar *et al.* (2007) showed that vegetation exhibits a longer "memory effect" than the one exhibited by the catchment groundwater system shown in Figure 6: trees are more likely to die if they experience multiple years of drought following a wet period or if a multi-year drought is combined with increased temperatures. They also demonstrated that growth rates for limber pine (*Pinus flexilis*) in the Sierra Nevada were more sensitive to changes in maximum temperature than minimum temperature (with no change in winter precipitation). In other regions, warmer average temperatures lead to increases or decreases in vegetation growth rates depending upon which resources are limiting (Running and Nemani, 1991; Aber *et al.*, 1995; Case and Petersen, 2005; van Mantgem and Stephenson, 2007). Millar *et al.* (2007) noted that water and energy are limiting resources in the Sierra Nevada. Because water availability may change with precipitation phase, we hypothesize that minimum temperatures above and below 0°C would be associated with different average tree growth rates. If both water and energy were to peak coincidentally, average growth rates would be higher. In places where the minimum temperature is below freezing, spring snowmelt may ensure that transpiration is not water-limited during the annual peak in incoming radiation. In places where the minimum temperature is above freezing, water availability may limit transpiration during the period of peak incoming radiation. The records analyzed by Millar *et al.* (2007) did not span 0°C, but our modeling work suggests that

temperature may affect the timing of water availability to plants and rates of evapotranspiration. For example, in the modeled Sagehen catchment, a 4°C temperature increase led to a ~50% increase in annual rainfall and associated decrease in peak SWE (Table 2). In response, peak evapotranspiration shifted earlier by ~2 weeks (Figure 11c). Much lower transpiration rates during the latter part of the summer may indicate that summer growth rates decreased because of water limitations, and it is unclear whether higher spring transpiration rates may be sufficient to permit similar annual rates of growth (Figure 11c). One could directly test the hypothesis outlined above by applying Millar *et al.*'s (2007) technique to plants along a gradient spanning a historical rain-snow threshold to determine relative annual growth rates and their sensitivity to water and energy limitations.

5. Conclusion

Low flows are important to human and ecological systems. We demonstrate that changes in snowpack volume affect subsequent summer and fall low flows in the Sierra Nevada of California. At all eight of our study catchments, summer and fall low flows are strongly correlated with annual peak Snow Water Equivalent (SWE), and in six of the eight catchments, low flows vary more than proportionally with variations in SWE from year to year. In these six catchments, linear extrapolations of the historical low-flow/SWE relationships suggest that low flows could drop to zero if peak SWE decreases by roughly 50 percent from historical norms. At two sites (Pitman Creek and Sagehen Creek), low flows depend on both the current year's snowpack and the previous year's snowpack. At these sites, streamflow is more sensitive to the current year's snowpack in years for which the previous year's snowpack was above average.

RHESSys model results indicate that, under scenarios of warming by 2 and 4 degrees, the more-than-proportional relationship between maximum SWE and low flow still holds, albeit over a narrower range of values. Net fall recharge at both sites (and winter recharge at Sagehen) increases with increasing temperatures that shift the phase of precipitation from snow to rain. This phase change alters the temporal distribution of recharge that in turn affects low flows. Evapotranspiration changes relatively little in the modeled warming scenarios, but the timing of peak evapotranspiration shifts slightly earlier to better coincide with the earlier peak water availability in a warmer climate. We did not examine how growth phenology, frost damage, vegetation die-off and species composition change could affect evapotranspiration rates; these effects could produce large changes not accounted for in our model. Monitoring studies, especially those conducted near the snow-rain boundary, should measure precipitation and unimpaired streamflows to understand how low flows in these systems respond to shifts in precipitation and temperature. Some streams' low flows will be very sensitive to such changes whereas other streams will be more robust to changes in climate. Our modeling work suggests that the current degree of groundwater dominance, rain/snow balance, and extent of vegetative cover all influence the resilience of catchment low flows to climate warming.

6. Acknowledgements

Funding from the NSF Graduate Research Fellowship Program and the Berkeley Water Center supported this research. The US Geological Survey, Natural Resources Conservation Service, and the California Department of Water Resources provided crucial data.

7. References Cited

Alo CA, Wang GL. 2008. Hydrological impact of the potential future vegetation response to climate changes projected by 8 GCMs. Journal of Geophysical Research – Biogeosciences 113(G3): G03011.

Aber JD, Ollinger SV, Federer A, Reich PB, Goulden ML, Kicklighter DW, Melillo JM, Lathrop RG. 1995. Predicting the effects of climate change on water yield and forest production in the northeastern United States. Climate Research 5: 207-222.

Bates, B.C., Z.W. Kundzewicz, S. Wu and J.P. Palutikof, Eds., 2008: Climate Change and Water. Technical Paper of the Intergovernmental Panel on Climate Change, IPCC Secretariat, Geneva, 210 pp.

Brady NC, Weil RC. 2008. The Nature and Properties of Soils (14th ed). Prentice Hall, 980 pp.
Case MJ, Petersen DL. 2005. Fine-scale variability in growth–climate relationships of Douglas-fir, North Cascade Range, Washington. Canadian Journal of Forest Research-Revue Canadienne De Recherche Forestiere 35: 2743–2755 doi: 10.1139/X05-191

Cayan DR, Dettinger MD, Caprio JM, Kammerdiener SA, Peterson DH. 2001a. Comments on "Changes in the onset of spring in the western United States" - Reply. Bulletin of the American Meteorological Society 82: 2265-2266

Cayan DR, Kammerdiener SA, Dettinger MD, Caprio JM, Peterson DH. 2001b. Changes in the onset of spring in the western United States. Bulletin of the American Meteorological Society 82: 399-415

Cayan DR, Riddle LG, Aguado E. 1993. The Influence of Precipitation and Temperature on Seasonal Streamflow in California. Water Resources Research 29: 1127-1140

Christensen L, Tague CL, Baron JS. 2008. Spatial patterns of simulated transpiration response to climate variability in a snow dominated mountain ecosystem. Hydrological Processes 22: 3576–3588, DOI: 10.1002/hyp.6961

Cleavitt NL, Fahey TJ, Groffman PM, Hardy JP, Henry KS, Driscoll CT. 2008. Effects of soil freezing on fine roots in a northern hardwood forest. Canadian Journal of Forest Research 38: 82-91, DOI: 10.1139/X07-133.

Conklin MH, Liu F. 2008. Groundwater Contributions to Baseflow in the Merced River: Processes, Flow Paths, and Residence Times. California Energy Commission, PIER Energy-Related Environmental Research Program. CEC-500-2007-116.

Dettinger MD, Cayan DR. 2003. Interseasonal covariability of Sierra Nevada streamflow and San Francisco Bay salinity. Journal of Hydrology 277: 164-181
Dettinger MD, Cayan DR, Meyer M, Jeton AE. 2004. Simulated hydrologic responses to climate variations and change in the Merced, Carson, and American River basins, Sierra Nevada, California, 1900-2099. Climatic Change 62: 283-317

Earman S, Campbell AR, Phillips FM, Newman BD. 2006. Isotopic exchange between snow and atmospheric water vapor: Estimation of the snowmelt component of groundwater recharge in the southwestern United States. Journal of Geophysical Research - Atmospheres 111(D9): D09302.

Erman NA, Erman DC. 1995. Spring Permanence, Trichoptera Species Richness, and the Role of Drought. Journal of the Kansas Entomological Society 68: 50-64.

Gleick PH. 1987. The Development and Testing of a Water-Balance Model for Climate Impact Assessment - Modeling the Sacramento Basin. Water Resources Research 23: 1049-1061

Gleick PH, Chalecki EL. 1999. The impacts of climatic changes for water resources of the Colorado and Sacramento-San Joaquin River Basins. Journal of the American Water Resources Association 35: 1429-1441

Hall FR. 1968. Base-Flow Recessions-a Review. Water Resources Research 4: 973-983

Hanson RT, Newhouse MW, Dettinger MD. 2004. A methodology to assess relations between climatic variability and variations in hydrologic time series in the southwestern United States. Journal of Hydrology 287: 252-269

Hayhoe K, Cayan D, Field CB, Frumhoff PC, Maurer EP, Miller NL, Moser SC, Schneider SH, Cahill KN, Cleland EE, Dale L, Drapek R, Hanneman RM, Kalkstein LS, Lenihan J, Lunch CK,

Neilson RP, Sheridan SC, Verville JH. 2004. Emissions pathways, climate change, and impacts on California. Proceedings of the National Academy of Sciences 101: 12422-12427

Jefferson A, Nolin A, Lewis S, Tague C. 2008. Hydrogeologic controls on streamflow sensitivity to climate variation. Hydrological Processes, DOI: 10.1002/hyp.7041

Kakue T, Kishi H. 2003. Investigations and tests for evaluating the permeability of pyroxene andesite in Groundwater Engineering: Recent Advances (Kono, Nishigaki and Komatsu (eds.)), Balkema, Lisse, 459-466

Kingsmill DE, Neiman PJ, Ralph FM, White AB. 2006. Synoptic and Topographic Variability of Northern California Precipitation Characteristics in Landfalling Winter Storms Observed during CALJET. Monthly Weather Review 134: 2072-2094

Knowles N, Cayan DR. 2002. Potential effects of global warming on the Sacramento/San Joaquin watershed and the San Francisco estuary. Geophysical Research Letters 29, DOI: 10.1029/2001GL014339

Lenihan JM, Bachelet D, Neilson RP, Drapek R. 2008. Response of vegetation distribution, ecosystem productivity, and fire to climate change scenarios for California. Climatic Change 87: S215-S230.

Lettenmaier DP, Gan TY. 1990. Hydrologic Sensitivities of the Sacramento-San-Joaquin River Basin, California, to Global Warming. Water Resources Research 26: 69-86

Lettenmaier DP, Sheer DP. 1991. Climatic Sensitivity of California Water-Resources. Journal of Water Resources Planning and Management-ASCE 117: 108-125

Lettenmaier DP, Wood AW, Palmer RN, Wood EF, Stakhiv EZ. 1999. Water resources implications of global warming: A US regional perspective. Climatic Change 43: 537-579

Leung LR, Qian Y, Bian XD, Washington WM, Han JG, Roads JO. 2004. Mid-century ensemble regional climate change scenarios for the western United States. Climatic Change 62: 75-113

Leung LR, Wigmosta MS. 1999. Potential climate change impacts on mountain watersheds in the Pacific Northwest. Journal of the American Water Resources Association 35: 1463-1471

Loheide SP, Richard S. Deitchman RS, Cooper DJ, Wolf EC, Hammersmark CT, Lundquist JD. 2008. A framework for understanding the hydroecology of impacted wet meadows in the Sierra Nevada and Cascade Ranges, California, USA. Hydrogeology Journal 17: 229-246, DOI 10.1007/s10040-008-0380-4.

Lundquist JD, Cayan DR, Dettinger MD. 2004. Spring onset in the Sierra Nevada: When is snowmelt independent of elevation? Journal of Hydrometeorology 5: 327-342

Lundquist JD, Huggett B, Roop H, Low N. 2009. Use of spatially distributed stream stage recorders to augment rain gages by identifying locations of thunderstorm precipitation and distinguishing rain from snow. Water Resources Research 45: DOI:10.1029/2008WR006995

May CL, Lee DC. 2004. The relationships among in-channel sediment storage, pool depth, and summer survival of juvenile salmonids in Oregon Coast Range streams. North American Journal of Fisheries Management 24: 761-774

Millar CI, Westfall RD, Delany DL. 2007. Response of high-elevation limber pine (Pinus flexilis) to multiyear droughts and 20th-century warming, Sierra Nevada, California, USA. Canadian Journal of Forest Research-Revue Canadienne De Recherche Forestiere 37: 2508-2520

Mote PW, Hamlet AF, Clark MP, Lettenmaier DP. 2005. Declining mountain snowpack in western North America. Bulletin of the American Meteorological Society 86: 39-49, DOI: 10.1175/BAMS-86-1-39

Nichols WD. 1994. Groundwater discharge by phreatophyte shrubs in the Great Basin as related to depth to groundwater. Water Resources Research 30: 3265-3274.

Panagoulia D, Dimou G. 1996. Sensitivities of groundwater-streamflow interaction to global climate change. Hydrological Sciences Journal 41: 781-796

Perkins RM, Jones JA. 2008. Climate variability, snow, and physiographic controls on storm hydrographs in small forested basins, western Cascades, Oregon. Hydrological Processes, DOI: 10.1002/hyp.7117

Post DA and Jakeman AJ. 1998. Relationships between catchment attributes and hydrological response characteristics in small Australian mountain ash catchments. Hydrological Processes 10: 877-892

Price DG. 2009. Engineering geology: principles and practice (de Freitas MH, ed.), Springer-Verlag, Berlin, 450 pp.

Price MV, Waser NM.1998. Effects of experimental warming on plant reproductive phenology in a subalpine meadow. Ecology 79:1261-1271.

Rademacher LK, Clark JF, Clow DW, Hudson GB. 2005. Old groundwater influence on stream hydrochemistry and catchment response times in a small Sierra Nevada catchment: Sagehen Creek, California. Water Resources Research 41, DOI: 10.1029/2003WR002805

Risbey JS, Entekhabi D. 1996. Observed Sacramento Basin streamflow response to precipitation and temperature changes and its relevance to climate impact studies. Journal of Hydrology 184: 209-223

Royce EB, Barbour MG. 2001. Mediterranean climate effects. II. Conifer growth phenology across a Sierra Nevada ecotone. American Journal of Botany 88: 919-932.

Running SW, Nemani RR. 1991. Regional hydrologic and carbon balance responses of forests resulting from potential climate change. Climatic Change 19: 349-368

Shun T, Duffy C. 1999. Low-frequency oscillations in precipitation, temperature, and runoff on a west facing mountain front: A hydrogeologic interpretation. Water Resources Research 35: 191-201

Singh KP. 1968. Some factors affecting baseflow. Water Resources Research 4: 985-999

Stewart IT, Cayan DR, Dettinger MD. 2004. Changes in snowmelt runoff timing in western North America under a 'business as usual' climate change scenario. Climatic Change 62: 217-232

Sylvester AF, Raines FL and students. 2007. Geology of the Sagehen Creek and Independence Lake hydrologic basins, Sierra and Nevada counties, California. Available at: http://www.geol.ucsb.edu/projects/tahoe/Sagehen/SageAbs01.html

Tague C, Grant G. 2009. Groundwater dynamics mediate low flow response to global warming in snow-dominated alpine regions. Water Resources Research 45: DOI:10.1029/2008WR007179
Tague C, Grant G, Farrell M, Choate J, Jefferson A. 2008. Deep groundwater mediates streamflow response to climate warming in the Oregon Cascades. Climatic Change 86: 189-210

Tague CL, Band LE. 2004. RHESSys: Regional Hydro-Ecologic Simulation System - An Object-Oriented Approach to Spatially Distributed Modeling of Carbon, Water and Nutrient Cycling. Earth Interactions 8: 1-42

Tallaksen LM. 1995. A Review of Baseflow Recession Analysis. *Journal of Hydrology* 165: 349-370

van Mantgem PJ, Stephenson NL. 2007. Apparent climatically induced increase of tree mortality rates in a temperate forest. Ecology Letters 10: 909-916

Weih M, Karlsson PS. 2002. Low winter soil temperature affects summertime nutrient uptake capacity and growth rate of mountain birch seedlings in the subarctic, Swedish Lapland. Arctic, Antarctic, and Alpine Research 34:434-439.

White JD, Running SW, Nemani R, Keane RE, Ryan KC. 1997. Measurement and remote sensing of LAI in Rocky Mountain montane ecosystems, Canadian Journal of Forest Research 27: 1714-1727.

White WN. 1932. A method of estimating ground-water supplies based on discharge by plants and evaporation from soil--results of investigations in Escalante Valley, Utah, Water Supply Paper Report Number 659-A. US Geological Survey.

Winograd IJ, Riggs AC, Coplen TB. 1998. The relative contributions of summer and cool-season precipitation to groundwater recharge, Spring Mountains, Nevada, USA. Hydrogeology Journal 6(1): 77-93.

Figure Captions

Figure 1. Gray lines are time series plots of (a) daily 15-day running median snow water equivalent (SWE) at the Independence Lake Snow Telemetry (SNOTEL) site located on the divide between the Sagehen Creek and Independence Lake basins, and (b) daily 15-day running median flow at Sagehen Creek (Q, log-scale). The minimum flow in Sagehen Creek varies from year to year, partly in response to changes in peak SWE, as indicated by the black cubic spline curves in (a) and (b).

Figure 2. Map of stream gauge and snow pillow locations selected for this study. See Table 1 for site information.

Figure 3. Relative minimum runoff, Q, as a function of relative maximum snow water equivalent, SWE, for each study catchment. The solid lines indicate the best-fit regression lines for each catchment. In most cases, the solid line has a slope that is significantly steeper than 1, indicating a more-than-proportional runoff response to changes in snowpack. The x-intercepts (shown on the truncated x-axes) of the best-fit lines also indicate that streams may run dry with relatively small decreases (~45% or more) from current average peak SWE. Data points alternate between black and gray solely to visually distinguish sites from one another.

Figure 4. Average of the annual hydrograph for the wettest (black) and driest (gray) five years of record at Sagehen Creek. Low flows are lower and reach a minimum value earlier in dry years than in wet years. The peak flow also occurs substantially earlier in dry years relative to wet ones.

Figure 5. The timing of melt out and the middle of the minimum flow period (as day of year) for all study catchments, plotted as functions of the relative maximum snowpack (SWE) with overall best-fit line shown. The upper graph (a) shows deviations from the mean first day of zero snowpack. The lower graph (b) shows deviations from the mean day of the low-flow period. The overall trends indicate that a 10% decrease in maximum SWE will result in snowmelt and the low-flow period occurring ~3-7 days earlier in the year. The low-flow period is defined as the range of days with flow less than the 25th percentile of flow (see text).

Figure 6. The annual minimum flow at (a) Sagehen Creek and (b) Pitman Creek depends not only on the current year's snowpack, but also on the snowpack of the previous year as measured at the Independence Lake or Tamarack Summit SNOTEL sites. Relative minimum flow (Q) is plotted as a function of the current year's relative maximum snowpack (SWE), normalized as described in the text and Figure 3. Two subsets of data are distinguished: the closed symbols indicate when the previous year's SWE was above average and the open symbols indicate when the previous year's SWE was below average. When the previous year's SWE is above average, minimum Q is more sensitive to the current year's maximum SWE. Two high-flow years (1983 and 1998) in Pitman are indicated in (b); without these years, there is no statistically significant memory effect.

Figure 7. Relative minimum runoff, Q, vs. relative maximum snowpack, SWE, in RHESSYS model results for the (a) Upper Merced and (b) Sagehen catchments under the base scenario of

no warming (black squares) and under the 4°C warming case (open circles). Note that the warming case exhibits a similar trend to the base case, but is limited to a smaller range of both flow and snowpack water content, that is, it is telescoped down to the lower left quadrant of the plots.

Figure 8. Time series for different elements of the water budget for the Upper Merced River. Black is the 4°C warming case and gray is the no-forcing case, representing the reference or current climate conditions. Shown are mean values for the given day of year across the entire record for (a) rainfall (mm/d), (b) 15-day running median snow water equivalent, SWE (mm), (c) 15-day running median flow (mm/d), note logarithmic scale on y-axis, (d) 15-day running median evapotranspiration (mm/d), (e) net change in storage (mm/d).

Figure 9. Time series for different elements of the water budget for Sagehen Creek. Panels and legend are as described in the caption for Figure 8.

Figure 10. Phase-change-only 4°C warming scenario time series for different elements of the water budget for the Upper Merced River. Panels are as described in the caption for Figure 8 and gray represents the reference no-forcing current climate scenario whereas black lines represent the phase-change only warming scenario (see text).

Figure 11. Phase-change-only 4°C warming scenario time series for different elements of the water budget for Sagehen Creek. Panels are as described in the caption for Figure 8 and gray still represents the reference no-forcing current climate scenario whereas black lines represent the phase-change only, 4°C warming scenario (see text).

Table Captions

Table 1. Site information for the eight study catchments in the Sierra Nevada. The last two columns indicate the best-fit slope and *x*-intercept of the minimum annual 15-day running median flow vs. the maximum annual 15-day running median snow water equivalent (SWE), as shown in Figure 3. The *x*-intercept value indicates the fraction of normal peak SWE at which low flows cease. The asterisk on the Pitman Creek values indicate that these are the linear best-fit parameter estimates, but as seen in Figure 3, the relationship is likely non-linear, and these values only broadly indicate the trend of the low-flow response to changes in SWE.

Table 2. Summary of changes observed in different components of the water budgets modeled by RHESSys for the current climate scenario and the 4°C warming scenarios that include or exclude vegetation warming responses for two sites in the Sierra Nevada mountains. The lower portion of the table indicates shifts in timing in units of days from the base case. Superscripts: a=differences in total annual rainfall between the two warming scenarios are due to variations in melting of the snowpack on days with precipitation; b=seasons are defined by Julian day (see text); c=15-day running median ET.

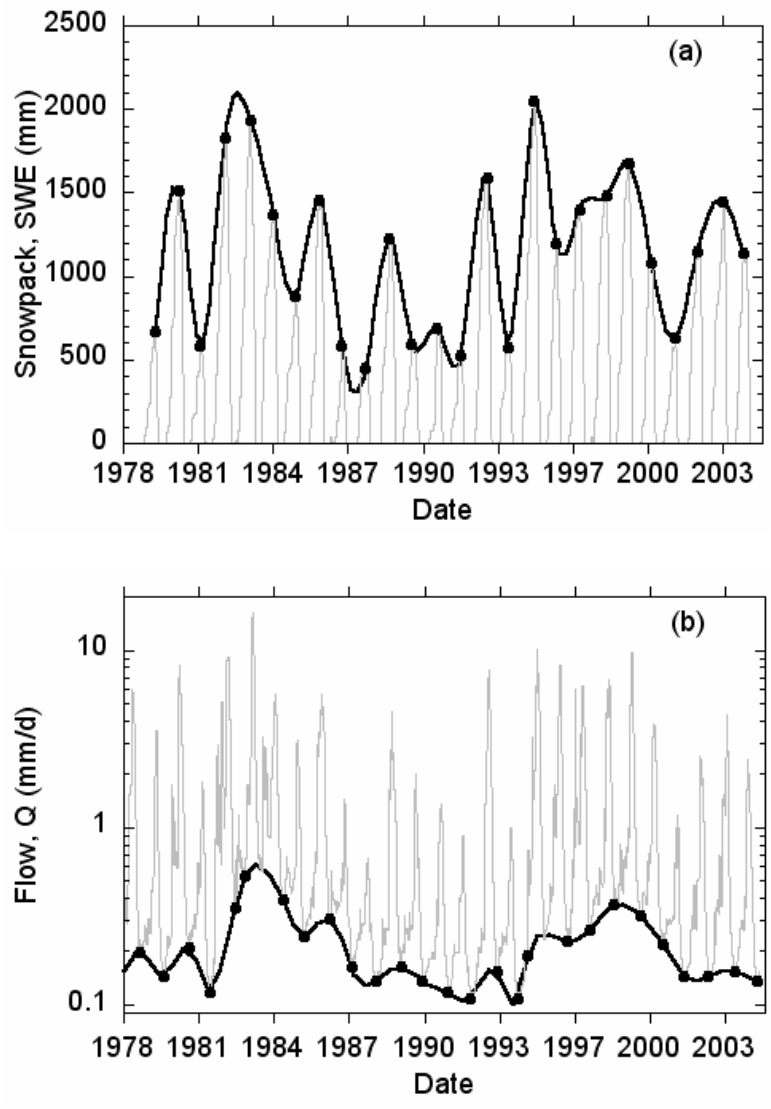
(a)
Snowpack, SWE (mm)
2500
2000
1500
1000
500
0
1978 1981 1984 1987 1990 1993 1997 2000 2003
Date
(b)
Flow, Q (mm/d)
10
1
0.1
1978 1981 1984 1987 1990 1993 1997 2000 2003
Date

Figure 1.

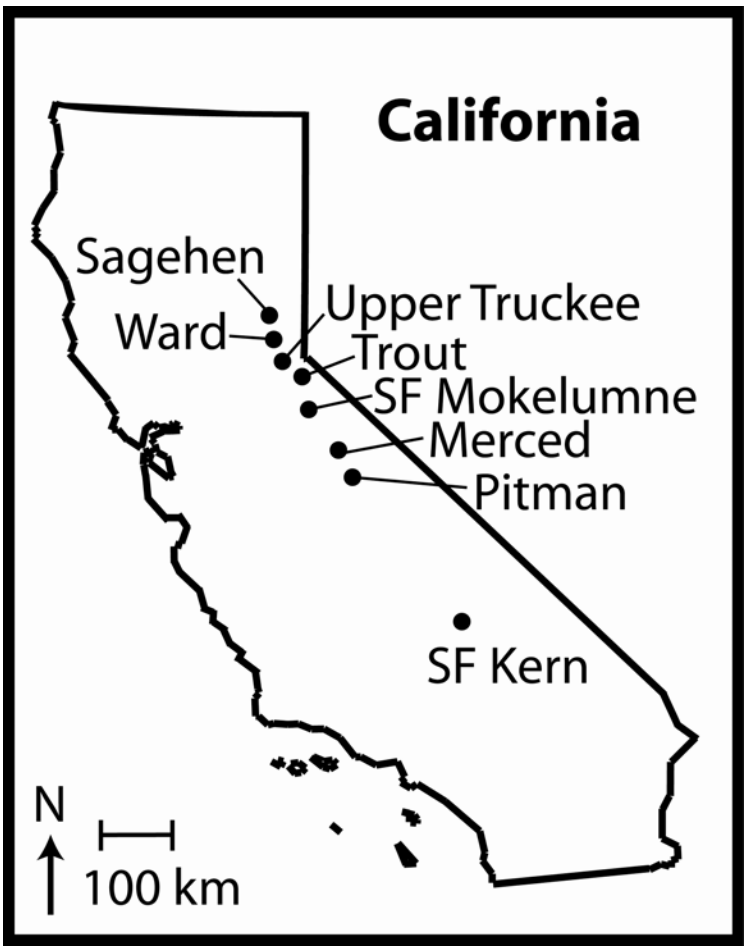
California
Sagehen
Ward
Upper Truckee
Trout
SF Mokelumne
Merced
Pitman
SF Kern
N
100 km

Figure 2.

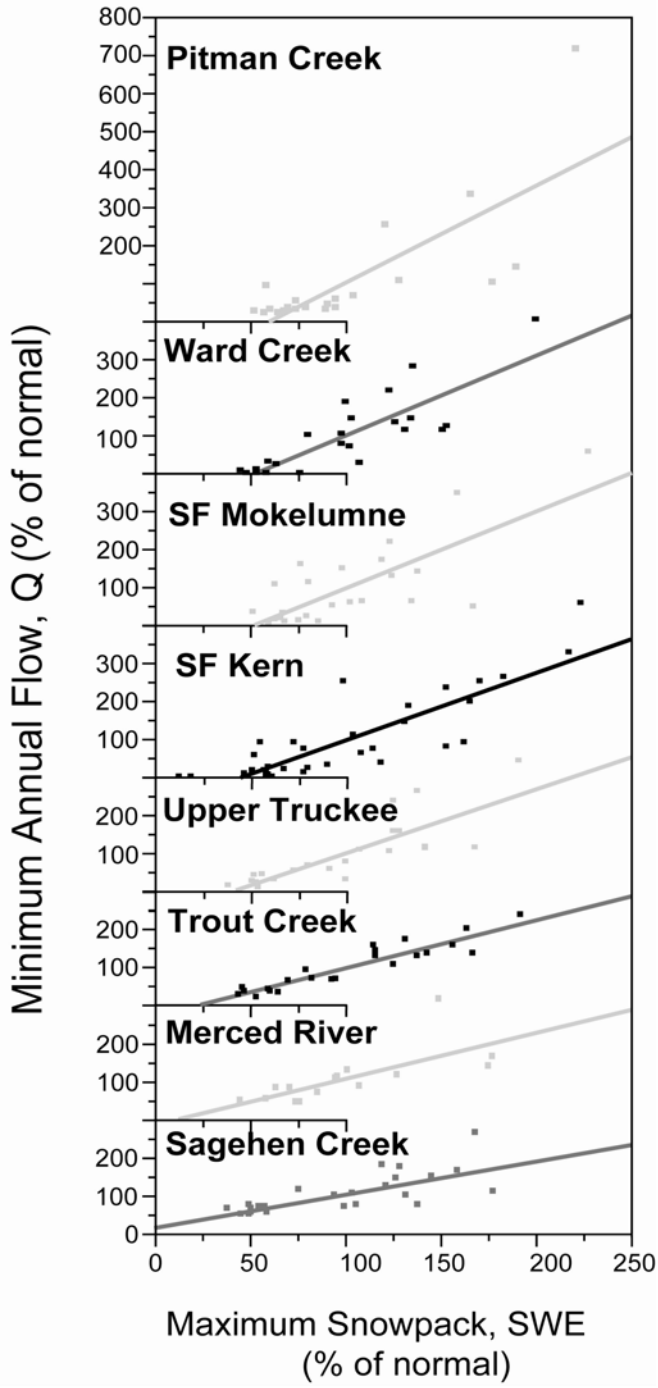
Pitman Creek
Ward Creek
SF Mokelumne
SF Kern
Upper Truckee
Trout Creek
Merced River
Sagehen Creek
Minimum Annual Flow, Q (% of normal)
Maximum Snowpack, SWE
(% of normal)
0
50
100
150
200
250

Figure 3.

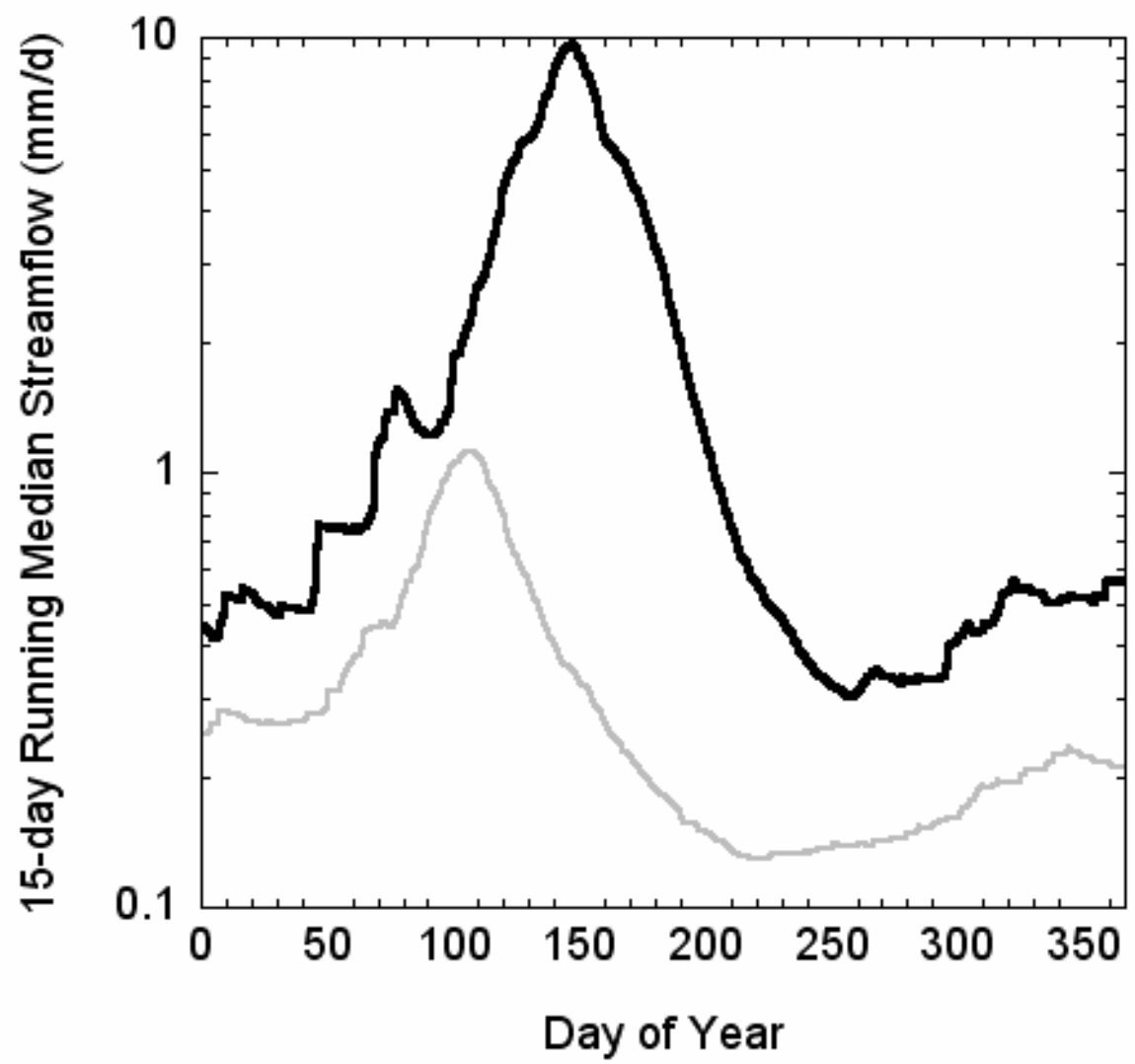
10
1
0.1
15-day Running Median Streamflow (mm/d)
0
50
100
150
200
250
300
350
Day of Year

Figure 4.

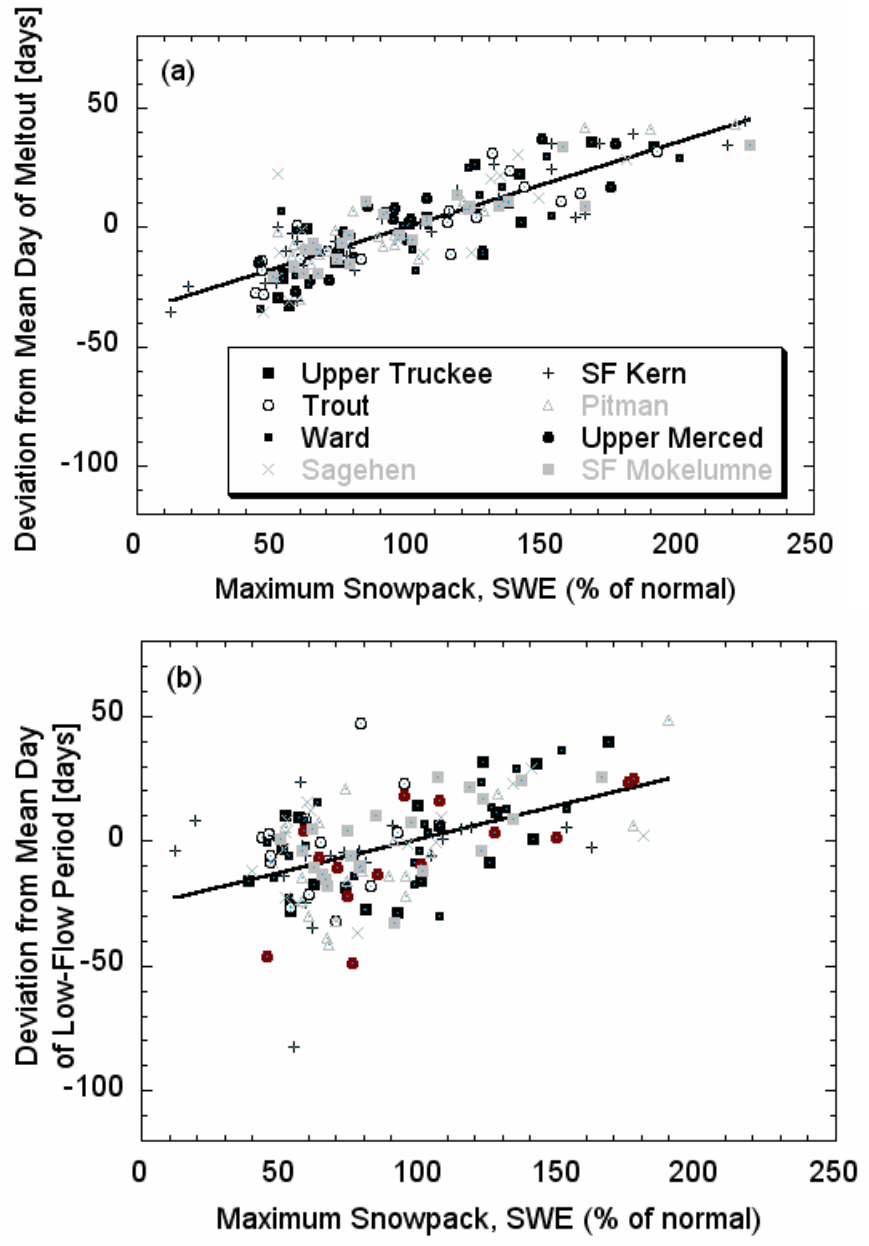
(a)
Deviation from Mean Day of Meltout [days]
50
0
-50
-100
0
50
100
150
200
250
Maximum Snowpack, SWE (% of normal)
Upper Truckee
Trout
Ward
Sagehen
SF Kern
Pitman
Upper Merced
SF Mokelumne
(b)
Deviation from Mean Day of Low-Flow Period [days]
50
0
-50
-100
0
50
100
150
200
250
Maximum Snowpack, SWE (% of normal)

Figure 5.

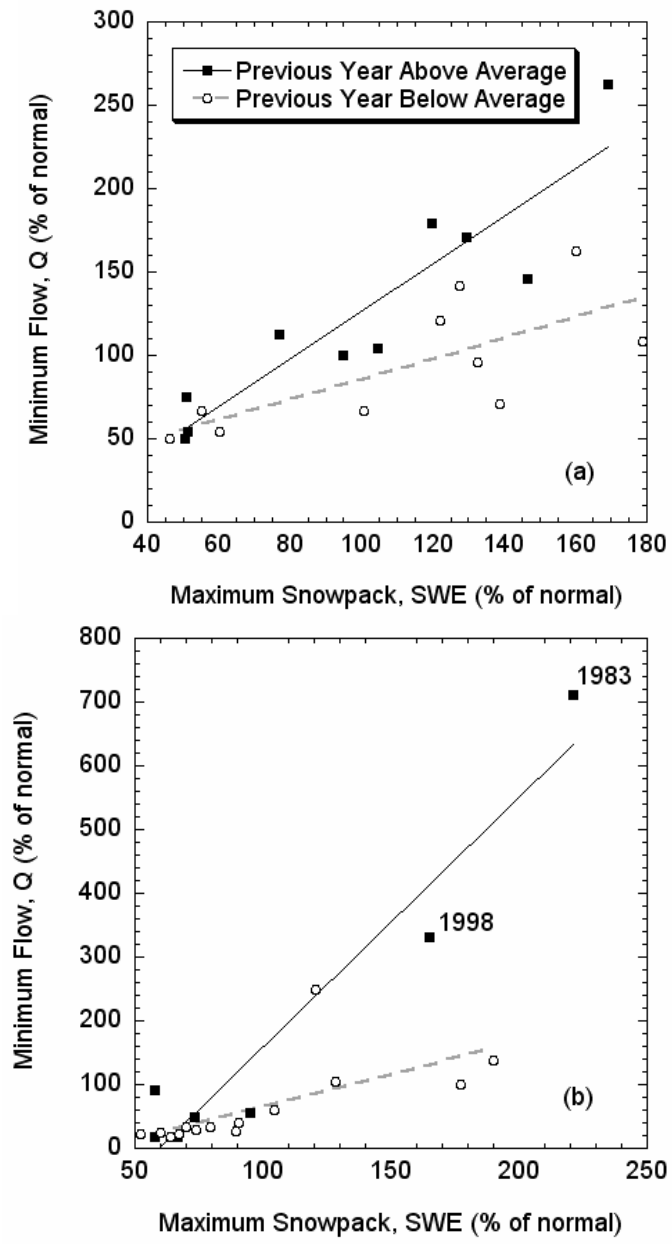
Previous Year Above Average
Previous Year Below Average
Minimum Flow, Q (% of normal)
Maximum Snowpack, SWE (% of normal)
(a)
1983
1998
(b)

Figure 6.

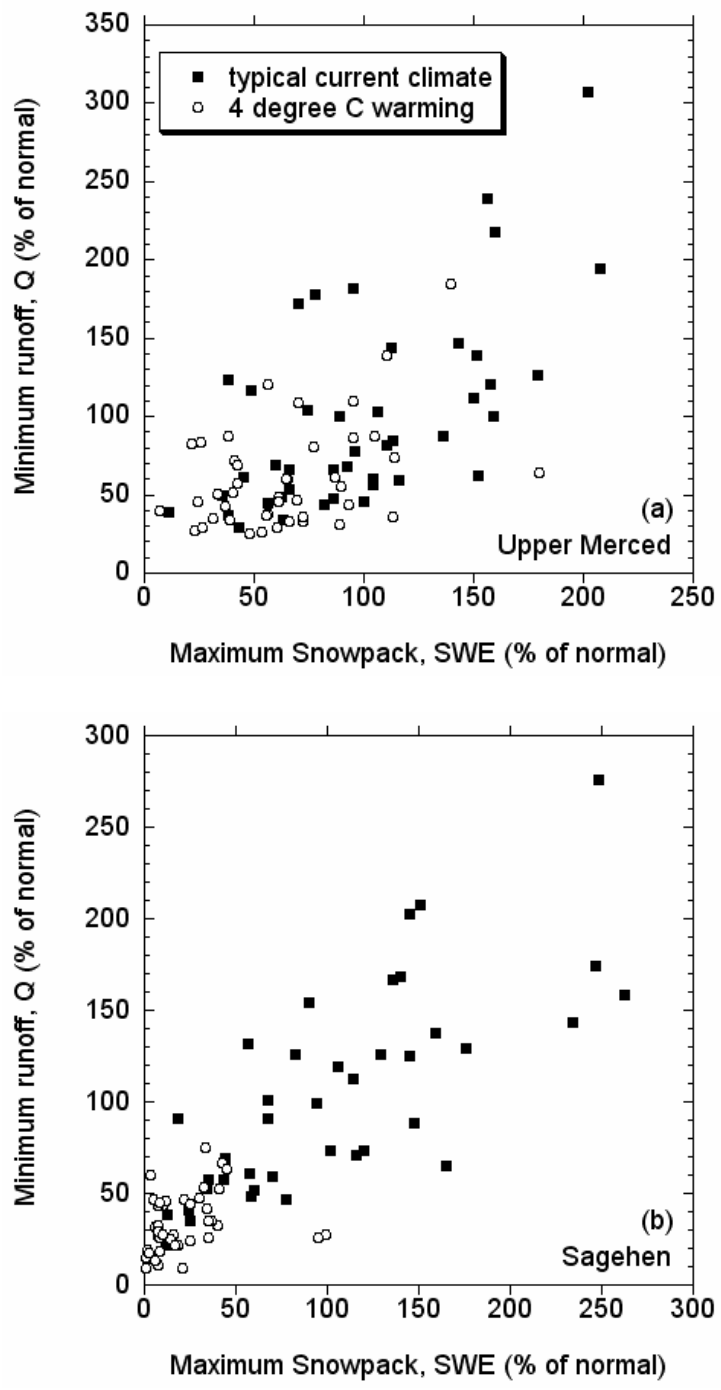
typical current climate
4 degree C warming
Minimum runoff, Q (% of normal)
Maximum Snowpack, SWE (% of normal)
(a)
Upper Merced
(b)
Sagehen
0
50
100
150
200
250
300
350

Figure 7.

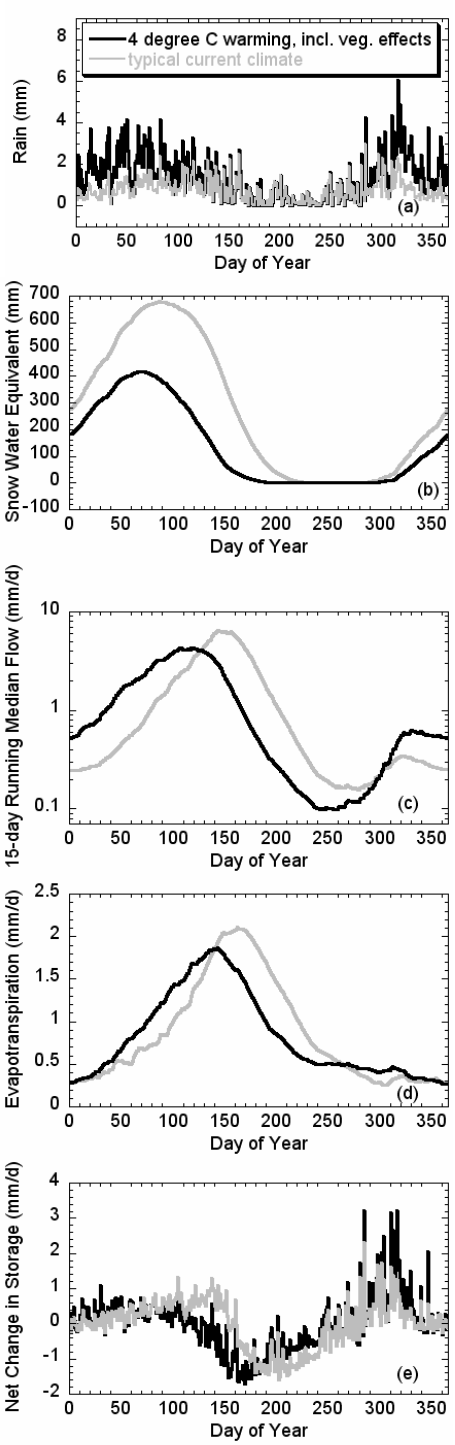
4 degree C warming, incl. veg. effects
typical current climate
Rain (mm)
(a)
Day of Year
Snow Water Equivalent (mm)
(b)
Day of Year
15-day Running Median Flow (mm/d)
(c)
Day of Year
Evapotranspiration (mm/d)
(d)
Day of Year
Net Change in Storage (mm/d)
(e)
Day of Year

Figure 8.

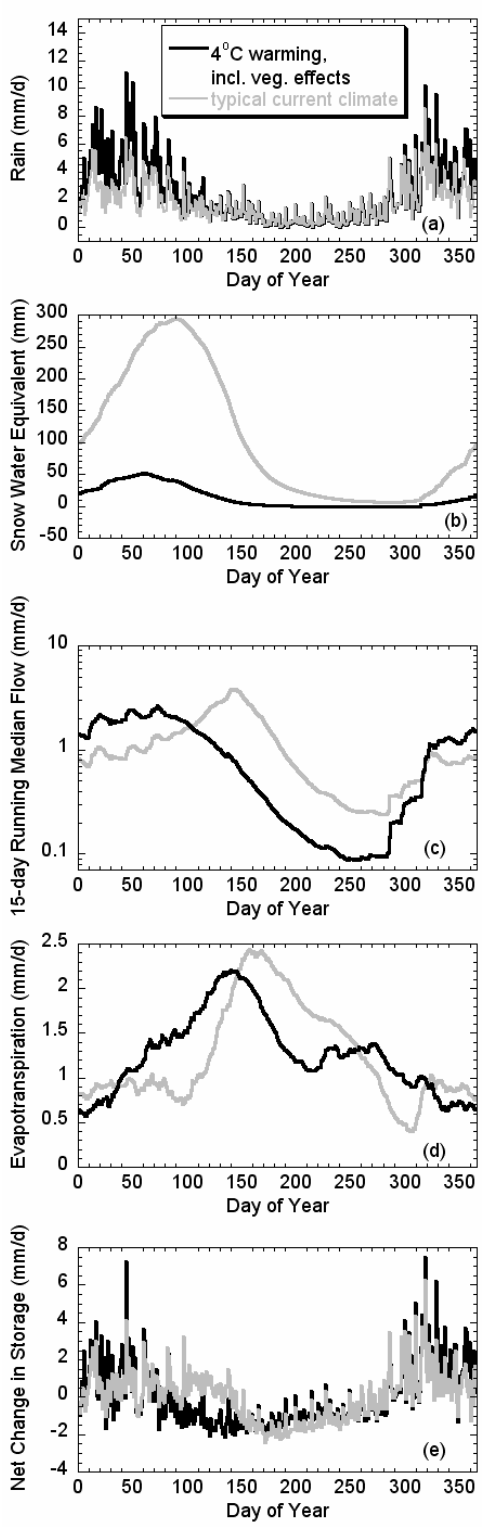
4°C warming,
incl. veg. effects
typical current climate
Rain (mm/d)
Snow Water Equivalent (mm)
15-day Running Median Flow (mm/d)
Evapotranspiration (mm/d)
Net Change in Storage (mm/d)
Day of Year
(a)
(b)
(c)
(d)
(e)

Figure 9.

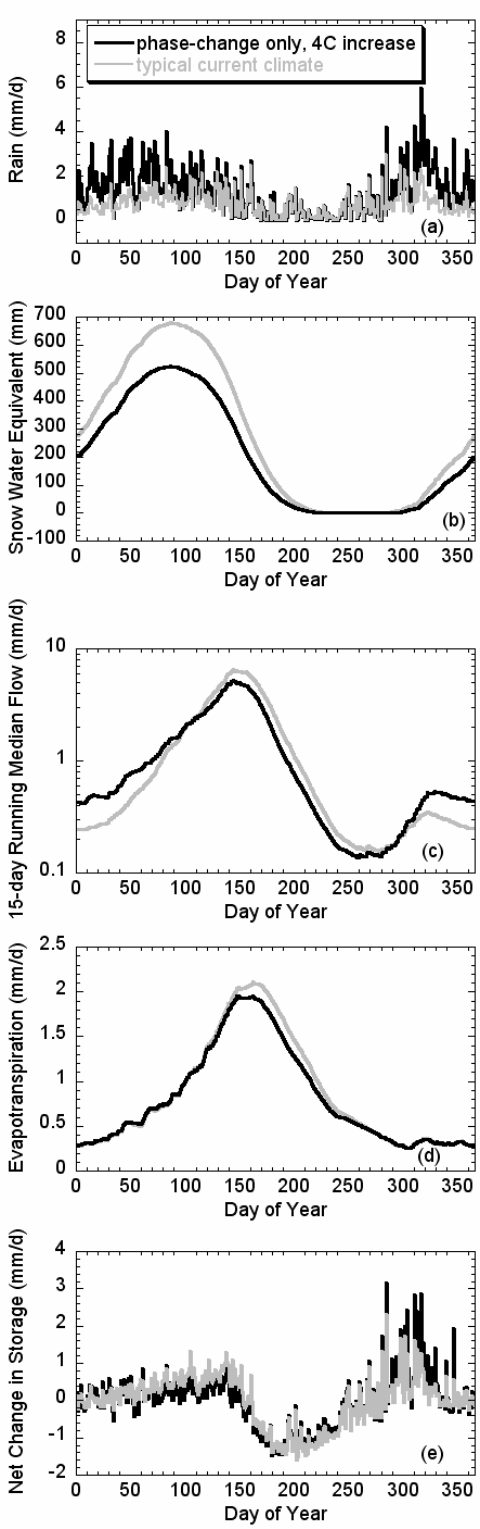
phase-change only, 4C increase
typical current climate
Rain (mm/d)
(a)
Day of Year
Snow Water Equivalent (mm)
(b)
Day of Year
15-day Running Median Flow (mm/d)
(c)
Day of Year
Evapotranspiration (mm/d)
(d)
Day of Year
Net Change in Storage (mm/d)
(e)
Day of Year
Figure 10.

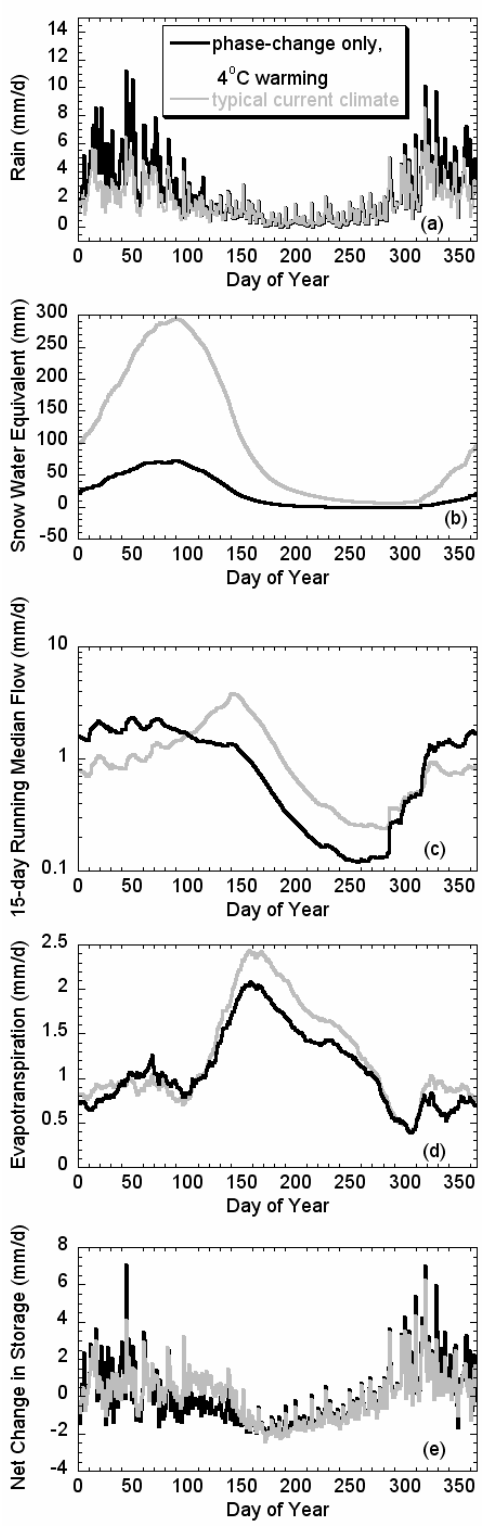
phase-change only,
4°C warming
typical current climate
Rain (mm/d)
Snow Water Equivalent (mm)
15-day Running Median Flow (mm/d)
Evapotranspiration (mm/d)
Net Change in Storage (mm/d)
Day of Year
(a)
(b)
(c)
(d)
(e)

Figure 11.

Name		Altitude (m)		Drainage Area (km^2)	Years of overlapping record	Snowpack vs. Q (% of normal)	
Snow Pillow	**Stream Gauge**	**Snow Pillow**	**Stream Gauge**			**Regression Slope (± s.e.)**	**x-intercept (± s.e.)**
Tamarack Summit (TMR)	Pitman Creek below Tamarack Creek	2349	2184	59	22	2.55 (0.47)*	61 (23)*
Ward Creek 3 (WC3)	Ward Creek at Hwy 89 near Tahoe Pines	2100	1948	25	23	2.08 (0.30)	52(17)
Black Springs (BLS)	SF Mokelumne near West Point	2022	607	195	24	2.02 (0.36)	51 (21)
Upper Tyndall Creek (UTY)	SF Kern River near Onyx	3547	902	1373	33	1.74 (0.19)	42 (13)
Echo Peak 5 (EP5)	Upper Truckee River at South Lake Tahoe	2427	1938	142	22	1.69 (0.26)	41(18)
Heavenly Valley (HVN)	Trout Creek near Tahoe Valley	2738	1942	95	24	1.25 (0.10)	20(9)
Ostrander Lake (STR)	Upper Merced River at Happy Isles Bridge near Yosemite	2551	1250	469	15	1.12 (0.30)	10 (30)
Independence Lake (IDP)	Sagehen Creek near Truckee	2629	1966	27	24	0.84 (0.16)	-19 (22)

Table 1.

	Sagehen			Upper Merced		
	base case, current climate	**4C warming, ppt phase change only**	**4C warming, ppt phase change + vegetation response**	**base case, current climate**	**4C warming, ppt phase change only**	**4C warming, ppt phase change + vegetation response**
annual average streamflow [mm/yr]	469	503	461	799	815	815
average annual rainfall [mm/yr]^a	663	910	914	278	481	505
average annual evapotranspiration [mm/yr]	507	475	519	314	299	299
gross recharge fluxes into groundwater storage [mm/yr]	459	549	560	195	228	245
annual average 15-d running median peak SWE [mm]	321	84	69	729	562	473
annual average 15-d running median low flow [mm/d]	0.16	0.08	0.05	0.11	0.10	0.07
std dev peak SWE [mm]	221	82	71	344	279	253
std dev low flow [mm/d]	0.09	0.05	0.03	0.07	0.07	0.04
winter net recharge (NR)^b [mm/season]	56	85	108	7	8	18
spring net recharge^b [mm/season]	44	-30	-64	53	29	6
summer net recharge^b [mm/season]	-136	-120	-99	-83	-81	-75
fall net recharge^b [mm/season]	59	86	76	23	45	52
winter ET^b,c [mm/season]	80	73	72	34	34	39
spring ET^b,c [mm/season]	113	110	159	110	108	131
summer ET^b,c [mm/season]	181	151	130	134	120	88
fall ET^b,c [mm/season]	84	75	103	38	38	43
std dev winter NR [mm/d]	1.0	1.5	1.5	0.2	0.3	0.4
std dev spring NR [mm/d]	0.8	0.9	1.0	0.3	0.3	0.5
std dev summer NR [mm/d]	0.5	0.5	0.5	0.4	0.4	0.5
std dev fall NR [mm/d]	1.5	1.7	1.8	0.6	0.8	0.9
timing [Julian day]						
melt-out	228	202	173	214	209	184
peak 15-d running median flow	141	50	73	144	144	119
minimum 15-d running median flow	282	257	257	279	259	259
peak 15-d running median net recharge	120	314	316	138	139	84
peak 15-d running median evapotranspiration rate	157	158	140	164	150	134

Table 2.

Chapter Four

Concentration-discharge relationships reflect chemostatic characteristics of US catchments

Published in Hydrological Processes

Abstract

Concentration-discharge relationships have been widely used as clues to the hydrochemical processes that control runoff chemistry. Here we examine concentration-discharge relationships for solutes produced primarily by mineral weathering in 59 geochemically diverse US catchments. We show that these catchments exhibit nearly chemostatic behavior; their stream concentrations of weathering products such as Ca, Mg, Na, and Si typically vary by factors of only 3-20 while discharge varies by several orders of magnitude. Similar patterns are observed at the inter-annual time scale. This behavior implies that solute concentrations in stream water are not determined by simple dilution of a fixed solute flux by a variable flux of water, and that rates of solute production and/or mobilization must be nearly proportional to water fluxes, both on storm and inter-annual timescales. We compared these catchments' concentration-discharge relationships to the predictions of several simple hydrological and geochemical models. Most of these models can be forced to approximately fit the observed concentration-discharge relationships, but often only by assuming unrealistic or internally inconsistent parameter values. We propose a new model that also fits the data and may be more robust. We suggest possible tests of the new model for future studies. The relative stability of concentration under widely varying discharge may help make aquatic environments habitable. It also implies that fluxes of weathering solutes in streams, and thus fluxes of alkalinity to the oceans, are determined primarily by water fluxes. Thus hydrology may be a major driver of the ocean-alkalinity feedback regulating climate change.

Introduction

Chemical weathering and solute transport are coupled with hydrology in catchments, and this coupling is reflected in the relationships between solute concentrations and stream discharge. Catchment hydrologists often study concentration-discharge relationships because the necessary data are frequently available and the initial analysis is straightforward. However, despite decades of work, there are still open questions about what concentration-discharge relationships can tell us about catchment behavior.

Concentrations of the major base cations and silica have generally been observed to decrease with discharge (Hem, 1948 & 1985; Johnson *et al.*, 1969 and references therein; Waylen, 1979; Walling and Webb, 1986; Clow and Drever, 1996). Typical concentration-discharge analyses have centered on mixing models of different source waters (*e.g.*, event and pre-event water; old and new water; or soil water, groundwater and precipitation) inferred from the shape of the concentration-discharge relationship for different solutes (Johnson *et al.*, 1969; Hall, 1970, 1971). In other studies, researchers have inferred the relative timing of mixing from hysteresis loops observed in concentration-discharge plots (Evans and Davies, 1998; Evans *et al.*, 1999; House and Warwick, 1998; Hornberger *et al.*, 2001; Chanat *et al.*, 2002). Evans and Davies (1998) proposed that the form and direction of hysteresis loops could uniquely identify the rank order of end-member concentrations in a three end-member mixing scenario. However, Chanat *et al.* (2002) showed that even the small number of assumptions required for this identification are not always valid, and that when the assumptions are violated, hysteresis loops cannot definitively distinguish the relative concentrations of different end-members. Nonetheless, other characteristics of concentration-discharge relationships may provide insight into the coupling of chemical weathering and hydrological processes in catchments.

In this paper, we identify common features of concentration-discharge relationships across a range of hydrochemically distinct catchments with minimal human impacts, and discuss the implications of those features. We then compare several simple models against the observed patterns in concentration-discharge relationships and evaluate whether their assumptions are generally valid across the study sites. Finally, we show that the concentration-discharge relationships observed in many catchments imply that changes in stream solute fluxes as a result of climatic forcing are, to first order, dependent upon changes in hydrology.

Observations

We plotted concentrations of the major weathering-derived cations (Mg, Na and Ca) and dissolved silica (Si) against instantaneous discharge on logarithmic axes for 59 sites in the United States Geological Survey's (USGS) Hydrologic Benchmark Network (HBN) (*e.g.*, Figure 1, discussed further below). The HBN was established in the mid-1960's to provide a long-term database to track changes in the flow and water quality of undisturbed streams and rivers, and to serve as a reference, or "benchmark," for discerning natural from human-induced changes in river ecosystems (Leopold, 1962). Most HBN sites have more than 30 years of hydrochemical data, and water samples were typically collected 5-7 times per year using standard USGS methods (Wilde *et al.*, 1998). The HBN is the only nationwide network of environmental monitoring sites that tracks the health of rivers draining mid-sized, undisturbed basins in the United States. The sites are located throughout the country, usually in National Parks, National Forests or reserves where minimal human influence is expected. Site characteristics compiled from USGS circulars (Mast and Turk, 1999a&b; Clark *et al.*, 2000; Mast and Clow, 2000) are summarized in Table 1. Drainage areas range from 6.1 to 5196 km^2 (median=146 km^2) and average annual runoff varies from 0.7 to 400 cm/yr (median=40 cm/yr). Many environments in the US are represented, including tropical forests, tundra and eight sites with <10 cm average annual runoff, which include arid and semi-arid grasslands, shrublands and semi-desert areas. Most catchments are forested, but several of the basins have substantial alpine and grassland areas. The 59 sites encompass a wide range of lithologic settings (Table 1). Solute concentrations in precipitation are not available at all sites for the entire period of record, so the reported concentrations are not corrected by the precipitation chemistry. Stream concentrations of Ca, Na and Mg are at least 10 to 100 times higher than available mean precipitation concentrations. Si concentrations in rainfall are not typically measured, but are normally orders of magnitude lower than Si concentrations in streamflow.

We plotted the concentrations of each of the major weathering-derived solutes against instantaneous discharge. We then calculated simple linear regression statistics for each of the sites and solutes, and, using Student's t test, determined whether the best-fit slope was significantly different from reference slopes of zero and -1 (whose meaning is discussed in detail below). We identified sites with nonlinear relationships between log concentration and log discharge by examining the residuals of the linear fit. Most of the catchments in the Hydrologic Benchmark Network exhibit much less variability in concentrations than in discharge (Figure 1). Figure 1 shows concentration as a function of discharge on logarithmic axes, with the same number of log units shown on each axis to facilitate a visual comparison of the relative variability of concentration and discharge. For example, between high flow and low flow, concentrations at Elder Creek increase by factors of 3 (Ca and Mg), 2.6 (Na), and 1.5 (Si), as

discharge changes by a factor of ~6000. Although not plotted in Figure 1, similar relationships also hold for Mg across the HBN sites.

As seen in Figure 1, concentration-discharge plots are often linear on logarithmic axes, indicating that there is a power-law relationship between concentration, C, and discharge, Q (i.e., $C = aQ^b$, where a and b are constants). The exponent in this power-law relationship (or equivalently, the slope of the concentration-discharge relationship on logarithmic axes) has a physical interpretation. A slope of zero would indicate that the catchment behaves chemostatically, that is, the system keeps concentrations constant as discharge varies. A slope of -1, on the other hand, would indicate that concentrations vary inversely with discharge, as might be expected if dilution were the dominant process controlling concentrations, such that approximately constant fluxes of solutes were diluted by variable fluxes of water.

Power-law concentration-discharge relationships like those shown in Figure 1 can be usefully summarized by their log-log slopes. The best-fit log(C)-log(Q) slopes for each solute can then be compared across all 59 of the HBN sites (Figure 2) and can be compared to reference slopes of zero (chemostatic behavior) and -1 (dilution). Uncertainty in the best-fit slope of +/-1 standard error (s.e.) is indicated by error bars, which are shown if they are larger than the plotting symbols. Across all sites, slopes are generally slightly less than zero. The means of the best-fit log-log concentration-discharge slopes vary between approximately -0.05 and -0.15 (standard error of the slope ~0.01-0.02) for each of the solutes. No slope is within two standard errors of -1 and only four (Na), six (Mg), eight (Ca) and 14 (Si) of the 59 sites have slopes within two standard errors of zero. Slopes across all sites and solutes are strikingly similar. In general, Si slopes are closer to zero than the slopes of the other solutes. With few exceptions (discussed below), nearly all of the concentration-discharge relationships in this study can be described by power-law relationships with small negative exponents. The data in Figure 2 show that most catchments behave almost chemostatically for chemical weathering products such as Ca, Mg, Na and Si.

Although this near-chemostatic behavior is common, examination of residual plots for all sites and solutes reveals that the best fits for up to 10% of the sites may not be power-law. Such sites are marked by open circles in Figure 2 and the plotted slope of the linear fit only provides a general sense of the concentration-discharge relationship for these sites. We also calculated the ratio of the standard deviation of log discharge to log concentration for all sites and solutes (not shown) to quantify the relative variability of discharge and concentration without making any assumptions about the form of the concentration-discharge relationship. Only Upper Three Runs, SC had Ca and Mg concentrations that were more variable than its discharge, and only Castle Creek, SD and Dismal River, NE had more variable Na concentrations. No sites had Si concentrations that were more variable than discharge. The ratio of the standard deviations of log discharge to log concentration ranged from just below 1 to 21.5, with the median ratio equal to 4.1 (Ca), 4.0 (Mg and Na), and 5.3 (Si). These observations reinforce the inference drawn from the shallow power-law slopes, namely that these catchments behave almost chemostatically. We also verified that the samples collected are representative of the range of flows at each site. At all sites, samples are collected across a range of flows from the 5th to 97th flow percentiles (as calculated from the complete flow record reported in the USGS National Water Information System database, excluding dates on which flow is zero). Most sites include samples from the 1st

to 99th percentiles of flow, and median HBN samples corresponded approximately to the 52nd flow percentile, suggesting that baseflows are not oversampled.

A handful of sites have positive slopes for one or more solutes, which indicate that concentration increases with increasing flow (*e.g.*, Upper Three Runs, SC for Ca and Mg and Steptoe Creek, NV for Na). In past studies, increased concentrations of more biologically active ions such as K^+ and NO_3^- with increased flow have been attributed to leaching from organic soil horizons during higher flows (Walling and Webb, 1986). At the HBN sites, the observed increase in concentration of the major weathering products with discharge may be due to a weak correlation between discharge and concentration, or due to limited variability in the sampled discharge (*e.g.*, discharge varies by only a factor of ~4 at Upper Three Runs). At Upper Three Runs, it also may be a result of analytical error or instrumentation changes in very dilute stream waters (Mast and Turk, 1999a, pp. 108-110). However, most sites show little variability in concentration with discharge and we focus on these sites for the rest of this paper.

One might postulate that concentrations are relatively constant across wide ranges of discharge simply because the volume of water stored in a catchment is much larger than the amount discharged during an individual storm event. Therefore we also tested whether catchments behave chemostatically on inter-annual time scales. Annualized concentration-discharge relations for each of the HBN sites were plotted as mean annual flow-weighted concentrations against annual water yield. Water yield was calculated by summing all daily flows in the water year, as available from the daily USGS streamflow record, and dividing by catchment area. Mean flow-weighted concentrations were calculated as $\Sigma(Q_iC_i)/\Sigma Q_i$, where the subscript i indicates each sample during the water year. We excluded years with fewer than four available concentration measurements from the inter-annual concentration-discharge analysis.

The plots of mean annual flow-weighted concentrations vs. annual water yield exhibit similar patterns to those observed on an event basis (Figures 3 and 4). Mean annual concentrations vary much less than water yield does from year to year. The concentration-discharge plots for inter-annual time scales (Figure 3) are similar to those for individual samples (Figure 1); both exhibit power-law relationships between solute concentrations and water yields, with small negative log-log slopes. Across the HBN sites, these log-log slopes are generally close to zero on both inter-annual time scales (Figure 4) and event time scales (Figure 2), although the error bars in Figure 4 are larger because the annualized concentration-discharge plots (*e.g.*, Figure 3) have fewer points and a smaller range of discharge. The near-zero slopes imply that catchments exhibit near-chemostatic behavior over both event and inter-annual timescales and across a wide range of hydrologically and geochemically diverse sites. Thus an interesting first-order question is not why concentrations of weathering products vary, but why they vary so little as discharge changes so much.

Assessment of alternative models

Consistent near-zero log(C)-log(Q) slopes imply that rates of solute production or mobilization must be nearly proportional to water fluxes on intra- and inter-annual timescales. Here we explore several simple quantitative explanations for the observed concentration-discharge patterns to verify if they hold across all the HBN sites, and to compare different

possible models at each site. We evaluate these explanations on the basis of several key criteria. They should generate power-law relationships between concentration and discharge with small negative slopes and little hysteresis. Furthermore, they should have reasonable physical and chemical parameters and should make plausible assumptions about catchment behavior. They should be as simple as possible and explain observations in a wide range of catchments. We examine several empirical, mixing and chemical models to gain insight into the linkages between chemical weathering and hydrologic processes that produce the observed concentration-discharge relationships. We quantitatively assess the models' performance at each site using the Akaike and Bayesian information criteria for each set of comparable models.

Empirical models

We first evaluated whether the slope of the concentration-discharge relationship can be predicted as a simple empirical function of each catchment's characteristics, or as a multivariate model of several characteristics. For each site, we plotted average low and high temperature, annual average runoff, area, and mean annual precipitation against the event-based concentration-discharge slope for each solute, and calculated the correlation between each of these site characteristics and each solute's concentration-discharge slope (using the non-parametric Spearman correlation coefficient because the distributions of site characteristics are not normal). Based on the site descriptions from the USGS circulars (Mast and Turk, 1999a&b; Clark *et al.*, 2000; Mast and Clow, 2000), we also coded each site according to the presence or absence of carbonates and volcanics in the underlying bedrock. We then used the F-test (Zar, 1984) to determine whether the presence of either of these broad rock types significantly affected the concentration-discharge slope for any solute. For the multivariate models, we systematically added and removed characteristics from a series of multiple linear regression models and evaluated their performance.

The site characteristics that we tested generally do not satisfactorily explain the observed slopes of the concentration-discharge relationships (Table 2). Steeper concentration-discharge slopes are associated with higher average annual runoff (although, surprisingly, not always with higher mean annual precipitation); these correlations are statistically significant for some solutes but not others. Sites with volcanic bedrock have significantly ($p<0.05$) steeper concentration-discharge slopes for Ca, Mg and Na compared to sites where volcanics are absent. Similarly, log-log slopes for Na are significantly ($p<0.02$) shallower at sites with carbonate bedrock, compared to sites without carbonates. Although some site characteristics show statistically significant effects on concentration-discharge slopes, their predictive power is weak because they explain only a small fraction of the variance; typical r^2 values are 0.1 or less. Multivariate models with combinations of these site characteristics could only explain <20% of the variability in log(C)-log(Q) slopes. We conclude that the observed variation in concentration-discharge slopes cannot be straightforwardly predicted by any of the site characteristics tested here. Other site characteristics, such as basin slope, soil permeability, or amount and type of soil and vegetation, might be useful explanatory variables, but they have not been quantified for most of the HBN basins. Basin slope and soil permeability, for example, might be important because they influence hydrological flowpaths and the residence time of water in the basins.

Mixing models

We turn from empirical models based on site characteristics to simple models based on the mixing of waters with different compositions. Isotopic studies and other hydrometric and hydrochemical evidence have shown that in many catchments, typical residence times are much longer than the duration of individual storm events (*e.g.*, Buttle, 1994). One can imagine that residence times may be long enough for weathering reactions to approach equilibrium, and that this explains the chemostatic behavior observed across the HBN sites. Sufficient storage capacity for the "old" water must exist for this option to be physically plausible, and we explore storage requirements for different models below. In general, we find that mixing models that assume a constant rate of solute supply generally cannot reproduce the observations well.

First, we present a simple "bucket" mixing model that treats the catchment as a single well-mixed reservoir whose volume (V, [m^3]) remains constant as discharge (Q_w, [m^3/s]) varies. The model likewise assumes that the solute flux (Q_s, [ppm-m^3/s]) produced by mineral weathering is constant through time. It further assumes that concentrations in precipitation are very dilute compared to streamflow (as is typically the case for the major weathering products), so that precipitation solute fluxes can be ignored in the mass balance. Under these conditions, the solute concentration (C, [ppm]) in the well-mixed reservoir, and thus in its outflow, will evolve according to the familiar mass-balance equation:

Eq. 1 $$dC/dt = (Q_s - Q_w C)/V$$

where Q_w is the average daily water flux through the reservoir, for which we use the USGS historical daily flow record. We fix the solute flux (Q_s) equal to the product of the average water flux and the flow-weighted average concentration, so that the average modeled solute flux will equal the observed long-term average. The reservoir volume (V) is the only free parameter, which is adjusted to reproduce the observed range of variation in outflow concentrations.

Constraining the concentrations modeled using equation (1) within the bounds of observed variability in the HBN data set requires a storage volume that is well-mixed to depths of several meters throughout the catchment (Table 3) for a porosity of 10% (averaged across both soil and underlying rock). Higher porosities require a smaller storage volume whereas lower porosities require a larger storage volume. Even with sufficiently large storage volumes, however, modeled concentration-discharge relationships do not match the observations well; the model results exhibit large hysteresis loops that are not present in the observations (Figure 5a). These loops result from the assumption that the catchment behaves as a simple well-mixed bucket: the integro-differential relationship in equation (1) implies a 90 degree phase lag between changes in discharge and changes in concentration, rather than the simultaneous variations in concentration and discharge that are usually observed. Hysteresis loops are frequently observed in concentration-discharge relationships, but the extent of looping modeled in Figure 5a is much greater than is typically observed (*e.g.*, Evans and Davies, 1998). To match the observed concentration-discharge relationships, this model would have to be modified to allow solutes to be: (1) produced at a variable rate, or (2) mobilized from different sources at variable rates.

Another well-known model that we consider is the Hubbard Brook "working model" (Johnson *et al.*, 1969) which assumes that discharge is proportional to storage volume (V, [m^3]),

and that solute concentrations (C, [ppm]) associated with each storage volume are fixed. Storage volume is defined as the subsurface pore space available above an "impermeable" layer. C is then inversely related to Q according to:

Eq. 2 $C = [d/(1+bQ)]+a$,

where a = concentration of solute in the low-concentration end-member [ppm], b=mean residence time/$V_{Q=0}$ (flows at the catchment outlet are assumed to cease at some non-zero storage volume, $V_{Q=0}$) [s/m^3], and d = concentration difference between high and low concentration waters [ppm]. Any non-zero flow is directly proportional to water in storage above the minimum volume. One can immediately see that this model does not represent a power-law relationship between C and Q, but instead that the relationship is a hyperbolic function. However, because it has an additional free parameter, equation (2) can also fit the data well (Figure 5b). A non-linear fitting algorithm which minimizes the sum of squared error between the model results and observed data is used to select best-fit values of a, b, and d. The parameter b depends only on the mean residence time of water in the catchment and the minimum volume required for flow in the stream. Importantly, b does not depend on the solute of interest; therefore, it should have the same value for all the solutes at an individual site. This consistency in b can be ensured by simultaneously fitting all solutes in a given catchment. Johnson *et al.* (1969) suggest that a should be thought of as the "rainwater" concentration of each solute. However, the best-fit a values exceed measured volume-weighted precipitation concentrations for Ca, Mg and Na (as reported in Mast and Turk, 1999a&b; Clark *et al.*, 2000; Mast and Clow, 2000) by up to two orders of magnitude (Table 4). Concentrations of Si in precipitation are not generally reported, but the best-fit a for Si is in the range of ~10 ppm. Instead of representing "rainfall" concentrations, the high best-fit a values could perhaps be thought of as "soil water" concentrations. In any case, the fact that the best-fit values of a are much higher than rainfall concentrations implies that important solute sources within the catchment are not captured by the model.

Chemical models

On the other end of the modeling spectrum, one could assume that waters react so rapidly with soil and rock that one can ignore mixing of waters of different ages altogether. If changes in chemical reactions were solely responsible for the concentration-discharge patterns we see, what would this imply? The simplest way to maintain chemical concentrations as discharge increases is through a combination of increasing reactive surface area and increasing reaction rates.

A simple approach was proposed by Langbein and Dawdy (1964) who assumed that dissolution rate varies between zero and the maximum dissolution rate, D, depending upon distance from equilibrium. They also assumed that the dissolved load is removed as quickly as it is formed, which is equivalent to assuming that mixing of water of different ages is negligible. To generalize their model from 1st order to nth-order reactions, one can let the forward reaction be equal to DA [mol/s] where A [m^2] is the reactive surface area, and let the back reaction be equal to $DA(C/C_s)^n$ where n [dimensionless] is the order of the reaction, C [mol/m^3] is the concentration and C_s [mol/m^3] is the concentration at saturation. The load, L [mol/s], would then be equal to the balance of the forward and backward reactions:

Eq. 3 $L=DA(1-(C/C_s)^n)$.

Assuming that the dissolved load is removed as quickly as it is formed, one can also write:

Eq. 4 $L=Q(C-C_o)$

where C_o [mol/m^3] is the initial (*i.e.*, rainfall) concentration, C [mol/m^3] is the final concentration and Q [m^3/s] is the discharge. For first- and second-order reactions (n =1 or 2, respectively), equations (3) and (4) can be solved for C as a function of Q:

Eq. 5a (for n=1) $$C = \frac{DA + QC_o}{Q + DA/C_s}$$ or

Eq. 5b (for n=2) $$C = \frac{Q - \sqrt{Q^2 + \frac{4DA}{S^2}(DA + QC_o)}}{-2DA/C_s^{\,2}}$$

where the negative root for n=2 gives the concentration that has physical meaning. Using these equations and the observed concentration-discharge relationships, one can determine the values of DA, C_s and C_o that are required to fit the data. With three adjustable parameters, the model approximately reproduces the observed concentration-discharge relationship with either n=1 or n=2, although the log-log relationship is curved rather than linear (Figure 5c). The order of the reaction does not strongly affect the overall quality of fit, but the dissolution rate times area (DA) parameter for the best-fit 2nd order scenario differs from the 1st order case. One cannot distinguish among models of different reaction order given only concentration-discharge data; additional *a priori* information about the order of the reaction or the dissolution rate and reaction area is needed to distinguish among the models. The best-fit saturated concentration is lower than the observed maximum concentration and the best-fit initial concentration is higher than the observed minimum concentration; the best-fit concentrations vary little as reaction order changes. In either case, the best-fit initial concentration is usually much higher than is realistic for rainfall. Rather than representing rainfall, the best-fit C_o probably reflects solutes acquired during infiltration through the soil column before reaching the groundwater system. Although multiple versions of the Langbein and Dawdy model fit the data reasonably well, the key assumption that there is no storage of water between storms and therefore negligible mixing of water of different ages is generally not valid (*e.g.*, Buttle, 1994).

Permeability-porosity-aperture model

Here we suggest another model that is the only general model that we know of that produces a power-law relationship between concentration and discharge, assumes a variable solute flux that is proportional to the reactive surface area, and allows for mixing of waters of different ages. This final point distinguishes this model from the Langbein-Dawdy model.

The full derivation is shown in the appendix. The key assumptions are: that permeability, porosity and average pore aperture or width, all decrease exponentially with depth; that Darcy's Law describes flow through the catchment; that the effective precipitation rate is approximately spatially uniform across a hillslope; that flows originating near the divide and stream are minimal; and that solute flux is proportional to reactive surface area such that secondary and back-reactions do not control solute fluxes.

One can show that under these assumptions, the volume-weighted mean concentration ($\overline{C}$, [mol/m^3]) draining a one-dimensional hillslope will be a power function of the water flux (Q_w),

Eq. 6 $$\overline{C} = a_o Q_w^{b_0} \quad , \quad b_0 = \left(\lambda_k / \lambda_\phi - \lambda_k / \lambda_p - 1 \right).$$

where the constant a_o is a function of solute and catchment characteristics, and the power-law exponent b_0 [dimensionless] depends on the rate at which permeability, porosity and pore aperture decrease exponentially with depth in the subsurface (represented by the e-folding length scales λ_k, λ_ϕ, and λ_p, all in [m]). Because λ_k, λ_ϕ, and λ_p are geometric properties of the subsurface and are not specific to individual solutes, equation (6) implies that b_o should be the same for all weathering-derived solutes at an individual site (see, for one example, Figure 5d showing Ca at Andrews Creek). We fitted a single value of b_o for each site, and a value of a_o for each site and solute, using a non-linear fitting algorithm that minimizes the error between the modeled and observed concentrations for all solutes simultaneously.

Because we fit some models to all the solutes simultaneously whereas we fit other models to each solute independently, comparing the models is not a straightforward exercise. Using the Akaike or Bayesian information criteria (AIC or BIC), or by looking at the example in Figure 5, it is clear that the Langbein-Dawdy model (5b) outperforms the simple mixing model (5a). The permeability-porosity-aperture model (5d) outperforms the Hubbard Brook Experimental Forest "working model" (5c) according to the AIC and BIC at each of the eight featured sites. Comparisons between the Langbein-Dawdy and permeability-porosity-aperture model cannot be made using the AIC or BIC because the models are based on different sets of data (fitting each solute independently vs. all solutes simultaneously). Regardless of model performance, a key test of each of these models is whether the best-fit parameters make physical and chemical sense in the real-world catchments in which they are applied.

Contrary to the prediction of the permeability-porosity-aperture model, that the log-log slope b_0 of the concentration-discharge relationship should be the same for different weathering products at an individual catchment, the log(C)-log(Q) slopes for different solutes at the same site often differ by more than their uncertainties. This result could be explained by different depth profiles in the abundances of different minerals (and thus their reactive surface areas per unit pore surface). Mathematically this could be represented as λ_p taking on different values for different solutes, although this would imply that p would reflect not only pore aperture but also the relative abundances of different minerals. However, because b_0 is usually close to zero for different solutes, it is possible that the variation in λ_p may be small. Another parameter, b_1, has been shown to relate storage and discharge in catchments, and is expressed as a function of the parameters λ_k and λ_ϕ (Kirchner, 2009; and see appendix, equation A12 and A13). The two log-log slopes b_0 and b_1 are not sufficient to uniquely constrain the three parameters λ_k, λ_ϕ, and λ_p, so the individual e-folding depths (as well as values of the reactivity parameter k_R for each solute, see appendix) could only be determined by direct measurement. Any such attempt at direct measurement, however, would be complicated by the spatial heterogeneity in subsurface properties, as well as the large differences between field and laboratory weathering rates (Schnoor, 1990; Brantley, 1992; White *et al.*, 1996).

The mechanism proposed here is in some ways analogous to that proposed by Clow and Drever (1996) to explain the relatively constant concentrations of weathering products in runoff from an alpine soil under widely varying rainfall. Clow and Drever (1996) argued that Si concentrations in their study catchment may be controlled by flushing and diffusion from micropores and seasonal precipitation/dissolution of metastable amorphous aluminosilicates. They argued that since both flushing and reaction rates increase with increasing discharge, this combination of mechanisms would allow concentrations to remain relatively constant with fluctuating discharge. But whereas Clow and Drever (1996) argued that the rate of Si dissolution from the mineral phase should be controlled by Si concentrations in solution (and thus by the fluid flushing rate), here we assume that silicate weathering reactions are always far from equilibrium and thus are unaffected by changes in solute concentrations. Instead, in the permeability-porosity-aperture model outlined in Equation 6 and in the appendix, reaction rates increase at higher discharges because the wetted mineral surface area increases. Others have also argued that because Si is retained by secondary minerals to varying degrees, its concentration may be controlled in large measure by equilibration with respect to the secondary minerals that form (Drever and Clow, 1995; Godderis *et al.* 2006). Secondary mineral formation should preferentially affect Si and may explain why the power-law concentration-discharge slopes for Si are generally shallower than for the other major weathering products. These examples illustrate that different mechanisms can potentially generate similar observed concentration-discharge relationships, so it is important to verify the site-specific plausibility of any proposed mechanism.

Further Possibilities

Many catchment-based chemical weathering models, such as Birkenes, ETD (Enhanced Trickle-Down), ILWAS (Integrated Lake Watershed Acidification Study), PROFILE/SAFE (Soil Acidification in Forested Ecosystems), MAGIC (Model of Acidification of Groundwater in Catchments), or WITCH (see review in Nordstrom, 2004, pp. 60-62; Godderis *et al*., 2006), and other mineral weathering models such as PHREEQC (Parkhurst and Appelo, 1999), allow the simulation of weathering processes. We do not use these models in this study because most of our sites have insufficient information to apply them. Instead we explore in this paper whether a simple general modeling approach is possible based primarily on the observed concentration-discharge relationship. We show that several simple models can fit the observations well, but often they require unrealistic or internally inconsistent parameter values. Because data limitations have precluded us from testing more complex models, we cannot say whether their added complexity, and additional data requirements, would be helpful in understanding catchments' concentration-discharge behavior. Future studies could also examine the geomorphic features, soil or regolith depth, presence of organic matter, or perennial/ephemeral status of the catchments, which may control weathering rates or fluxes in some catchments (*e.g.*, Oliva *et al*., 1999; Drever 1994; Johnson *et al*., 2001). These characteristics have not been considered in this study.

The relative constancy of concentrations across wide ranges of discharge requires solute production or solute mobilization at rates nearly proportional to the water flux. Depending on the relationship between reaction times and water transit times, one can infer the relative importance of production and mobilization. Based on field experiments, reaction rates have sometimes been

inferred to be fast enough that the time to equilibrium is much shorter than average water transit times, such that waters are effectively always near equilibrium (*e.g.*, Anderson and Dietrich, 2001). Buttle (1994) and many others have documented that most water reaching a stream during a storm event is so-called "old" (*i.e.*, pre-storm) water. Mean transit times in many catchments are on the order of ~1 year (McGuire and McDonnell, 2006, Table 1), so this "old" water may be near equilibrium with respect to certain minerals, with the consequence that solute fluxes mobilized by this "old" water must be nearly proportional to water flux. However, studies of silicate weathering have typically found that reaction rates are slow (even relative to mean transit times of a year) and have assumed that catchments are kinetically-limited systems (see discussion in Brantley, 2004). Because the chemical weathering kinetics of silicates and carbonates differ (*e.g.*, Brantley, 2004), one might expect different log(C)-log(Q) behavior or explanatory models for catchments dominated by the distinct lithologies. However, for most of the solutes considered, the concentration-discharge slopes are not significantly different between the different lithologic settings. This suggests that differences in lithology and in reaction kinetics between carbonates and silicates do not significantly alter the relationship between concentration and discharge across the study sites. Time to equilibrium in the laboratory for mineral-water equilibrium reactions has been reported as a week to a year or longer (*e.g.*, Bricker, 1968; Langmuir, 1997, Table 2.1) and field rates are even slower (Schnoor, 1990; Brantley, 1992; White *et al.*, 1996). This suggests that mineral weathering reactions would be unlikely to stay close to equilibrium, particularly during high flows. Determining the average time to equilibrium in the field is challenging: flow paths are heterogeneous and reactions and reactive surface areas are difficult to define. Nonetheless, as the preceding discussion illustrates, there would be much to be gained from determining how close weathering reactions are to equilibrium in the field.

Implications

Because concentrations are relatively constant with discharge across these diverse study catchments (Figures 1 and 2), solute fluxes (defined as concentration times discharge) from these catchments change nearly proportionally to discharge, both on an event basis and on an inter-annual basis (*e.g.*, Figure 6). Although our observations are drawn from US catchments, these results are likely to be broadly generalizable because the HBN catchments include a broad range of climatic and lithologic environments (see Table 1). A similar relationship between concentration and discharge is also seen in granitic boreal catchments in permafrost regions of Russia (Zakharova *et al*., 2005), suggesting these observations and implications may be globally applicable. Climate change may substantially alter stream flows (especially if precipitation and evapotranspiration change in opposite directions). Such hydrologic changes will have little effect on concentrations but will alter fluxes almost proportionally.

Alkalinity flux to the ocean can be estimated as the sum of the Ca and Mg concentrations (McSween *et al*., p. 147), or the hardness of the water. Raymond and Cole (2003) used this approach to estimate alkalinity for the Mississippi River for years before 1973 using hardness. They showed that overlapping alkalinity and carbonate hardness (=total hardness-noncarbonate hardness) measurements are accurate to 99.8+/-0.8%. Thus, we can estimate alkalinity fluxes based on the relationships between Ca, Mg and discharge presented in Figures 2 and 4. Raymond and Cole (2003) found that discharge and alkalinity flux in the Mississippi River increased by

approximately 44% and 70%, respectively, over 48 years (1953-2001), attributed partially to changes in climate as well as changes in cropping patterns and additions from groundwater pumping. Based on the patterns in Figure 6 (and similar results for other solutes), one would expect solute flux from most watersheds across North America to vary nearly proportionally to water fluxes. Unlike the Mississippi River, most of the streams and rivers in the HBN are minimally affected by land use change or large amounts of groundwater pumping. Nonetheless, the nearly chemostatic behavior demonstrated across so many diverse sites implies that alkalinity flux is largely determined by stream discharge. Streamflows at high latitudes are expected to increase by 10-40% over the next century, according to the latest report of the Intergovernmental Panel on Climate Change (IPCC, 2007). For a 10% increase in average annual flows, we would expect an approximately proportional 10% increase in alkalinity fluxes to the oceans. Carbonic acid weathering is one of the main mechanisms generating alkalinity; thus, an increase in alkalinity fluxes implies a concomitant increase in CO_2 consumption.

On the other hand, if discharges were to drop sharply, solute fluxes would also be expected to decrease. As an example, the seaward total dissolved solids flux from the Huanghe (Yellow) River, China has decreased by more than half over the past approximately 40 years because of a sharp decrease in water discharge in the lower reaches of the river (Chen *et al.*, 2005). Diversions, irrigation, and reservoir use are primarily responsible for the decrease in water discharge, and despite an increase of ~5-10 mg/L/yr in total dissolved solids in the middle and lower reaches of the river, there has been an overall decrease in solute flux (Chen *et al.*, 2005). Climate change models predict that flows in the southwestern US and other dry areas are likely to decrease by 10-40% by 2090-2099 relative to 1980-1999 in a scenario in which global average temperatures increase by 2.8°C over the same period (IPCC, 2007). One would expect solute flux of the major base cations and silica from streams and rivers in these regions to decrease by an amount that is approximately proportional to the decrease in flows.

The stability of concentrations of weathering products across a wide range of flow regimes may be important both for the health of individual organisms and for the diversity of aquatic ecosystems. At an organismal level, mortality from acidification-induced aluminum toxicity is closely linked to decreases in alkalinity and base cation concentrations (Jeffries *et al.*, 1992; Thornton and Dise, 1998). Metals and other contaminants are more toxic to juvenile fish in waters with lower hardness, which as noted above, is usually equal to sum of the concentration of Ca and Mg (*e.g.*, Hall, 1991). The greater the stability of base cation concentrations across a wide range of flows, the smaller the likelihood that toxicity thresholds will be crossed during hydrological extremes because concentrations will not drop precipitously when flows increase.

At a species to community level, site-to-site comparisons reveal that benthic macroinvertebrate and diatom species diversity is a function of total dissolved solid concentration, conductivity or salinity in some streams, lakes and fjords (Metzeling, 1993, Ryves *et al.*, 2004). Solute fluxes, especially the amount of Si relative to other potentially limiting nutrients, can be a predictor of phytoplankton blooms and diatom growth (LePape *et al.*, 1996; Grenz *et al.*, 2000). Si concentrations relative to concentrations of Fe, N and P strongly control diatom nutrient uptake and growth rates. Increased N and P concentrations relative to Si concentrations and decreased Si flux due to river regulation have shifted ecosystems dominated by siliceous phytoplankton or diatoms to those dominated by non-siliceous algae or flagellate

communities (*e.g.*, Officer and Ryther, 1980; Egge & Aksnes, 1992; Turner *et al*., 1998; Billen and Garnier, 2007). Oceanic Si limitations have been seen in the eastern equatorial Pacific and North Atlantic as well as in coastal communities that have experienced eutrophication problems due to increased N and/or P loads relative to Si loads (Ragueneau *et al*., 2000). Furthermore, rare taxa are more sensitive to changes in salinity than common taxa in site-to-site comparisons (Metzeling, 1993). Species that are more tolerant to salinity variations may be able to disperse widely into different rivers feeding an estuary or coastal region and negatively affect native populations, which may be adapted to the narrow range of concentrations seen in their particular chemostatic catchment (Bringolf *et al*., 2005). Therefore, the chemostatic behavior of catchments may enhance hydrochemical stability across a wide range of flows and thus promote biodiversity, but also suggests that streams subject to anthropogenic salinity variations or estuarine influences are more vulnerable to invasive species.

Conclusions

Concentrations of weathering-derived solutes vary little with discharge for 59 USGS Hydrologic Benchmark Network (HBN) streams, indicating that these catchments exhibit nearly chemostatic behavior. Concentrations vary by only a factor of 3 to 20 as discharge varies by several orders of magnitude, and annual mean concentrations are similarly insensitive to changes in annual water yield. Concentrations of the major base cations and silica typically exhibit power-law relationships with discharge, with small negative exponents. Broad qualitative lithologic differences, such as the presence or absence of volcanics or carbonates, are associated with statistically significant differences in the power-law concentration-discharge slope among different sites. Other site characteristics such as area, low temperature and average annual runoff are significantly rank-correlated with site-to-site variations in concentration-discharge slopes for some solutes, but the predictive power of site characteristics to quantify concentration-discharge slopes is limited. The narrow range of concentration variability with discharge implies that rates of solute production and mobilization must be nearly proportional to water fluxes. Because concentrations remain nearly constant across wide ranges in discharge, solute yield from catchments (and, at continental scale, alkalinity fluxes to the oceans) are predominantly determined by water yield.

It is difficult to find simple generalizable models that accurately represent the typical form of the concentration-discharge relationship, that are internally consistent, and that make plausible assumptions about catchment behavior. A simple “bucket” model cannot reproduce the observed concentration-discharge behavior. The Hubbard Brook "working model" can fit the observations, but the required best-fit “rainfall” concentrations are much higher than observed concentrations, suggesting that key physical or chemical processes are not captured by the model. A Langbein-Dawdy chemical reaction model that assumes that reaction rates vary with distance from equilibrium can also fit the observed concentration-discharge relationships, but requires relatively high input concentrations (and therefore likely requires an important role for soil water) and assumes that no mixing of waters of different ages can occur. Finally, a new chemical and mixing model can explain the observed power-law relationships between concentration and discharge in terms of depth profiles of porosity, characteristic pore size, and hydraulic conductivity in the catchment. In this model, changes in discharge correspond to changes in the depth of saturation in the subsurface. These in turn alter solute fluxes by altering

the reactive wetted surface area. The assumptions of this new model should be tested at a subset of the HBN sites. An internally-consistent model of hydrology, chemical weathering and transport is needed to explain the power-law concentration-discharge relationships that are observed across hydrochemically diverse catchments.

Acknowledgments

We thank Tom Meixner, Madeline Solomon, Steve Sebestyen, Jake Peters and Kathleen Lohse for helpful discussions, and thank the 2003 Sagehen Watershed Symposium for stimulating the collaboration that led to this work. This work was supported by NSF grant EAR-0125550, the Miller Institute for Basic Research in Science and an NSF Graduate Research Fellowship.

Cited References

Anderson SP, Dietrich WE. 2001. Chemical weathering and runoff chemistry in a steep headwater catchment. *Hydrological Processes* **15**: 1791-1815.

Billen G, Garnier J. 2007. River basin nutrient delivery to the coastal sea: Assessing its potential to sustain new production of non-siliceous algae. *Marine Chemistry* **106**: 148-160.

Brantley SL. 1992. Kinetics of dissolution and precipitation - experimental and field results. In *Proceedings of the 7th Water-Rock Interaction Symposium - Park City, UT (Vol. 1)*, Kharak YF, Maest AS (eds). AA Balkema: Rotterdam; 3-6.

Brantley SL. 2004. Reaction kinetics of primary rock-forming minerals under ambient conditions. In *Treatise on Geochemistry: Surface and ground water, weathering, and soils*, Drever JI, Holland HD, Turekian KK (eds). Elsevier Pergamon: Amsterdam; 73-117.

Bricker OP. 1968. Cations and silica in natural waters: control by silicate minerals. In *Geochemistry, precipitation, evaporation soil-moisture, hydrometry – General Assembly of Bern, Reports and Discussions, IAHS Publ. 78*. IAHS: Bern; 110-119.

Bringolf RB, Kwak TJ, Cope WG, Larimore MS. 2005. Salinity tolerance of flathead catfish: Implications for dispersal of introduced populations. *Transactions of the American Fisheries Society* **134**: 927-936.

Buttle JM. 1994. Isotope hydrograph separations and rapid delivery of pre-event water from drainage basins. *Progress in Physical Geography* **18**: 16-41.

Chanat JG, Rice KC, Hornberger GM. 2002. Consistency of patterns in concentration-discharge plots. *Water Resources Research* **38**: 22. DOI: 10.1029/2001WR000971.

Chen J, Wang F, Meybeck M, He D, Xia X, Zhang L. 2005. Spatial and temporal analysis of water chemistry records (1958-2000) in the Huanghe (Yellow River) basin. *Global Biogeochemical Cycles* **19**: GB3016. DOI: 10.1029/2004GB002325.

Clark ML, Eddy-Miller CA, Mast MA. 2000. *Environmental Characteristics and Water Quality of Hydrologic Benchmark Network Stations in the West-Central United States, 1963-95. USGS Circular 1173-C*. USGS: Reston; 115.

Clow DW, Drever JI. 1996. Weathering rates as a function of flow through an alpine soil. *Chemical Geology* **132**: 131-141.

Drever JI. 1994. The Effect of Land Plants on Weathering Rates of Silicate Minerals. *Geochimica Et Cosmochimica Acta* **58**: 2325-2332.

Drever JI, Clow DW. 1995. Weathering rates in catchments. In *Chemical Weathering Rates of Silicate Minerals*, 463-483.

Egge JK, Aksnes DL. 1992. Silicate as Regulating Nutrient in Phytoplankton Competition. *Marine Ecology-Progress Series* **83**: 281-289.

Evans C, Davies TD. 1998. Causes of concentration/discharge hysteresis and its potential as a tool for analysis of episode hydrochemistry. *Water Resources Research* **34**: 129-137.

Evans C, Davies TD, Murdoch PS. 1999. Component flow processes at four streams in the Catskill Mountains, New York, analysed using episodic concentration/discharge relationships. *Hydrological Processes* **13**: 563-575.

Godderis Y, Francois LM, Probst A, Schott J, Moncoulon D, Labat, D, Viville, D. 2006. Modelling weathering processes at the catchment scale: The WITCH numerical model. *Geochimica Et Cosmochimica Acta* **70**: 1128-1147.

Grenz C, Cloern JE, Hager SW, Cole BE. 2000. Dynamics of nutrient cycling and related benthic nutrient and oxygen fluxes during a spring phytoplankton bloom in South San Francisco Bay (USA). *Marine Ecology-Progress Series* **197**: 67-80.

Hall FR. 1970. Dissolved solids-discharge relationships 1. Mixing models. *Water Resources Research* **6**: 845-850.

Hall FR. 1971. Dissolved solids-discharge relationships 2. Applications to field data. *Water Resources Research* **7**: 591-601.

Hall LW. 1991. A Synthesis of Water-Quality and Contaminants Data on Early Life Stages of Striped Bass, Morone-Saxatilis. *Reviews in Aquatic Sciences* **4**: 261-288.

Hem JD. 1948. Fluctuations in concentration of dissolved solids of some southwestern streams. *Transactions, American Geophysical Union* **29**: 80-84.

Hem JD. 1985. *Study and Interpretation of the Chemical Characteristics of Natural Water. 3rd edition. USGS Water Supply Paper 2254*. USGS: Alexandria, VA; 263.

Hornberger GM, Scanlon TM, Raffensberger JP. 2001. Modelling transport of dissolved silica in a forested headwater catchment: the effect of hydrological and chemical time scales on hysteresis in the concentration-discharge relationship. *Hydrological Processes* **15**: 2029-2038. DOI: 10.1002/hyp.254.

House WA, Warwick MS. 1998. Hysteresis of the solute concentration/discharge relationship in rivers during storms. *Water Research* **32**: 2279-2290.

IPCC. 2007. *Climate Change 2007: Synthesis Report. Contribution of Working Groups I, II and III to the Fourth Assessment Report of the Intergovernmental Panel on Climate Change*. Core Writing Team, Pachauri, R.K and Reisinger, A. (eds). IPCC: Geneva, Switzerland; 104.

Jeffries DS, Lam DCL, Wong I, Bloxam RM. 1992. The predicted effect of SO_2 emission controls on the water-quality of eastern Canadian lakes. *Environmental Monitoring and Assessment* **23**: 99-113.

Johnson DW, Susfalk RB, Dahlgren RA, Caldwell TG, Miller WW. 2001. Nutrient fluxes in a snow-dominated, semi-arid forest: Spatial and temporal patterns. *Biogeochemistry* **55**: 219-245.

Johnson NM, Likens GE, Bormann FH, Fisher DW, Pierce RS. 1969. A working model for the variation in stream water chemistry at the Hubbard Brook Experimental Forest, New Hampshire. *Water Resources Research* **5**: 1353-1363.

Kirchner JW. 2009. Catchments as simple dynamical systems: catchment characterization, rainfall-runoff modeling, and doing hydrology backwards. *Water Resources Research* **45**: DOI:10.1029/2008WR006912.

Langbein WB, Dawdy DR. 1964. *Occurrence of dissolved solids in surface waters in the United States. USGS Prof. Paper 501-D*. USGS: Washington, DC; D115-D117.

Langmuir D. 1997. *Aqueous Environmental Geochemistry*. Prentice Hall: Upper Saddle River, NJ; 600.

Leopold, LB. 1962. *A national network of hydrologic bench marks, USGS Circular 460-B*. USGS: Washington, DC; 4.

LePape O, Del Amo Y, Menesguen A, Aminot A, Quequiner B, Treguer P. 1996. Resistance of a coastal ecosystem to increasing eutrophic conditions: The Bay of Brest (France), a semi-enclosed zone of Western Europe. *Continental Shelf Research* **16**: 1885-1907.

Mast MA, Clow DW. 2000. *Environmental Characteristics and Water Quality of Hydrologic Benchmark Network Stations in the Western United States, 1963-95. USGS Circular 1173-D*. USGS: Reston; 114.

Mast MA, Turk JT. 1999a. *Environmental Characteristics and Water Quality of Hydrologic Benchmark Network Stations in the Eastern United States, 1963-95. USGS Circular 1173-A*. USGS: Denver; 158.

Mast MA, Turk JT. 1999b. *Environmental Characteristics and Water Quality of Hydrologic Benchmark Network Stations in the Midwestern United States, 1963-95. USGS Circular 1173-B.* USGS: Denver; 130.

McGuire KJ, McDonnell JJ. 2006. A review and evaluation of catchment transit time modeling. *Journal of Hydrology* **330**: 543-563.

McSween HY, Richardson SM, Uhle ME. 2003. Geochemistry: Pathways and Processes. Columbia University Press: New York; 363.

Metzeling L. 1993. Benthic macroinvertebrate community structure in streams of different salinities. *Australian Journal of Marine and Freshwater Research* **44**: 335-351.

Murdoch PS, Stoddard JL. 1992. The role of nitrate in the acidification of streams in the Catskill Mountains of New York. *Water Resources Research* **28**: 2707-2720.

Nordstrom DK. 2004. Modeling low-temperature geochemical processes. In *Treatise on Geochemistry: Surface and Ground Water, Weathering, and Soils*, Drever JI, Holland HD, Turekian KK(eds). Elsevier Pergamon: Amsterdam; 37-72.

Officer CB, Ryther JH. 1980. The Possible Importance of Silicon in Marine Eutrophication. *Marine Ecology-Progress Series* **3**: 83-91.

Oliva P, Viers J, Dupre B, Fortune JP, Martin F, Braun JJ, Nahon D, Robain H. 1999. The effect of organic matter on chemical weathering: Study of a small tropical watershed: Nsimi-Zoetele site, Cameroon. *Geochimica Et Cosmochimica Acta* **63**: 4013-4035.

Parkhurst DL, Appelo CAJ. 1999. *User's Guide for PHREEQC (version 2) - A Computer Program for Speciation, Batch-Reaction, One-Dimensional Transport, and Inverse Geochemical Calculations. WRI Report 99-4529*. USGS: Denver; 312.

Ragueneau O, Treguer P, Leynaert A, Anderson RF, Brzezinski MA, DeMaster, DJ, Dugdale, RC, Dymond J, Fischer G, Francois R, Heinze C, Maier-Reimer E, Martin-Jezequel V, Nelson DM, Queguiner B. 2000. A review of the Si cycle in the modem ocean: recent progress and missing gaps in the application of biogenic opal as a paleoproductivity proxy. *Global and Planetary Change* **26**: 317-365.

Raymond PA, Cole JJ. 2003. Increase in the export of alkalinity from North America's largest river. *Science* **301**: 88-91.

Ryves DB, Clarke AL, Appleby PG, Amsinck SL, Jeppesen E, Landkildehus F, Anderson NJ. 2004. Reconstructing the salinity and environment of the Limfjord and Vejlerne Nature Reserve, Denmark, using a diatom model for brackish lakes and fjords. *Canadian Journal of Fisheries and Aquatic Sciences* **61**: 1988-2006. DOI: 10.1139/F04-127.

Schnoor JL. 1990. Kinetics of chemical weathering: a comparison of laboratory and field weathering rates. In *Aquatic Chemical Kinetics: Reaction rates of processes in natural waters*, Stumm W (ed). John Wiley & Sons: New York; 475-504.

Thornton GJP, Dise NB. 1998. The influence of catchment characteristics, agricultural activities and atmospheric deposition on the chemistry of small streams in the English Lake District. *Science of the Total Environment* **216**: 63-75.

Turner RE, Qureshi N, Rabalais NN, Dortch Q, Justic D, Shaw RF, Cope J. 1998. Fluctuating silicate:nitrate ratios and coastal plankton food webs. *Proceedings of the National Academy of Sciences of the United States of America* **95**: 13048-13051.

Waylen MJ. 1979. Chemical weathering in a drainage basin underlain by old red sandstone. *Earth Surface Processes* **4**: 167-178.

Walling DE, Webb BW. 1986. Solutes in river systems. In *Solute Processes*, Trudgill ST (ed). John Wiley & Sons: Chichester; 251-327.

White AF, Blum AE, Schulz MS, Bullen TD, Harden JW, Peterson ML. 1996. Chemical weathering rates of a soil chronosequence on granitic alluvium: I. Quantification of mineralogical and surface area changes and calculation of primary silicate reaction rates. *Geochimica et Cosmochimica Acta* **60**: 2533-2550.

Wilde FD, Radtke DB, Gibs J and Iwatsubo RT (eds), 1998. *National Field Manual for the Collection of Water-Quality Data v.9*. USGS: Denver.

Zakharova EA, Pokrovsky OS, Dupre B, Zaslavskaya MB. 2005. Chemical weathering of silicate rocks in Aldan Shield and Baikal Uplift: insights from long-term seasonal measurements of solute fluxes in rivers. *Chemical Geology* **214**: 223-248.

Zar JH. 1984. *Biostatistical Analysis (2nd edition)*. Prentice Hall: Englewood Cliffs, NJ; 718.

Appendix

Here we develop the new permeability-porosity-aperture model, briefly discussed in the main text, in which chemical weathering and hydrological mixing jointly control the relationship between solute concentrations and water fluxes.

First, we assume that permeability (k, [m/s]), porosity (ϕ, [dimensionless]) and average pore aperture or width (p, [m]) all decrease exponentially with depth (z, [m]) from their values at the soil surface (k_o, ϕ_o, and p_o, respectively):

Eq. A1 $$k = k_o e^{-z/\lambda_k}$$

Eq. A2 $$\phi = \phi_o e^{-z/\lambda_\phi}$$

Eq. A3 $$p = p_o e^{-z/\lambda_p}.$$

The rates at which these variables decrease with depth, as expressed by the e-folding distances (λ_k, λ_ϕ, λ_p, all [m]), do not need to be equal to one another. Permeability and porosity are known to decrease roughly exponentially with depth at many sites. An exponential decrease in aperture with depth is less well characterized, but this assumption is plausible and testable. Invoking Darcy's law with an approximately constant head gradient along the hillslope, and using equation (A1), one can express specific discharge (q, [m/s]) in a similar manner as an exponential function that varies as permeability decreases with depth:

Eq. A4 $$q = q_o e^{-z/\lambda_k}.$$

where q_o is a reference discharge that equals k_o times the hillslope gradient. Thus water discharge (Q_w, [m^2/s]) per unit hillslope width can be calculated as:

Eq. A5a $$Q_w = \int_z^\infty q\,dz = \lambda_k q_o e^{-z/\lambda_k}$$

One can also assume that water discharge is proportional to effective precipitation inputs:

Eq. A5b $$Q_w = Rx,$$

where R [m/s] is the effective precipitation rate and x [m] is distance from the hill crest to any point along the hillslope. By setting equations (A5a) and (A5b) equal to one another, one can solve for depth of the hydrologically active region (*i.e.*, soil and bedrock) as a function of distance along the hillslope:

Eq. A6 $$z(x) = -\lambda_k \ln\left(\frac{Rx}{\lambda_k q_o}\right).$$

Equation (A6) assumes that effective precipitation is spatially uniform along the hillslope and that flow originating near the divide and near the stream (*i.e.*, in the non-linear portions of the hillslope) is negligible, and thus that the approximation of a constant hillslope gradient in equation (A4) is valid.

We can also define the solute flux per unit hillslope width (Q_s, [mol m^{-1} s^{-1}]) so that it is proportional to the reactive surface area per unit land area, A_* [dimensionless]. Pore volume is the product of porosity and total volume (V, [m^3]), and reactive surface area per unit volume of pores and medium can be defined as

Eq. A7 $$surface\ area/(volume\ of\ pores + medium) = \frac{V\phi\gamma}{pV} = \frac{\phi\gamma}{p}$$

where γ [dimensionless] is a shape factor that is assumed to be constant with depth. We then integrate to get reactive surface area per unit land area, A_*:

Eq. A8 $$A_* = \int_z^\infty \gamma \frac{\phi}{p} = \int_z^\infty \gamma \frac{\phi_o}{p_o} e^{-z\left(1/\lambda_\phi - 1/\lambda_p\right)} = \frac{\gamma\phi_o}{p_o\left(1/\lambda_\phi - 1/\lambda_p\right)} e^{-z\left(1/\lambda_\phi - 1/\lambda_p\right)}$$

Note that there is a larger wetted reactive surface area per unit land area, A_*, at higher flow rates in this model as a result of the relationship between z and R (equation (A6)). For a surface dissolution reaction in which secondary and back reactions can be ignored, solute flux per unit hillslope width (Q_s) is the product of the reaction constant, k_R [mol m^{-2} s^{-1}], and the reactive surface area per unit land area, A_*, integrated along the linear segment of the hillslope from the base (x=0) to near the ridge (x=L) using the relationships derived in equations (A6) and (A8):

$$Q_s = \int_0^L k_R A_* dx = \int_0^L \frac{k_R\gamma\phi_o}{p_o\left(1/\lambda_\phi - 1/\lambda_p\right)} e^{\left(\lambda_k/\lambda_\phi - \lambda_k/\lambda_p\right)\ln\left(\frac{Rx}{\lambda_k q_o}\right)} dx$$

$$= \int_0^L \frac{k_R\gamma\phi_o}{p_o\left(1/\lambda_\phi - 1/\lambda_p\right)} \left(\frac{Rx}{\lambda_k q_o}\right)^{\left(\lambda_k/\lambda_\phi - \lambda_k/\lambda_p\right)} dx$$

Eq. A9 $$= \frac{k_R\gamma\phi_o}{p_o\left(1/\lambda_\phi - 1/\lambda_p\right)} \left(\frac{1}{1 + \lambda_k/\lambda_\phi - \lambda_k/\lambda_p}\right) \left(\frac{\lambda_k q_o}{R}\right) \left(\frac{Rx}{\lambda_k q_o}\right)^{\left(\lambda_k/\lambda_\phi - \lambda_k/\lambda_p + 1\right)} \Bigg|_0^L$$

$$= \frac{Lk_R\gamma\phi_o}{p_o\left(1/\lambda_\phi - 1/\lambda_p\right)\left(1 + \lambda_k/\lambda_\phi - \lambda_k/\lambda_p\right)} \left(\frac{RL}{\lambda_k q_o}\right)^{\left(\lambda_k/\lambda_\phi - \lambda_k/\lambda_p\right)}$$

The volume-weighted mean concentration in the water flux ($\overline{C}$, [mol/m^3]) is equal to the ratio of the solute flux (equation (A9)) to the water flux (=RL), both expressed per unit hillslope width,

$$\overline{C} = \frac{Q_s}{Q_w} = \frac{\int_0^L k_R A_* dx}{Q_w}$$

Eq. A10 $$= \frac{Lk_R\gamma\phi_o}{p_o\left(1/\lambda_\phi - 1/\lambda_p\right)\left(1 + \lambda_k/\lambda_\phi - \lambda_k/\lambda_p\right)} \left(\frac{1}{\lambda_k q_o}\right)^{\left(\lambda_k/\lambda_\phi - \lambda_k/\lambda_p\right)} (RL)^{\left(\lambda_k/\lambda_\phi - \lambda_k/\lambda_p - 1\right)}.$$

$$= a_o Q_w^{b_0}$$

A power-law concentration-discharge relationship can thus be expressed for a one-dimensional hillslope, with the constant a_o $\left[\text{mol} \cdot \text{s}^{\left(\frac{\lambda_k}{\lambda_\phi}-\frac{\lambda_k}{\lambda_p}-1\right)} \Big/ \text{m}^{\left(\frac{2\lambda_k}{\lambda_\phi}-\frac{2\lambda_k}{\lambda_p}+1\right)} \right]$ equal to all of the other constants before the *RL* term, and the power-law exponent b_0 [dimensionless] equal to:

Eq. A11 $$b_0 = \left(\lambda_k / \lambda_\phi - \lambda_k / \lambda_p - 1 \right).$$

Furthermore, storage (S, [m]) can be defined as the integral of porosity over total depth:

Eq. A12 $$S = \int_z^\infty \phi = \lambda_\phi \phi_o e^{-z/\lambda_\phi}.$$

By combining equations (A5a) and (A12), one can see that discharge (Q_w) varies as a power function of storage:

Eq. A13a $$Q_w / Q_o = (S / S_o)^{b_1},$$

where Q_o and S_o are reference values of discharge and storage, such that Q_w=Q_o at S=S_o, and the power-law exponent, b_1 [dimensionless] is:

Eq. A13b $$b_1 = \frac{\lambda_\phi}{\lambda_k} \quad .$$

The value of b_1 can be determined from recession analysis, because equation (A13a) implies that a plot of $-\mathrm{d}Q_w/\mathrm{d}t$ as a function of Q_w should have a log-log slope of $2-(1/b_1)$, derived during periods when both evapotranspiration and precipitation are small relative to discharge (for example, during rain-free nights) (Kirchner, 2009).

Figure Captions

Figure 1. Concentration-discharge relationships for Si, Ca, and Na at eight Hydrologic Benchmark Network streams. Each plot has consistent axes (same number of log units for both concentration and discharge), so concentrations determined by dilution of fixed weathering fluxes would have the same slope as the gray diagonal lines shown (log-log slope of -1). Instead, concentration-discharge relationships conform more closely to chemostatic behavior (log-log slope near zero).

Figure 2. Log-log slopes of concentration-discharge relationships for 59 Hydrologic Benchmark Network streams arranged alphabetically by site name. Gray lines indicate slope values expected for ideal chemostatic behavior (concentration held constant; log-log slope=0) and for simple dilution of a constant solute flux (concentration inversely proportional to discharge; log-log slope=-1). With few exceptions, these catchments exhibit nearly ideal chemostatic behavior for Ca, Mg, Na, and Si. Error bars indicate ±1 standard error, and are shown where they are larger than the plotting symbols. Open symbols indicate that the observed relationship appears to be non-linear in log-log space.

Figure 3. Annually averaged concentration-discharge relationships for Si, Ca, and Na at the same eight Hydrologic Benchmark Network streams shown in Figure 1. Each plot has consistent axes (same number of log units for both concentration and discharge), so concentrations determined by dilution of fixed weathering fluxes would have the same slope as the gray diagonal lines shown (log-log slope of -1). Even on inter-annual time scales, concentration-discharge relationships do not generally follow the predictions of a simple dilution model, instead conforming more closely to chemostatic behavior (log-log slope near zero).

Figure 4. Log-log slopes of relationships between mean annual flow-weighted concentrations and mean annual discharge for 57 Hydrologic Benchmark Network streams (slopes are not shown for Limpia Creek, TX or Tallulah River, GA because too few years of data are available). Gray lines indicate slope values expected for ideal chemostatic behavior (concentration held constant; log-log slope = 0) and for simple dilution of a constant solute flux (concentration inversely proportional to discharge; log-log slope = -1). Even on inter-annual time scales, almost all of these catchments exhibit nearly ideal chemostatic behavior for Ca, Mg, Na, and Si. Error bars indicate ±1 standard error calculated from a weighted least squares fit to the log annual flow-weighted concentration for each water year vs. log annual water yield. The weighting function is equal to the inverse unbiased weighted variance of the log concentration. By unbiased, we mean that we account for a potential loss in the degrees of freedom introduced by variable flow by calculating the effective number of solute measurements per water year.

Figure 5. Concentration(C)-discharge(Q) relationships for several models plotted with the observed values for Ca at Andrews Creek in Mazama, WA. (a) A well-mixed reservoir model (equation (1)) with a very large storage volume can reproduce the observed range in concentration variability, but only with excessively large hysteresis loops that are not observed in the real data. (b) Inverse relationship between *C* and *Q* as specified by the Hubbard Brook "working model" (Johnson *et al.*, 1969) generally matches the form for each solute, but best-fit *a* parameters (Equation 2) exceed observed rainfall concentrations. See Table 4. (c) Langbein and Dawdy's (1964) chemical mixing model can fit the data well but allows no storage of water or mixing of waters of different ages in the catchment. (d) The permeability-porosity-aperture model (see text) can also fit the data reasonably well, although its assumptions still need to be tested in the field. The slight overestimate of concentration at high discharges is due to the simultaneous fitting to all four solutes with one hydrologic parameter, b_0, which is the best-fit slope to all four solutes' concentration-discharge data. See text for more detailed discussion.

Figure 6. Annual silicon fluxes in streamflow as a function of annual water yield for the eight Hydrological Benchmark Network streams shown in Figures 1 and 3. The diagonal gray line indicates solute fluxes proportional to discharge (*i.e.*, constant concentration).

Table Captions

Table 1. Site characteristics for the 59 Hydrologic Benchmark Network sites discussed in this analysis, as compiled from USGS Circulars 1173 A-D, unless otherwise indicated by one of the following superscripts: a=Hydroclimatic Data Network (HCDN), b=Murdoch and Stoddard (1992), c=Desert Research Institute (DRI), d=National Weather Service of the National Oceanic and Atmospheric Administration (NWS/NOAA), e=mean annual temperature (not low or high) and therefore not used in empirical model, f=data from Silas Little Experimental Forest, g=National Climatic Data Center (NCDC/NOAA), h=low elevation estimate, i=varies strongly with elevation, j=North Carolina State University (NCSU/NOAA), k=mean annual precipitation in Hilo, HI, l=mean annual precipitation in Amanda Park, WA.

Table 2. Statistical tests of association between site characteristics and concentration-discharge slopes across the 59 HBN streams. Single and double asterisks indicate statistical significance at the $p<0.05$ and $p<0.02$ levels, respectively. Several of the tested relationships are statistically significant but their explanatory power is low. Sites with volcanic bedrock have steeper concentration-discharge slopes for Ca, Mg, and Na than sites without volcanics, and slopes for Na are shallower at sites with carbonate bedrock compared to sites without carbonates. Nonparametric (Wilcoxon) tests agree with the parametric (F-test) results. Average annual runoff is significantly correlated with Ca and Si slopes, and average low temperature and MAP with Si slopes, according to the robust Spearman rank correlation coefficient.

Table 3. Subsurface storage depths required for a simple "bucket" model assuming a constant 5%, 10% and 30% porosity for the model described in equation (1) of the text. The porosity is a single average value for all soil and underlying bedrock to the specified depth. The specified storage depth indicates the volume required to maintain the observed variability in concentrations at a given site (reported value is the median storage for all four solutes based on the observed ratio of maximum to minimum concentrations at each site, the median of which is ~4 across all sites and solutes).

Table 4. Best-fit parameter *a* in the Hubbard Brook "working model" and observed precipitation concentrations for the major base cations at eight representative sites. (Observed Si concentrations in precipitation were not available.) The best-fit concentrations, *a*, are observed to be one to two orders of magnitude higher than the observed concentrations. This suggests that the model is unable to represent some mixing or reaction processes occurring in the catchment. In all cases, all three parameters in equation (2) were fit simultaneously for all four solutes; *a* and *d* were constrained to be ≥ 0, and *b*, which depends only on hydrology and is independent of the solute, was forced to be a single value for all four solutes at each site.

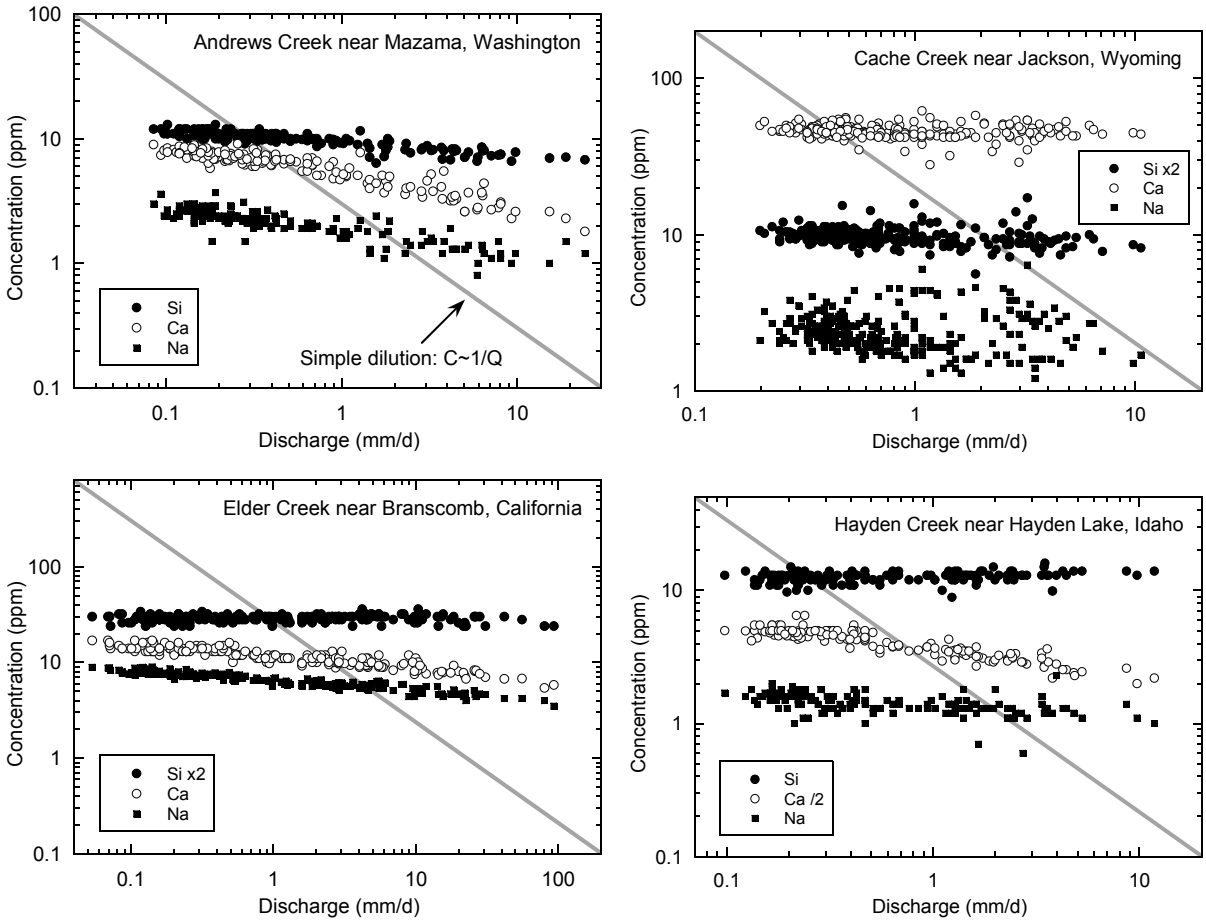
Andrews Creek near Mazama, Washington
Concentration (ppm)
Discharge (mm/d)
Si
Ca
Na
Simple dilution: C~1/Q
Cache Creek near Jackson, Wyoming
Si x2
Ca
Na
Elder Creek near Branscomb, California
Hayden Creek near Hayden Lake, Idaho
Ca /2

Figure 1 a-d.

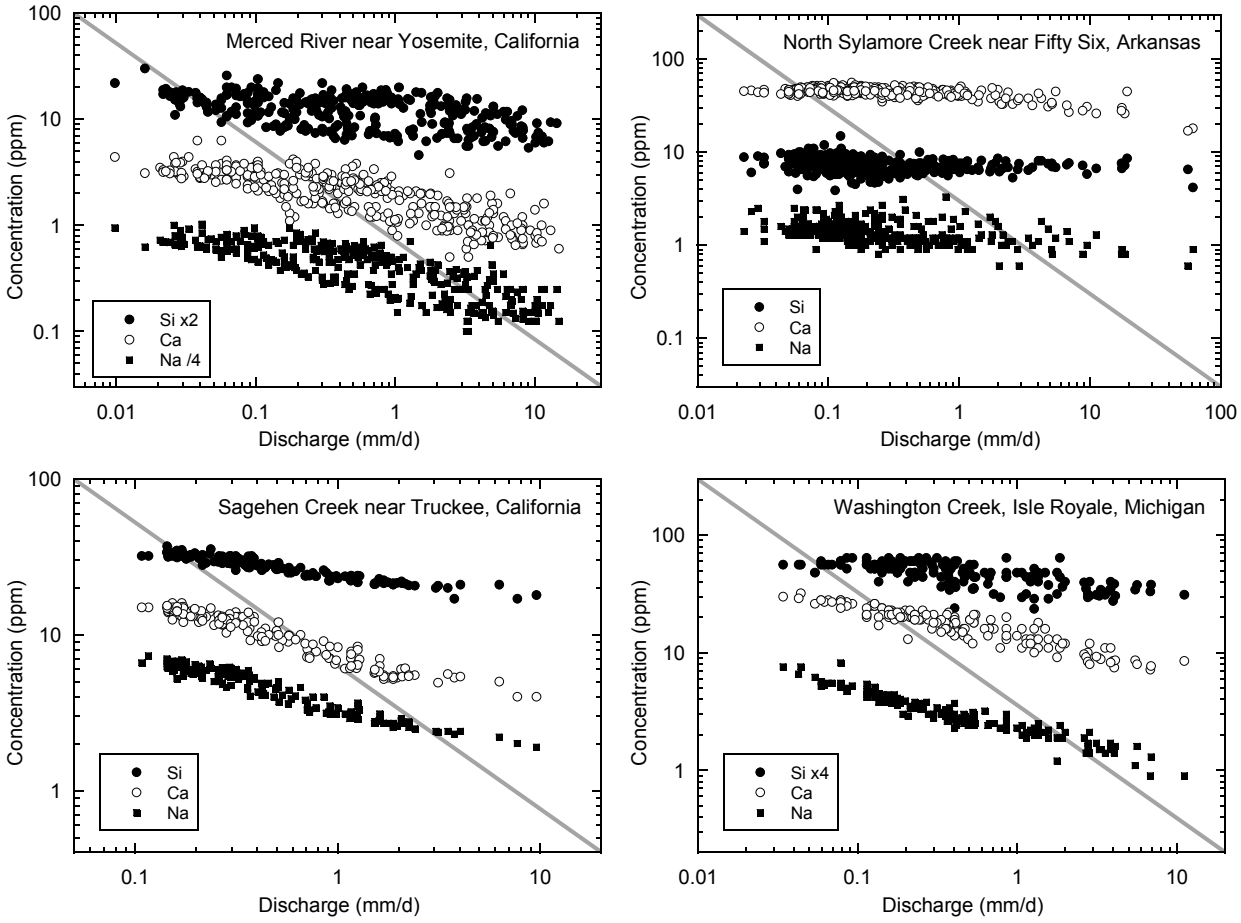
Merced River near Yosemite, California
Si x2
Ca
Na /4
Concentration (ppm)
Discharge (mm/d)
North Sylamore Creek near Fifty Six, Arkansas
Si
Ca
Na
Concentration (ppm)
Discharge (mm/d)
Sagehen Creek near Truckee, California
Si
Ca
Na
Concentration (ppm)
Discharge (mm/d)
Washington Creek, Isle Royale, Michigan
Si x4
Ca
Na
Concentration (ppm)
Discharge (mm/d)

Figure 1 e-h.

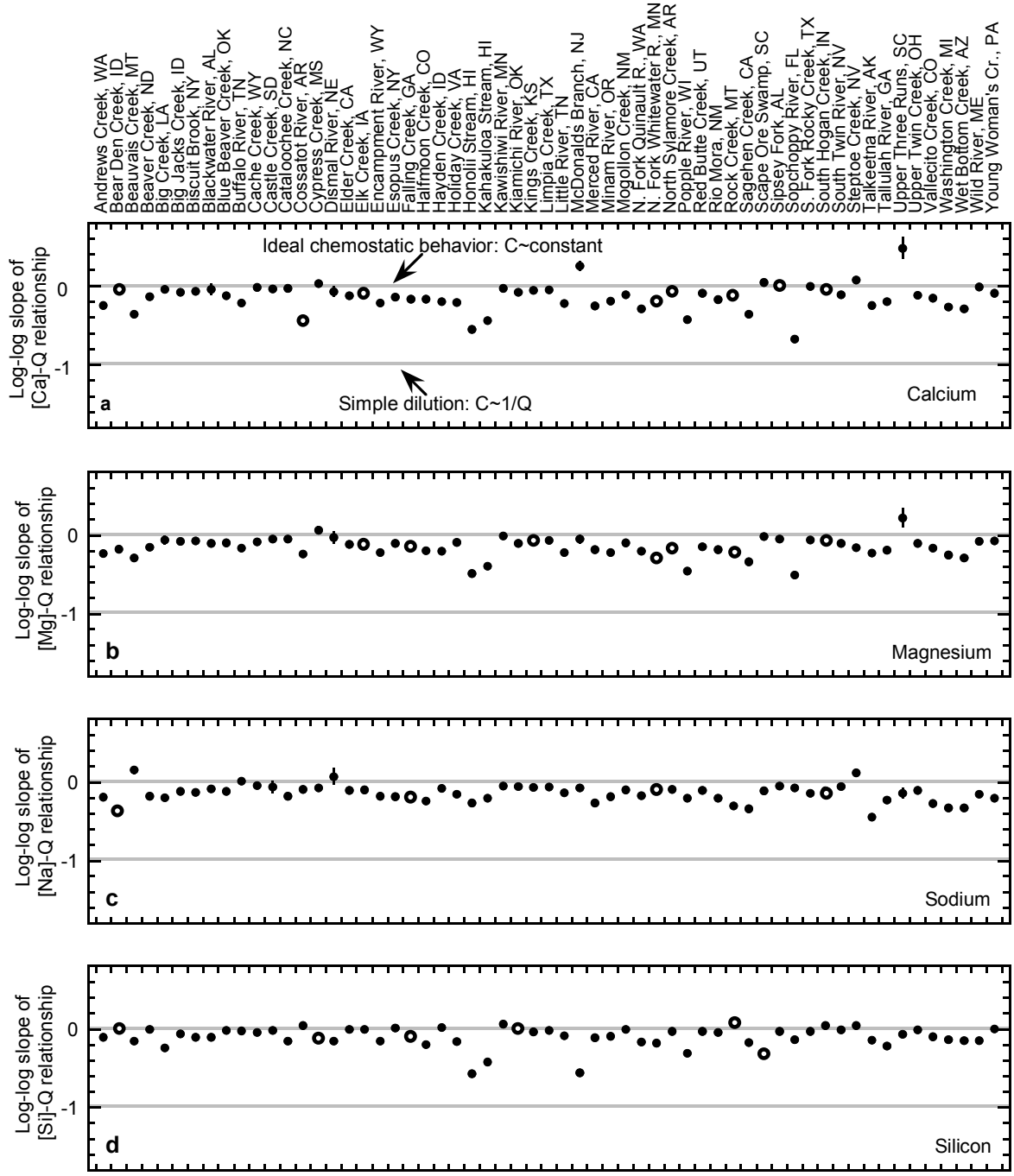
Andrews Creek, WA
Bear Den Creek, ID
Beauvais Creek, MT
Beaver Creek, ND
Big Creek, LA
Big Jacks Creek, ID
Biscuit Brook, NY
Blackwater River, AL
Blue Beaver Creek, OK
Buffalo River, TN
Cache Creek, WY
Castle Creek, SD
Cataloochee Creek, NC
Cossatot River, AR
Cypress Creek, MS
Dismal River, NE
Elder Creek, CA
Elk Creek, IA
Encampment River, WY
Esopus Creek, NY
Falling Creek, GA
Halfmoon Creek, CO
Hayden Creek, ID
Holiday Creek, VA
Honolii Stream, HI
Kahakuloa Stream, HI
Kawishiwi River, MN
Kiamichi River, OK
Kings Creek, KS
Limpia Creek, TX
Little River, TN
McDonalds Branch, NJ
Merced River, CA
Minam River, OR
Mogollon Creek, NM
N. Fork Quinault R., WA
N. Fork Whitewater R., MN
North Sylamore Creek, AR
Popple River, WI
Red Butte Creek, UT
Rio Mora, NM
Rock Creek, MT
Sagehen Creek, CA
Scape Ore Swamp, SC
Sipsey Fork, AL
Sopchoppy River, FL
S. Fork Rocky Creek, TX
South Hogan Creek, IN
South Twin River, NV
Steptoe Creek, NV
Talkeetna River, AK
Tallulah River, GA
Upper Three Runs, SC
Upper Twin Creek, OH
Vallecito Creek, CO
Washington Creek, MI
Wet Bottom Creek, AZ
Wild River, ME
Young Woman's Cr., PA
Ideal chemostatic behavior: C~constant
Simple dilution: C~1/Q
Log-log slope of [Ca]-Q relationship
Log-log slope of [Mg]-Q relationship
Log-log slope of [Na]-Q relationship
Log-log slope of [Si]-Q relationship
0
-1
a
Calcium
b
Magnesium
c
Sodium
d
Silicon

Figure 2.

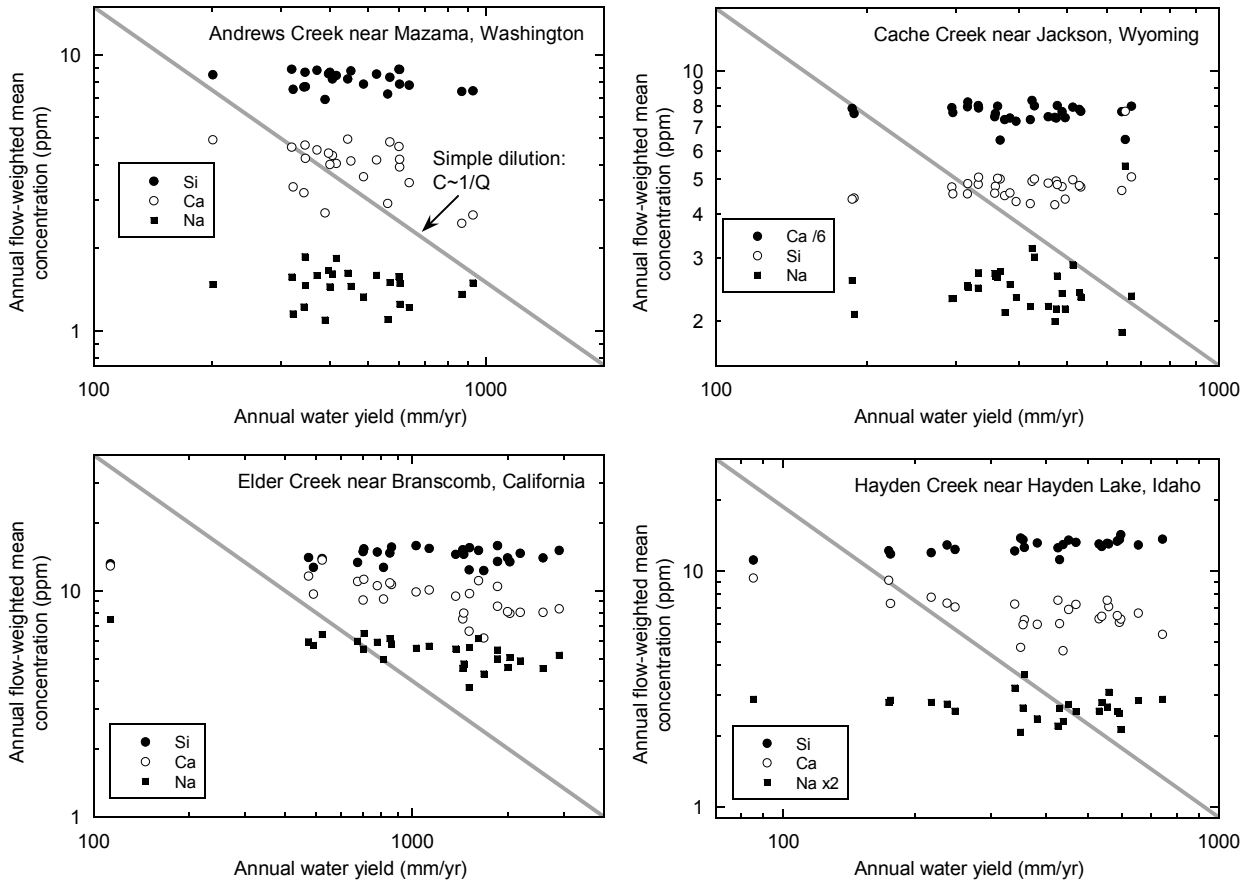
Andrews Creek near Mazama, Washington
Annual flow-weighted mean concentration (ppm)
Annual water yield (mm/yr)
Simple dilution:
C~1/Q
Si
Ca
Na
Cache Creek near Jackson, Wyoming
Ca /6
Si
Na
Elder Creek near Branscomb, California
Hayden Creek near Hayden Lake, Idaho
Na x2

Figure 3a-d.

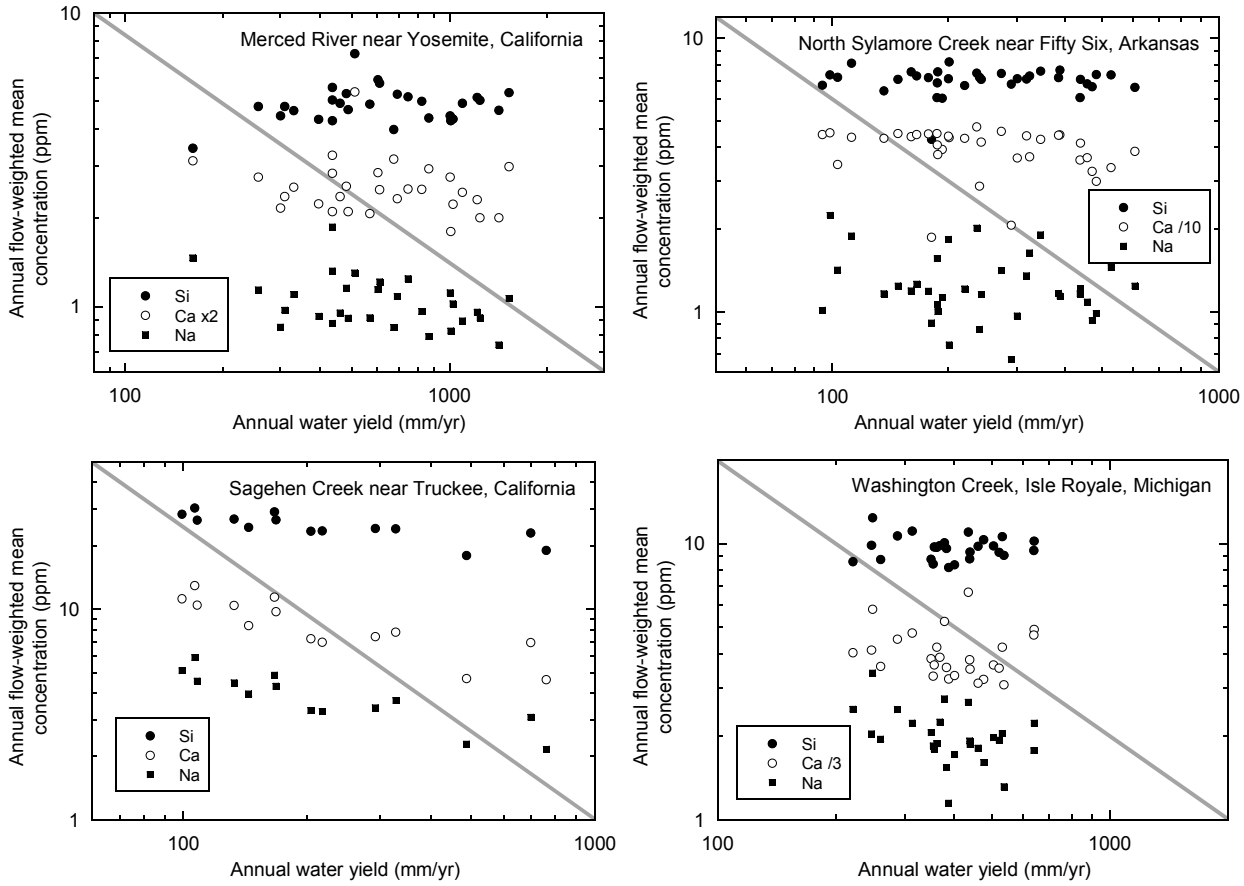
Merced River near Yosemite, California
Si
Ca x2
Na
North Sylamore Creek near Fifty Six, Arkansas
Si
Ca /10
Na
Sagehen Creek near Truckee, California
Si
Ca
Na
Washington Creek, Isle Royale, Michigan
Si
Ca /3
Na
Annual flow-weighted mean concentration (ppm)
Annual water yield (mm/yr)
10
1
100
1000

Figure 3e-h.

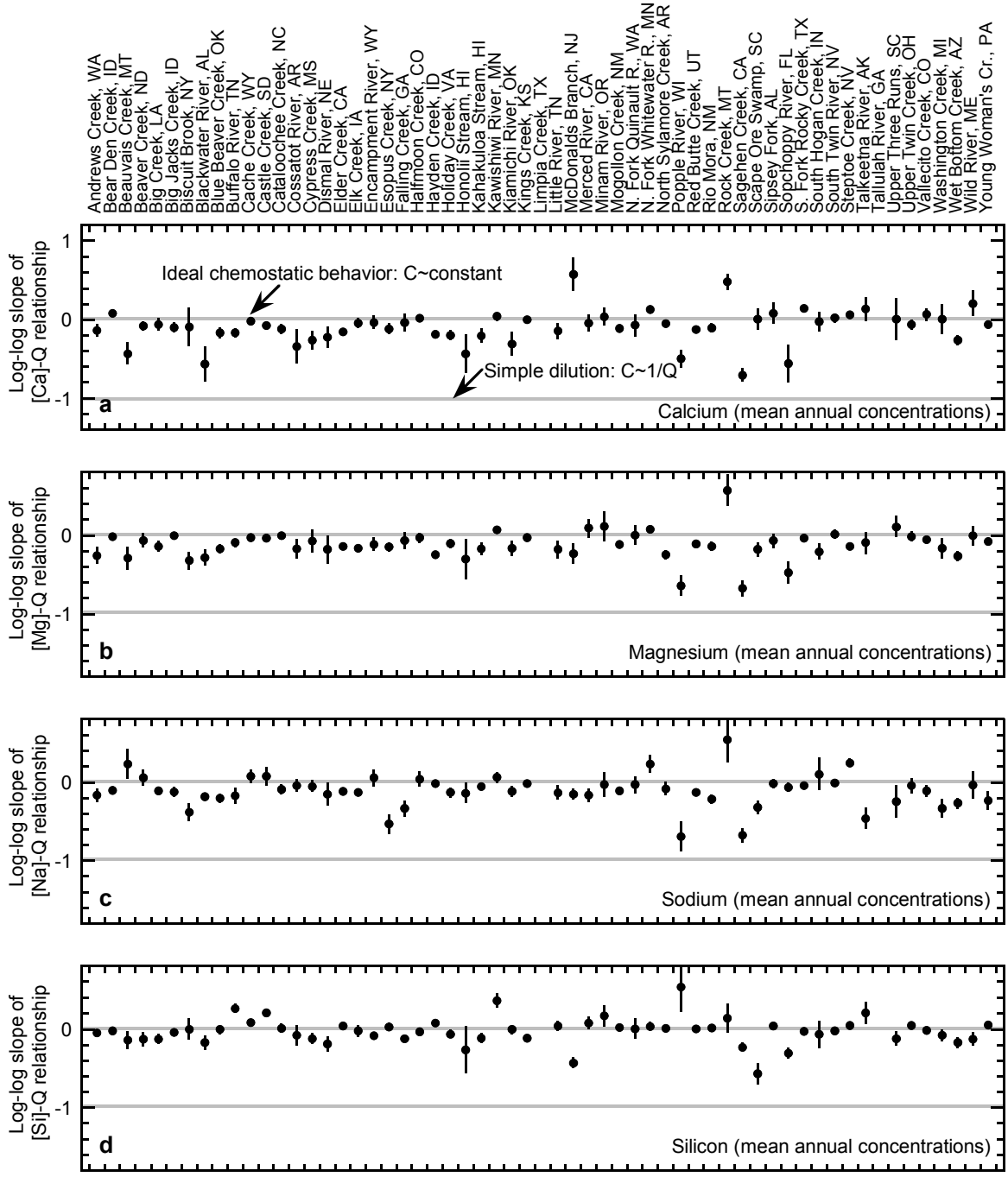
Andrews Creek, WA
Bear Den Creek, ID
Beauvais Creek, MT
Beaver Creek, ND
Big Creek, LA
Big Jacks Creek, ID
Biscuit Brook, NY
Blackwater River, AL
Blue Beaver Creek, OK
Buffalo River, TN
Cache Creek, WY
Castle Creek, SD
Cataloochee Creek, NC
Cossatot River, AR
Cypress Creek, MS
Dismal River, NE
Elder Creek, CA
Elk Creek, IA
Encampment River, WY
Esopus Creek, NY
Falling Creek, GA
Halfmoon Creek, CO
Hayden Creek, ID
Holiday Creek, VA
Honolii Stream, HI
Kahakuloa Stream, HI
Kawishiwi River, MN
Kiamichi River, OK
Kings Creek, KS
Limpia Creek, TX
Little River, TN
McDonalds Branch, NJ
Merced River, CA
Minam River, OR
Mogollon Creek, NM
N. Fork Quinault R., WA
N. Fork Whitewater R., MN
North Sylamore Creek, AR
Popple River, WI
Red Butte Creek, UT
Rio Mora, NM
Rock Creek, MT
Sagehen Creek, CA
Scape Ore Swamp, SC
Sipsey Fork, AL
Sopchoppy River, FL
S. Fork Rocky Creek, TX
South Hogan Creek, IN
South Twin River, NV
Steptoe Creek, NV
Talkeetna River, AK
Tallulah River, GA
Upper Three Runs, SC
Upper Twin Creek, OH
Vallecito Creek, CO
Washington Creek, MI
Wet Bottom Creek, AZ
Wild River, ME
Young Woman's Cr., PA
Log-log slope of [Ca]-Q relationship
Ideal chemostatic behavior: C~constant
Simple dilution: C~1/Q
a
Calcium (mean annual concentrations)
Log-log slope of [Mg]-Q relationship
b
Magnesium (mean annual concentrations)
Log-log slope of [Na]-Q relationship
c
Sodium (mean annual concentrations)
Log-log slope of [Si]-Q relationship
d
Silicon (mean annual concentrations)
1
0
-1

Figure 4.

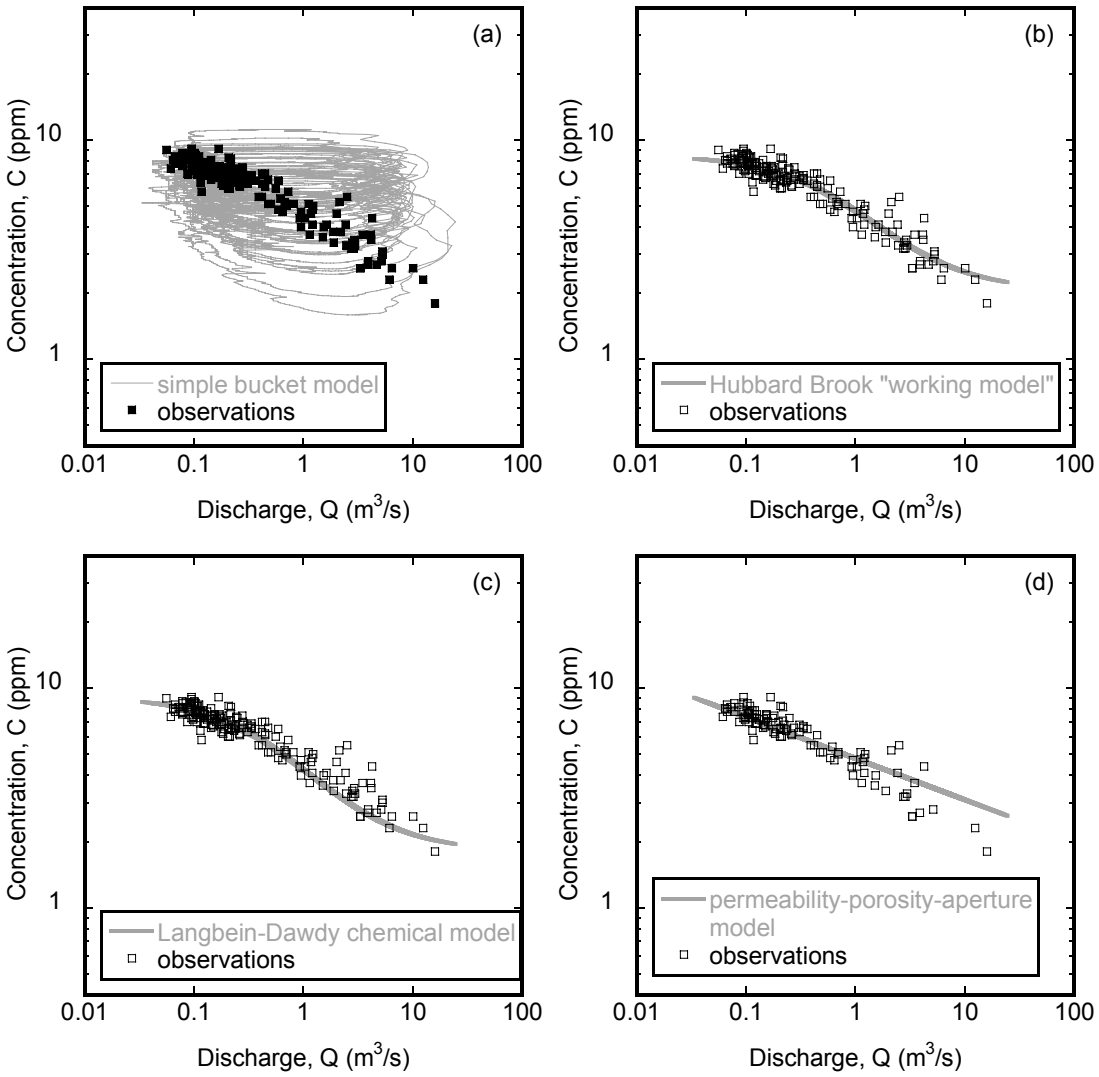
(a)
(b)
(c)
(d)
Concentration, C (ppm)
10
1
0.01
0.1
1
10
100
Discharge, Q (m3/s)
simple bucket model
observations
Hubbard Brook "working model"
observations
Langbein-Dawdy chemical model
observations
permeability-porosity-aperture model
observations

Figure 5.

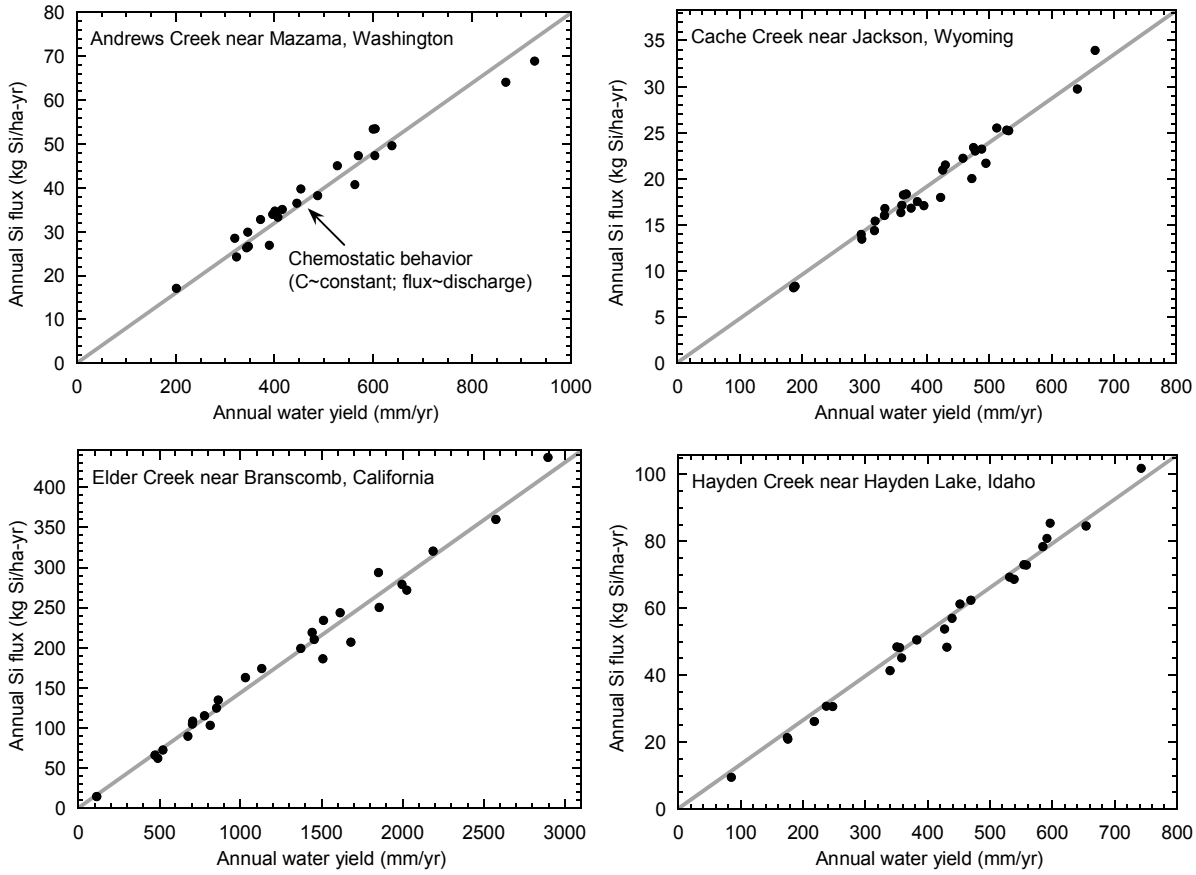
Andrews Creek near Mazama, Washington
Annual Si flux (kg Si/ha-yr)
Annual water yield (mm/yr)
Chemostatic behavior
(C~constant; flux~discharge)
Cache Creek near Jackson, Wyoming
Annual Si flux (kg Si/ha-yr)
Annual water yield (mm/yr)
Elder Creek near Branscomb, California
Annual Si flux (kg Si/ha-yr)
Annual water yield (mm/yr)
Hayden Creek near Hayden Lake, Idaho
Annual Si flux (kg Si/ha-yr)
Annual water yield (mm/yr)

Figure 6 a-d.

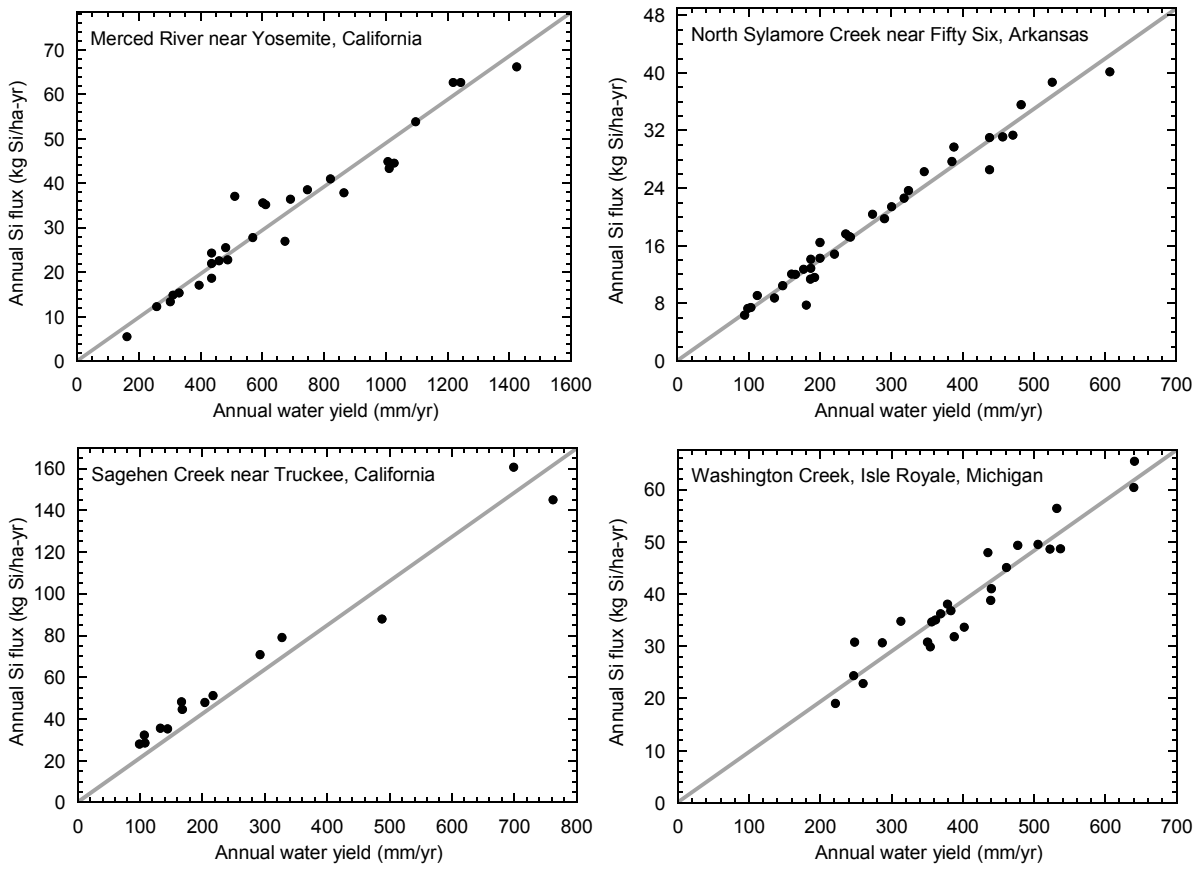
Merced River near Yosemite, California
Annual Si flux (kg Si/ha-yr)
Annual water yield (mm/yr)
North Sylamore Creek near Fifty Six, Arkansas
Annual Si flux (kg Si/ha-yr)
Annual water yield (mm/yr)
Sagehen Creek near Truckee, California
Annual Si flux (kg Si/ha-yr)
Annual water yield (mm/yr)
Washington Creek, Isle Royale, Michigan
Annual Si flux (kg Si/ha-yr)
Annual water yield (mm/yr)

Figure 6 e-h.

Station name	Station No.	Drainage Area	Average annual runoff	Land Cover/Use	Lithology	Low Mean Monthly Temperature	High Mean Monthly Temperature	Mean Annual Precipitation
		km^2	cm			degrees C	degrees C	cm
Andrews Creek near Mazama, WA	12447390	57	48	subalpine forest	quartz monzonite, quartz diorite	4	10	89[a]
Bear Den Creek near Mandaree, ND	6332515	192	3	grassland, agriculture	sandstone, siltstone, alluvium, colluvium	-12.3	20.5	39
Beauvais Creek near St. Xavier, MT	6288200	259	9	prairie	slate, shale, sandstone	-11.1[a]	31.5[c]	38[a]
Beaver Creek near Finley, ND	5064900	415	2	prairie, agriculture, grazing	glacial till	-14.8	21	49
Big Creek at Pollock, LA	7373000	132	44	pine forest, agriculture, residential	unconsolidated alluvium	8.2	27.8	148
Big Jacks Creek near Bruneau, ID	13169500	655	0.7	sagebrush	rhyolite/basalt	-0.5	22.9	19.6
Biscuit Bk above Pigeon Bk at Frost Valley, NY	1434025	10	91	mixed forest, residential	shales, sandstones, conglomerates	5[e,b]	n/a	157[b]
Blackwater River near Bradley, AL	2369800	227	59	pine forest hills, bay wetland	sandstone	9.1	26.2	150
Blue Beaver Creek near Cache, OK	7311200	64	19	grassland/prairie	rhyolite, conglomerates, sandstone	3	27.8	77
Buffalo River near Flat Woods, TN	3604000	1158	59	deciduous forest, agriculture, residential	limestones, siltstone, shale	3.3	25	127
Cache Creek near Jackson, WY	13018300	27	40	pine/fir, grassland	limestone, dolomite, siltstone, sandstone, shale	-9.2	16	61[a]
Castle Ck above Deerfield Res. near Hill City, SD	6409000	205	5	pine forest	schist, limestone	-7.3	15.5	51
Cataloochee Creek near Cataloochee, NC	3460000	127	78	broadleaf forest	sandstone	0	16	145
Cossatot River near Vandervoort, AR	7340300	232	78	pine-oak forest, residential	metamorphosed sedimentary: chert, sandstone, shale, novaculite	5	27.2	130
Cypress Creek near Janice, MS	2479155	136	70	pine forest	fine-grained sedimentary, quartz, salt dome	9.1	27.4	152
Dismal River near Thedford, NE	6775900	2500	7	prairie, grazing	chalk, limestone, shale, unconsolidated sediments	-5.4	23.7	54
Elder Creek near Branscomb, CA	11475560	16.8	129	mixed forest, chaparral, grassland	sandstone, argillite	6	31	215
Elk Creek near Decatur City, IA	6897950	136	23	prairie, deciduous trees, agriculture	limestone, shale, alluvium, loess	-6.6	24.6	92
Encampment River above Hog Park Creek near Encampment, WY	6623800	188	50	montane/subalpine forest, grassland	granite, quartz monzonite, granodiorite, felsic gneiss, calcareous siltstone, shale, mudstone, till	-5.8	17.2	76
Esopus Ck at Shandaken, NY	1362198	165	74	mixed forest, residential	shale, sandstone, conglomerate	-4.2	21.5	157

Falling Creek near Juliette, GA	2212600	187	30	mixed forest	gneiss, gabbro	7.3	26.6	122
Halfmoon Creek near Malta, CO	7083000	61	40	coniferous forest, tundra	biotite gneiss, schist, migmatite	-8.9	12.2	53[a]
Hayden Creek below N Fork near Hayden Lake, ID	12416000	57	44	coniferous forest	quartzite, argillite, siltstone, dolomite, limestone	-2	21	89
Holiday Creek near Andersonville, VA	2038850	22	35	mixed forest	phyllite, schist, gneiss	3	25	105
Honolii Stream near Papaikou, HI	16717000	31	377	lava, tropical vegetation	basalt	17.6[c]	28.8[c]	328[c,k]
Kahakuloa Stream near Honokohau, Maui, HI	16618000	8	197	dense tropical vegetation	basalt	17.4[d]	31.1[d]	n/a
Kawishiwi River near Ely, MN	5124480	655	28	mixed forest	anorthosite, igneous intrusives, till	-14.4	19.2	70
Kiamichi River near Big Cedar, OK	7335700	104	74	mixed forest	shale, siltstone, sandstone	4.9	27.2	130
Kings Creek near Manhattan, KS	6879650	10.6	20	tallgrass prairie	shale, limestone	-1.8	26.6	84
Limpia Creek above Ft. Davis, TX	8431700	135	1.6	deciduous forest, desert & riparian plants	andesite, basalt	7.1[c]	25[c]	45[c]
Little River above Townsend, TN	3497300	275	93	broadleaf forest	phyllite, sandstone, slate, limestone	4	23	152[i,j]
McDonalds Branch in Lebanon State Forest, NJ	1466500	6.1	32	broadleaf forest/swamp	unconsolidated sediments	12.8	25[f]	116
Merced River at Happy Isl. Bridge near Yosemite, CA	11264500	469	66.5	mixed forest, meadow	granite, granodiorite	3	22	94
Minam River at Minam, OR	13331500	622	65	coniferous forest, grasslands, meadow	granite, intruded by aplite, pegmatite, basalt	-7.2	14.6	100[h,i]
Mogollon Creek near Cliff, NM	9430600	179	17	mixed forest, meadow	rhyolite, quartz latite, porphyritic flows, plagioclase, biotite, sanidine	3.6	24.4	37
North Fork Quinault R near Amanda Park, WA	12039300	192	402	conifers, alpine vegetation, bare rock	basalt, semi-consolidated sediments, slate	1.4[c]	25.4[c]	328[c,l]
North Fork Whitewater River near Elba, MN	5376000	262	17	agriculture, broadleaf forest	limestone, dolomite, shale, sandstone, till	-10.7	22.7	84
North Sylamore Creek near Fifty Six, AR	7060710	150	28	hardwood/pine forest	sandstone, dolomite, shale, limestone	1.9	26.2	112
Popple River near Fence, WI	4063700	360	29	mixed forest	granite and granitoid gneiss	-17.1	20.9	78
Red Butte Ck at Ft. Douglas near Salt Lake City, UT	10172200	18.8	20	mixed forest, grassland	quartzite, sandstone, limestone	-0.7	25.4	74[a]
Rio Mora near Terrero, NM	8377900	138	20	coniferous forest, meadow	granite, amphibolite, tonalite, quartz diorite, quartzite, schist, limestone	-2.2	15.8	45

Rock Ck below Horse Ck near Intl Boundary, MT	6169500	850	1.5	prairie, agriculture, grazing	shale, unconsolidated sediments	-13.5	18.8	29
Sagehen Creek near Truckee, CA	10343500	27	40	coniferous forest, meadow	granite, andesite, breccia, hornfels, till, alluvium	-3	17	94
Scape Ore Swamp near Bishopville, SC	2135300	249	38	mixed forest, agriculture	arkosic and argillaceous sands	5.5	25.5	115
Sipsey Fork near Grayson, AL	2450250	239	62	mixed forest	limestone, sandstone, shale, mudstone, claystone, non-persistent coal beds	5	25.5	145
Sopchoppy River near Sopchoppy, FL	2327100	265	67	mixed forest	limestone, unconsolidated marine sediment	12.2	27.4	145
South Fork Rocky Creek near Briggs, TX	8103900	86	11	arid grassland	limestone, marl, dolomite	8.4	28.2	75
South Hogan Creek near Dillsboro, IN	3276700	99	39	broadleaf forest, agriculture, grazing	limestone, shale, glacial till, loess	-1.9	22.9	100
South Twin River near Round Mountain, NV	10249300	52	11.4	forest, sagebrush, semidesert	felsite, tuff, quartzite, limestone, dolostone, quartz	-1.4	22.2	20[h,i]
Steptoe Creek near Ely, NV	10244950	29	22	forest, scrub, semidesert	limestone, shale	-4.3	19.6	24[h,i]
Talkeetna River near Talkeetna, AK	15292700	5196	70	mixed forest, mixed shrubs, tundra	glacial drift, colluvium, igneous bedrock	-11.7[g]	14.9[g]	72[g]
Tallulah River near Clayton, GA	2178400	146	116	broadleaf forest	gneiss, schist, amphibolite	3.3	21.6	182
Upper Three Runs near New Ellenton, SC	2197300	255	36	mixed forest	arkosic sands	7.5	27.1	120
Upper Twin Creek at McGaw, OH	3237280	31.6	38	broadleaf forest	sandstone, shale	0	24.4	105
Vallecito Creek near Bayfield, CO	9352900	187	70	coniferous forest, alpine tundra	slate, schist, quartzite, breccia, limestone, conglomerate, quartz monzonite, granite	-5.9	17.6	117[a]
Washington Creek at Windigo Isle Royale, MI	4001000	34	42	mixed forest	basalt, andesite, sandstone, glacial drift	3.4[e]	n/a	77
Wet Bottom Creek near Childs, AZ	9508300	94	15.5	semidesert, grassland, woodlands	granite, basalt, andesite, siltstone, dolomite, limestone	7.7	29.4	63.5
Wild River at Gilead, ME	1054200	180	89	mixed forest	sandstone, shale, siltstone, gneiss, mica schists, quartzites	-9	19	119
Young Womans Creek near Renovo, PA	1545600	120	56	mixed forest	sandstone, siltstone, shale, conglomerate, discontinuous coal beds	-3.3	22.5	105

Table 1.

F ratio	Ca	Mg	Na	Si
Volcanics (present vs. absent)	5.32*	6.51*	4.59*	3.77
Carbonates (present vs. absent)	0.07	0.02	12.47**	2.54
Spearman correlation coefficient, r_s	Ca	Mg	Na	Si
Avg Annual Runoff (cm)	-0.27*	-0.19	-0.21	-0.28*
Average low temperature (deg C)	-0.02	0.10	0.06	-0.30*
Average high temperature (deg C)	-0.06	0.06	0.25	-0.16
MAP, Mean annual precipitation (cm)	0.03	0.05	-0.08	-0.28*
Area (km^2)	-0.11	-0.08	0.00	0.04

Table 2.

Site	Storage Depth [m]		
	5% porosity	10% porosity	30% porosity
Andrews	10.8	5.4	1.8
Cache	10.1	5.0	1.7
Elder	83.7	41.9	14.0
Hayden	6.0	3.0	1.0
Merced	9.8	4.9	1.6
N Sylamore	6.5	3.3	1.1
Sagehen	21.7	10.9	3.6
Washington	9.2	4.6	1.5

Table 3.

all [ppm]	best-fit a_{Ca}	Observed Ca in precipitation	best-fit a_{Mg}	Observed Mg in precipitation	best-fit a_{Na}	Observed Na in precipitation
Andrews	2.04	0.03	0.31	0.02	0.97	0.07
Cache	44.1	0.19	12.3	0.02	2.20	0.04
Elder	7.21	0.04	2.34	0.04	4.32	0.18
Hayden	4.23	0.11	1.31	0.04	1.13	0.01
Merced	0.72	0.05	0.10	0.01	0.56	0.04
N Sylamore	28.6	0.14	1.89	0.02	0.82	0.05
Sagehen	3.56	0.05	1.36	0.01	1.75	0.04
Washington	7.99	0.16	2.44	0.03	1.14	0.02

Table 4.